

Magneto-transport in (Ga,Mn)As-based alloys and hybrids



Dissertation
zur
Erlangung des Doktorgrades
der Naturwissenschaften
(Dr. rer. nat.)

dem

**Fachbereich Physik
der Philipps-Universität Marburg**

vorgelegt von

Shuangli Ye

aus

der V. R. China

Marburg/Lahn 2005

Vom Fachbereich Physik der Philipps-Universität als

Dissertation angenommen am:.....08. 06. 2005

Erstgutachter:Prof. Dr. W. Heimbrodt

Zweitgutachter:.....Prof. Dr. P. Thomas

Tag der mündlichen Prüfung:.....28. 06. 2005

Zusammenfassung

In der vorliegenden Arbeit wurden die Eigenschaften des Magnetotransports von Legierungen und Hybriden auf (Ga,Mn)As Basis untersucht.

In paramagnetischen GaAs:Mn-Schichten, die mittels MOVPE abgeschieden wurden, wurden bei tiefen Temperaturen ungewöhnliche positive und negative Magnetowiderstände (MR) beobachtet, die, wie auch in verdünnt-magnetischen II(Mn)-VI-Halbleitern, empfindlich von der Mn-Konzentration abhängen.

Man vermutet, daß das Wechselspiel zweier Effekte eine bedeutende Rolle für die beobachteten Magnetowiderstände spielt. Einer ist die vom Magnetfeld abhängige Aufspaltung des Valenzbandes aufgrund der s,p-d-Austauschwechselwirkung. Der andere ist der durch den Manganeinbau induzierte Unordnungseffekt. Die Konkurrenz dieser beiden Effekte ist für die komplizierten MR-Effekte verantwortlich. Die experimentellen Magnetowiderstände in verdünnt-magnetischen II(Mn)-VI und III(Mn)-V-Halbleitern wurden qualitativ durch theoretische Berechnungen mit einem Netzwerk- und einem Beweglichkeitsmodell beschrieben.

Im Gegensatz zu durch MBE hergestellten ferromagnetischen $\text{Ga}_{1-x}\text{Mn}_x\text{As}$ -Legierungen, die ein negatives $N_0\beta$ zeigen, findet man in den durch MOVPE abgeschiedenen paramagnetischen GaAs:Mn-Schichten durch MCD-Messungen ein positives $N_0\beta$. Andererseits wechselt das Vorzeichen von $N_0\beta$ in den MOVPE-Proben durch Te-Dotierung nach negativ. Diese Ergebnisse deuten darauf hin, daß Betrag und Vorzeichen von $N_0\beta$ durch Veränderungen der lokalen elektronischen Struktur der Mn-Ionen eingestellt werden können, was zu vielfältigen intrinsischen bzw. extrinsischen Magnetotransporteffekten führt.

In paramagnetisch-ferromagnetischen GaAs:Mn/MnAs-Hybridstrukturen, die durch MOVPE hergestellt wurden und die MnAs-Cluster mit NiAs-Struktur enthalten, beobachtet man große, ungewöhnliche Magnetowiderstandseffekte. Sie zeigen beispielsweise in einem Magnetfeld von 10 T bei tiefen Temperaturen einen negativen MR von 30%, der mit steigender Temperatur zu einem positiven MR von 160% wechselt. An den ferromagnetischen MnAs-Clustern finden bei tiefen Temperaturen Lokalisierungsprozesse der Ladungsträger statt, während die Cluster bei hohen Temperaturen als Spin-Filter wirken, was für die beobachteten MR-Effekte verantwortlich sein könnte.

Es konnte gezeigt werden, daß die magnetischen Eigenschaften und Magnetotransporteigenschaften von GaAs:Mn/MnAs-Hybridstrukturen stark von den Wachstumsparametern abhängen. Tempert man die durch Tieftemperatur-MBE hergestellten $\text{Ga}_{1-x}\text{Mn}_x\text{As}$ -Schichten nach dem Wachstum, so bilden sich zwei Arten von MnAs-Clustern, und es zeigt sich in den bei höheren Temperaturen getemperten Hybridstrukturen lediglich ein geringer positiver MR-Effekt.

Durch Variation der Kristallzuchtparameter wurde bestätigt, daß die Größe des Spin-Filter-Effektes sowohl durch Form und Größe der Cluster, als auch durch deren Dichte abgestimmt werden kann.

Es zeigte sich, daß die ungewöhnlichen Magnetowiderstands- und Halleffekte in durch MOVPE hergestellten GaAs:Mn/MnAs-Hybridstrukturen auch durch unterschiedliche Geometrien sowie durch hydrostatischen Druck verändert werden können. Die Ergebnisse deuten darauf hin, daß die Stärke der Wechselwirkung zwischen den Ladungsträgerspins und der Magnetisierung der MnAs-Cluster von äußeren physikalischen Parametern abhängt, was zu Veränderungen der Magnetotransporteigenschaften führt.

Contents:

1. Introduction	1
1.1 <i>Introduction to spintronics</i>	1
1.2 <i>Magnetic semiconductors and dilute magnetic semiconductors</i>	4
1.3 <i>Origin of the magnetism in II(Mn)-VI and III(Mn)-V DMS</i>	5
1.3.1. The nature of Mn ions in DMS	6
1.3.2. sp-d exchange interaction between Mn ions and band states	8
1.3.3. Exchange integrals $N_0\alpha$ and $N_0\beta$ in II(Mn)-VI and III(Mn)-V DMS	11
1.3.4. Antiferromagnetic superexchange interaction between the Mn ions in II-Mn-VI DMS	15
1.3.5. Origin of the ferromagnetism in III-V DMS	15
1.4 <i>Magneto-transport in DMS</i>	18
1.4.1. MR effect in II(Mn)-VI DMS	18
1.4.2. MR effects in III(Mn)-V DMS	19
1.4.3. MR in ferromagnet(FM)/semiconductor hybrids	20
2. Preparation and structural properties of the studied GaMnAs-based alloys and hybrids.....	25
2.1 <i>MOVPE and MBE growth</i>	25
2.2 <i>Six studied series of (Ga,Mn)As-based samples</i>	27
2.2.1 Paramagnetic GaAs:Mn alloys (MOVPE grown)	27
2.2.2 Co-doped GaAs:Mn,Te alloys (MOVPE grown)	28
2.2.3 p-GaAs:Mn/MnAs hybrids and their magnetic and structural properties (MOVPE grown)	28
2.2.4. p-GaInAs:Mn/MnAs hybrids (MOVPE grown)	33
2.2.5. p-Ga _{1-x} Mn _x As alloys (MBE grown)	34
2.2.6. p-GaAs:Mn/MnAs hybrids (MBE growth followed by post-annealing)	35
3. Transport properties of paramagnetic GaAs:Mn and co-doped GaAs:Mn,Te.....	39
3.1 <i>Resistivity and Hall measurements</i>	39
3.2 <i>MR effects of the paramagnetic GaAs:Mn alloys</i>	40
3.3. <i>Experimental MR results in the context of theoretical models</i>	44
3.4. <i>Hall measurements of paramagnetic GaAs:Mn alloy (MOVPE grown)</i>	47
3.5 <i>MR and Hall results of the paramagnetic GaAs:Mn,Te co-doped alloys</i>	50
3.6. <i>Summary</i>	53
4. Magneto-transport in GaAs:Mn/MnAs-based paramagnetic-ferromagnetic hybrids prepared by MOVPE and post-growth annealing of MBE-grown Ga_{1-x}Mn_xAs alloys ...	57
4.1. <i>Unusual MR effects in MOVPE-grown GaAs:Mn/MnAs hybrids</i>	58
4.2. <i>Qualitative and quantitative discussion of the microscopic mechanism for the negative MR in MOVPE-grown GaAs:Mn/MnAs hybrids</i>	61

4.3. Qualitative description of the microscopic mechanism for the positive MR in MOVPE-grown GaAs:Mn/MnAs hybrids.....	66
4.4. Unusual Hall effects in MOVPE-grown GaAs:Mn/MnAs hybrid	69
4.5. MR and Hall effects in MOVPE-grown GaInAs:Mn/MnAs hybrids	73
4.6. MR effects in GaAs:Mn/MnAs by post-growth annealing of MBE-grown $Ga_{1-x}Mn_xAs$ alloys	75
4.7. Summary.....	80
5. Studies of the geometry and hydrostatic pressure dependence of the MR effects and of local transport in GaAs:Mn/MnAs hybrids.....	83
5.1 Geometry dependence of MR effects in GaAs:Mn/MnAs hybrids	83
5.2. Hydrostatic pressure dependence of MR and Hall effects in GaAs:Mn/MnAs hybrids	88
5.3. Transport AFM measurements of GaAs:Mn/MnAs hybrids.....	94
6. Summary and Outlook.....	99
Acknowledgements.....	103
Curriculum Vitae	105

1. Introduction

1.1 Introduction to spintronics

Since 1994 the Defense Advanced Research Projects Agency (DARPA) started a new program called ‘spintronics’ (spin transport electronics), the idea to use the spin property of electrons in semiconductor electronic devices based on new operating principles has been considered as one of the promising trends for future electronics. In such devices the spin character of the carriers plays a crucial role in addition to or instead of the charge character, i.e., the carriers are in a defined orientation spin-state, either spin ‘up’ or spin ‘down’. These two spin states of carriers respond differently to an external (internal) magnetic, electric, or optical field, leading to the observation of spin-polarized current, polarized light emission or magnetic properties in semiconductors. One reason for a semiconductor-based spintronics is that semiconductors offer a tunability of the carrier concentration by orders of magnitude (ranging from almost insulating to metallic behavior) by controlled doping with donor or acceptor impurities. Furthermore, diamagnetic semiconductors can have very large spin-life times^[1-2] and the spin-carrying carriers in semiconductor can be manipulated in a controlled way by light, electric and magnetic fields. Therefore, the natural integration of spin-sensitive and normal semiconductor functionalities will lead to opportunities for integrating electronics, magnetics and photonics into a single technology with multifunctional capabilities. Furthermore, the study of the properties of electron spins in semiconductor is an important step into the quantum world, e.g. the possibility to realize quantum computers in the future.

One of the main topics in semiconductor-based spintronics is spin-dependent current transport (similar to metal-based magnetoelectronics), where the resistance of the device can be modified by changing the spin orientation of localized ions or free carriers and then altering the spin density of states. The change of the resistance caused by the magnetic force (e.g. magnetic fields) is called magnetoresistance (MR) defined as $\Delta\rho(H)/\rho_0 = (\rho(H)-\rho_0)/\rho_0$, where ρ_0 and $\rho(H)$ are the resistivity in zero-field and at an applied H field, respectively. For example, in 1988 Albert Fert^[3] in Paris and Peter Grünberg^[4] in Jülich respectively performed MR experiments with an electric current passing through ferromagnetic films separated by non-magnetic metallic spacer layers (as shown in the left of the Fig. 1.1). They found that the corresponding resistivity shows unexpectedly large changes when the relative alignment of the magnetizations of these two ferromagnetic films changes from parallel to antiparallel

alignment. This MR effect is usually referred to as the giant magneto-resistance (GMR) effect. It is not a material property, but a property of the artificially designed layer structure. The mechanism leading to such MR effects can be usually understood within Mott's two current model^[5] which assumes two independent current channels for spin-up and spin-down electrons, i.e., spin conservation for the electrons within the structure. In many materials where spin magnetism is present, one can examine the two spin directions separately, having spin-up and spin-down Bloch functions as eigenfunctions of the system. This leads to two different conductance coefficients g_{\downarrow} and g_{\uparrow} for the two spin directions, yielding a spin-dependent current. One can imagine that the corresponding resistances are connected in parallel. The aim of such artificial structures is to manipulate the current (or the resistance) by switching the magnetization in parts of the device. In this fashion one can, for example, create a magnetic switch, by a triple layer ferromagnetic-metal-ferromagnetic structure which has a low resistance when the two magnetizations are aligned in parallel, but high resistance when they are aligned antiparallel. The GMR effect is already being used widely in commercial devices, for example, in sensors embodied in read heads of hard disks in common PCs to obtain much higher read-out speed as well as higher storage densities.

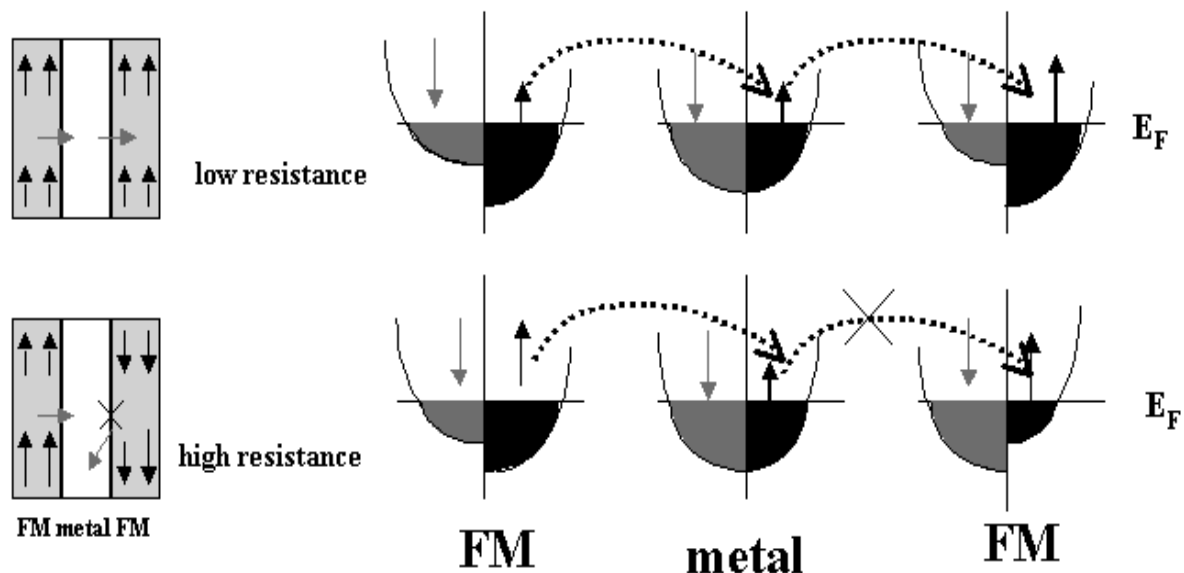


Fig. 1.1. Ferromagnetic double layer separated by a non-magnetic metal layer. When the magnetizations of the ferromagnetic layers have a parallel alignment, the resistance is low; when the ferromagnetic layers have an antiparallel alignment of magnetizations, the resistance is high.

Current efforts in designing and manufacturing spin-based devices involve two different approaches. The first, magnetoelectronics, is perfecting the existing GMR-based technology by either developing new materials with larger spin polarization of electrons or making improvements or variations in the existing devices that allow for better spin filtering. The second effort, spintronics, which is more radical, focuses on a new vista based on the great functionality, engineerability of semiconductor material in general and the development of new device ideas, e.g. for spin-opto-electronics which is not possible with metal technology.

In the traditional context of solid state physics, the term electronics comprises all effects in electric transport which depend on the charge of the electron only, without accounting for the randomly oriented spin of the electron. Magnetism, on the other hand, studies the interactions between electron spins yielding the magnetic moments in magnetic materials and giving rise to all kinds of magnetic properties of solids which are not related to current transport. These two disciplines, electronics and magnetism, contribute differently to traditional information technology, i.e., data processing by transistors and integrated circuits based on semiconductors on the one hand, and data storage on high density hard disk based on ferromagnetic materials on the other hand. Spintronics goes a step further and combines both disciplines. It makes use of collective phenomena, involving the mutual interaction of charge and spin degrees of freedom of the electron. A key issue in spintronics is combining ferromagnetism with semiconductors to develop magneto-optical and magneto-electronic devices (man-designed materials), which would be easy to be integrated with traditional semiconductor technology. Therefore, an important goal is to design and to build all semiconductor spintronic multi-functional devices, which will be compatible with existing chip technology. In addition, semiconductor spintronics may even offer more interesting possibilities for information processing since semiconductors have the ability to amplify both optical and electrical signals, which is not possible in metallic devices.

While there are clear advantages for introducing semiconductors in novel spintronic applications, many basic questions related to combining semiconductors with other magnetic materials to produce a viable spintronics technology remain open. To successfully incorporate spins into existing semiconductor technology, one has to resolve technical issues such as efficient injection, transport, control and manipulation, and detection of spin polarization as well as of spin-polarized currents. The major challenges addressed by experiment and theory include the optimisation of electron spin-lifetimes, the detection of spin coherence in nanoscale structures, transport of spin-polarized carriers across relevant length scales and heterointerfaces, and the manipulation of both electron and nuclear spins on sufficiently fast

time scales. For example, whether placing a semiconductor in contact with another material would impede spin transport across the interface is far from being well-understood. Therefore, the success of these ventures depends on a deeper understanding of fundamental spin interactions in solid-state materials as well as of the roles of dimensionality, defects, and semiconductor band structure in modifying these dynamics.

1.2. Magnetic semiconductors and dilute magnetic semiconductors

Tab. 1.1. The history of magnetic semiconductors and dilute magnetic semiconductors

<p>EuO; CdCr₂Se₄ $T_C < 100$ K</p>	<p>II(Mn)-VI DMS PM; AF; SG; T_C: a few Kelvins</p>	<p>III(Mn)-V DMS GaMnAs $T_C \sim 180$ K</p>	<p>GaN:Mn; GaP:Mn ZnO:Cr; ZnO:Mn $T_C > T_{\text{room}}$?</p>
1960s	1980s	1990s-present	future

The history of the research interest in magnetic semiconductors and dilute magnetic semiconductor (DMS) is shown in the Tab. 1.1. For the first time, the coexistence of ferromagnetism and semiconducting properties was explored in rare-earth chalcogenides^[6] (e.g. EuO) and semiconducting spinel structures (e.g. CdCr₂Se₄). In these magnetic semiconductors all magnetic atoms are periodically arranged in the crystal lattice. The magnetic exchange interaction between neighboring magnetic moments is mediated by the electrons in the bands yielding rather moderate ferromagnetic transition temperatures usually not exceeding 100 K, i.e. far below room temperature. Another kind of magnetic semiconductor are manganite oxides (LaMnO₃). These research activities have been particularly enhanced in recent years leading to compounds with high Curie temperatures even above 350 K. Only d electrons are involved in the ferromagnetism and the ferromagnetism originates from the spin coupling of d electrons between Mn³⁺ and Mn⁴⁺ by double exchange. However, as the crystal structure of the rare-earth chalcogenides and the manganites is quite different from that of technologically relevant semiconductors such as GaAs or Si, these materials are rather difficult to integrate into semiconductor heterostructures for spintronic applications.

Since the early 1980s, the interest has began to shift to a different class of dilute magnetic semiconductor in which the magnetic moments are chemically doped on random lattice sites

in a non-magnetic semiconductor. The first studies of DMS and their heterostructures have mainly focused on II-VI semiconductors, such as CdMnTe and ZnMnSe. However, as the magnetic interaction in the II-VI DMS is dominated by antiferromagnetic exchange between the transition metal moments, only paramagnetic, antiferromagnetic, spin-glass behavior, or ferromagnetism with a few Kelvins have been observed.^[7] However, these II(Mn)-VI DMS are relatively easy to be prepared in bulk form as well as thin epitaxial layers. The difficulty in creating high p- and n-type doping levels, which is essential for obtaining high Curie temperatures T_C , makes these systems less attractive for applications. Recently, the discovery of ferromagnetism in the III-V based DMS, i.e., (In,Mn)As and (Ga,Mn)As, has attracted much attention. It is already well established that the ferromagnetic transition observed in (Ga,Mn)As can be as high as 180 K and theory predicts even higher values for T_C . An alternative to a ferromagnetic alloy is a semiconductor-based hybrid structure, which has the two-fold advantages of being ferromagnetic at room temperature while keeping excellent compatibility with modern semiconductor technology. Besides these advantages and a high degree of crystalline perfection, large MR and magneto-optical effects have been observed in them. Until now, there are already a lot of spintronic devices based on the II(Mn)-VI and III(Mn)-V DMS and their hybrid structures. They have been successfully designed and tested at low temperatures. Some of current ideas are the spin-filter, spin diodes, spin-LED, spin-valve, magnetic bipolar transistor, magnetic tunneling transistor, spin laser, even spin-based solid-state quantum computing^[8] etc. Therefore, it can be anticipated that the combination of the spin and traditional semiconductor devices will yield new spintronic devices functioning at room temperature in the future.

1.3. Origin of the magnetism in II(Mn)-VI and III(Mn)-V DMS

In addition to find a successful way to synthesize DMS at room temperature, it is important to understand the physical origins of their magnetism, in order to optimise their application in spintronic devices. In the case of Eu compounds, the ferromagnetic s-f coupling and the presence of s-f hybridization compete with the antiferromagnetic cation-anion-cation interactions, leading to an overall ferromagnetic behaviour for EuS, but a complicated mediated magnetic behaviour for EuTe. For II(Mn)-VI and III(Mn)-V DMS, the magnetic properties of DMS are determined by the four important contributions: 1) The sp-d exchange interaction between the Mn ions and the band states. 2) The Mn-Mn or d-d exchange between the Mn ions. 3) Especially for III(Mn)-V DMS, the local electronic configuration of the Mn-

ion^[9], A^0 or A^- , i.e. $3d^5+\text{hole}$ or $3d^5$. 4) The concentrations of the magnetic ions and free carriers. The interplay of these contributions leads to various kinds of magnetic behaviour: antiferromagnetism, paramagnetism, spin glass, ferromagnetism. First of all, we have to understand the nature of the Mn center in the hosts. What is the electronic configuration of Mn in II-VI or III-V hosts? How does Mn interact with the band states?

1.3.1. The nature of Mn ions in DMS

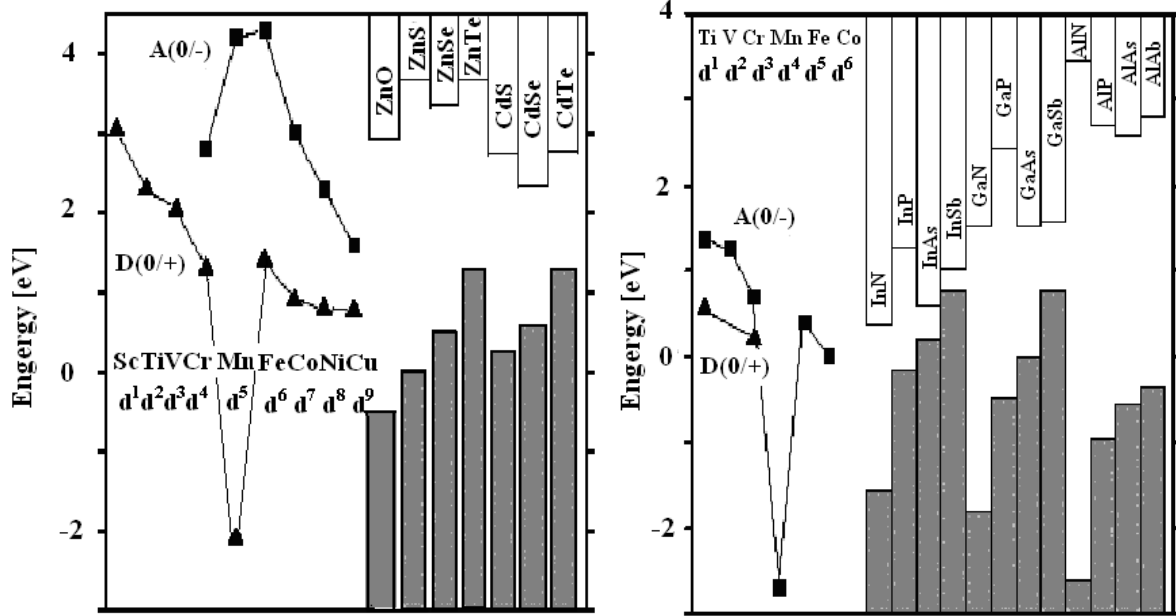


Fig. 1.2. Approximate position of transition metal levels relative to the conduction and valence band edges of II-VI (left panel) and III-V (right panel) compounds. By triangles the d^N/d^{N-1} donor and by squares the d^N/d^{N+1} acceptor states are denoted. ^[10]

As we know, a free Mn atom has the $3d^5 4s^2$ configuration, with the spins of the five 3d electrons aligned in the ground state according to Hund's rule. In this state the atom has a total spin quantum number $S=5/2$ and a total angular momentum $L=0$. When the Mn atom is placed substitutionally on a cation site of a II-VI host lattice, it is well established that Mn is divalent with high spin $3d^5$ configuration characterized by $S=5/2$ and $g=2.0$, i.e., the Mn ions neither introduce nor bind carriers as shown on the left panel of Fig. 1.2.^[10] However, the Mn ions contribute the localized d states and spin, which gives rise to the hybridization between anion p and Mn d states leading to the superexchange interaction. The presented two energy levels of Mn in II-VI compounds correspond to the majority (occupied) and minority (unoccupied) states of the 3d orbital. The location of the former level is about 3.5 eV below the top of the valence band, the location of the latter is less certain, but inverse photoemission

experiments indicate that it lies some 3.5 eV above the top of the valence band. In reality, these levels will be further split by the tetrahedral crystal field, and broadened into bands by hybridization with the p orbital.

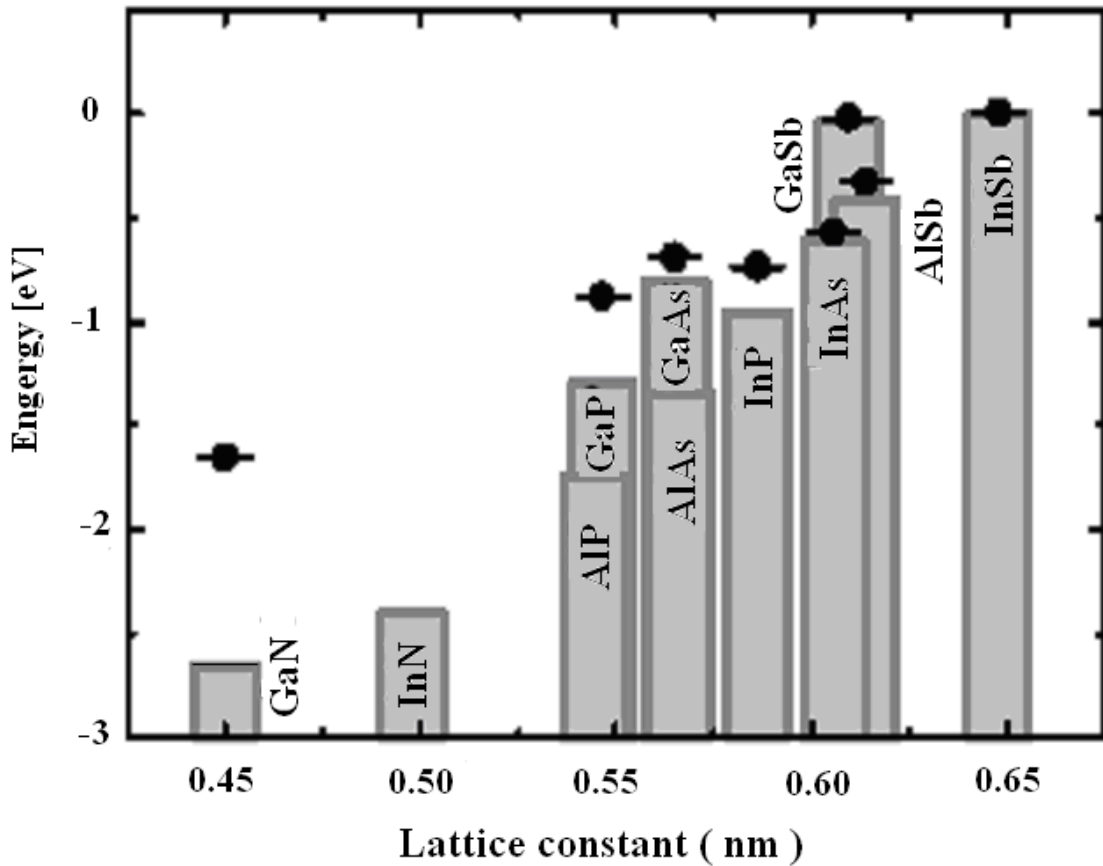


Fig. 1.3. Experimental energies of Mn acceptor levels in the gap of III-V compounds with respect to valence-band edges, whose relative positions are taken from [13].

The situation becomes much more complicated in III(Mn)-V semiconductors. Recent investigations show that there are essentially three types of Mn centers in III-V semiconductors. These are as follows: The first one is formed by manganese Mn^{3+} , which is in a d^4 configuration with ground state spin $S=2$, regarded as a neutral acceptor center $A(d^4)$. The second type of Mn center constitutes when the first type traps an electron and binds it tightly at the d-shell. Such a center can be regarded as a d^5 configuration with $S=5/2$, denoted as $A^-(d^5)$. This second Mn center is negatively charged and can attract and bind (weakly) a hole, forming a (d^5+h) complex, which is the third one as $A^0(d^5+h)$. The Mn ion acts as an effective mass acceptor $(d^5+h)^{[11]}$ in III-V antimonides and arsenides, which is confirmed by electron spin resonance (ESR) studies^[12], photoluminescence and x-ray magnetic circular dichroism (XMCD) in metallic or nearly metallic (Ga,Mn)As. The ESR is not only consistent

with such configuration and reveals the presence of two features in the density of states brought about by the Mn constituent: the original Mn $3d^5$ states located around 4.0 eV below the Fermi energy E_F as shown on the right panel of Fig. 1.2. The new states corresponds to acceptors merging with the valence band in the vicinity of E_F as shown in Fig. 1.3.^[13] This does not occur in II(Mn)-VI DMS where Mn is incorporated isoelectronically for the group II cation. Therefore, it is important to note that the Mn ions, which provide the localized spins, are electrically neutral in II-VI but act as effective mass acceptors in many III-V compounds. This leads to a more complicated magnetic and transport behavior in III-V than in II-VI DMS. Due to the Mn ion incorporation, the Hamiltonian including all the of spin-spin interaction in the II(Mn)-VI DMS and paramagnetic III(Mn)-V DMS can be written as follows:

$$\begin{aligned}
 H_{mag}(\vec{S}_j, \vec{S}_i) = & \underbrace{H_{Landau} + \sum_j g\mu_B \vec{B} \cdot \vec{s}_j}_{\text{normal Zeeman splitting}} - \underbrace{\sum_{i,j} J_{ij} \vec{S}_i \cdot \vec{s}_j}_{\text{s-d or p-d interaction}} - \underbrace{\sum_{i \neq j} J'_{ij} \vec{S}_i \cdot \vec{S}_j}_{\text{d-d interaction}} \\
 + & \underbrace{\sum_i g' \mu_B \vec{B} \cdot \vec{S}_i}_{\text{Mn-Spins in B-Field}}
 \end{aligned} \tag{1.1}$$

The first term is the normal Zeeman splitting and Landau quantization in the normal non-magnetic semiconductor, the second is the interaction between the Mn ions and the carriers in the conduction band or valence band, the third is the interaction between Mn ions, the fourth describes the spin alignment of the Mn ions in the magnetic field. In following we discuss the physical origins for each term in detail.

1.3.2. sp-d exchange interaction between Mn ions and band states

When magnetic Mn ions are incorporated into II-VI and III-V semiconductors, a strong interaction between the d-electrons of the magnetic ions and the s-like or the p-like states of the conduction band (CB) or valence band (VB) at $k = 0$ arises, which is called the sp-d exchange interaction. It originates from the spatially extended electronic wavefunction of carriers overlapping with a large number of the aligned local magnetic spin moments in the presence of an external magnetic field. The exchange interaction is expressed by a Heisenberg Hamiltonian

$$H_{ex} = \sum_{R_i} J_{sp-d} (r - R_i) \vec{S}_i \cdot \vec{\sigma}_i \quad (1.2)$$

where J_{sp-d} is the exchange coupling constant which is related to the exchange integrals $N_0\alpha$ and $N_0\beta$ as explained latter; \vec{s}_i and $\vec{\sigma}_i$ are the spin operators for the Mn^{2+} and the band electrons, respectively, R_i and r are their spatial coordinates.

In the following the relation between s,p-d exchange and GaAs-like band structure of (Ga,Mn)As is discussed. GaAs is a direct semiconductor with a band gap $E_g = 1.51$ eV at $T = 4$ K at the center of the Brillouin zone, the CB (s -like) is two-fold degenerate ($l=0$, these states are: $m_s = +1/2, -1/2$) while the VB (p -like) is six-fold degenerate ($l=1, m_l = -1, 0, 1; m_s = +1/2, -1/2$). The spin-orbit interaction couples the orbital angular momentum \vec{l} to the spin momentum \vec{S} by

$$H_{SO} = \lambda \vec{l} \cdot \vec{s} \quad (1.3)$$

where λ is the spin-orbit coupling constant. The spin-orbit interaction splits the eigenstates of the total angular momentum $j = 1/2$ from the $j = 3/2$ state in the valence band of the semiconductor. The splitting is known as the spin-orbit splitting Δ_0 of the valence band at the

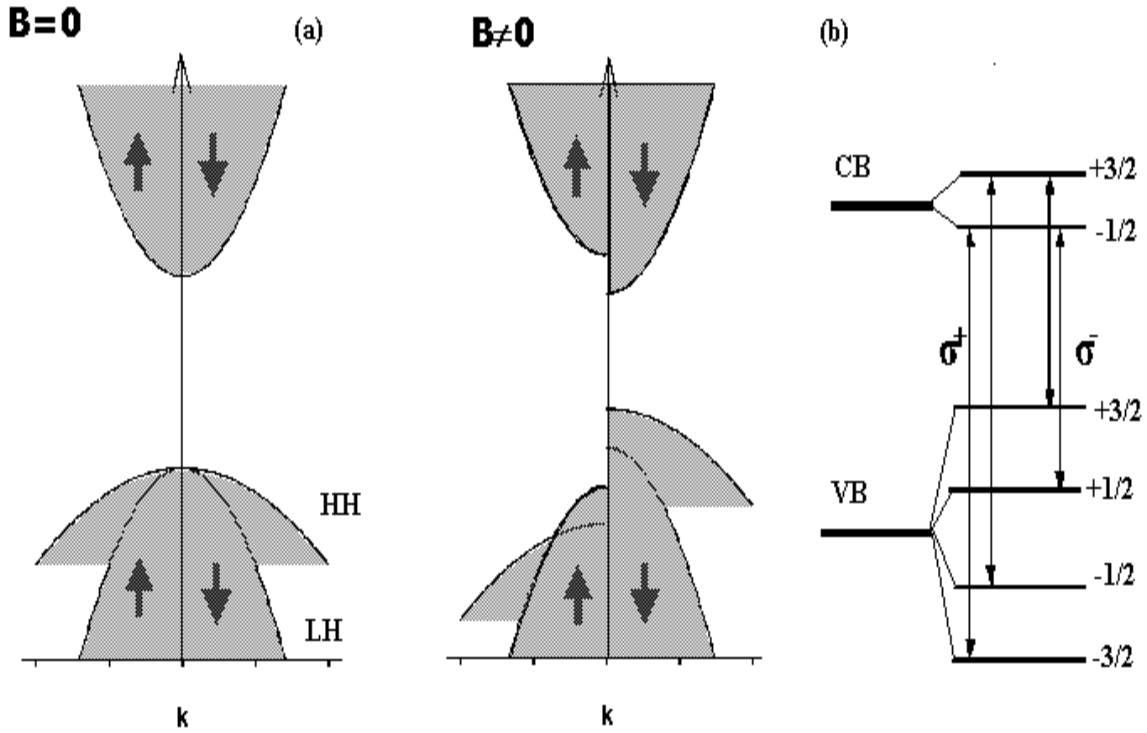


Fig. 1.4.(a) Zeeman splitting at the Γ -point in DMS. (b) Optical selection rules in DMS.

Γ -point, which is typically hundreds of meV (350 meV in GaAs) and causes the eigenstates with the total angular momentum $j=1/2$ to be negligible when dealing with processes taking place in the vicinity of the band gap. The $j=3/2$ states form the VB maximum. In zincblende material one distinguishes between light hole and heavy hole states with pseudo-spins $j_z = \pm 3/2$ and $j_z = \pm 1/2$, respectively.

Fig. 1.4 schematically shows the effect of the giant Zeeman splitting on the states at the Γ -point at the band gap. The effect of the giant Zeeman splitting of the four hole states at the VB edge and the two electron states at the CB edge dominates the transport properties and interband transitions between these states dominate optical measurements in magnetic fields. As an example, Fig. 1.4.(b) illustrates magnetic circular dichroism (MCD) to detect the difference in the absorption or emission of right σ^+ and left σ^- circularly polarized light according to the optical selection rule $\Delta m_j = \pm 1$. Due to the giant Zeeman splitting under an applied magnetic field, the spin substates of the electrons (holes) in the CB (VB) split as follows

$$E(s_z) = E_g \pm \left(g_e^* \mu_B H - N_0 \alpha x \langle S_z \rangle \cdot s_z \right) \quad \left(s_z = \pm \frac{1}{2} \right) \quad (1.4)$$

$$E(j_z) = E_g \pm \left(g_h^* \mu_B H - \frac{1}{3} N_0 \beta x \langle S_z \rangle \cdot j_z \right) \quad \left(j_z = \pm \frac{1}{2}, \frac{3}{2} \right) \quad (1.5)$$

where N_0 is the number of cation sites, α and β are the exchange integrals of the s-like carriers in the CB, and p-like carriers in the VB, respectively. The sign of $N_0\alpha$ and $N_0\beta$ determines the type of magnetic interaction, i.e., positive $N_0\alpha$ (or $N_0\beta$) indicates ferromagnetic interaction and negative $N_0\alpha$ (or $N_0\beta$) indicates antiferromagnetic alignment between the spin of the Mn ion and the spin of the carriers. From this equation it can be found that the magnitude of the CB and VB splitting is determined by the sp-d exchange coupling constants $N_0\alpha$ and $N_0\beta$, the effective Mn concentration x , and $\langle S_z \rangle$, which is the average spin per Mn site given by a modified Brillouin function:

$$\langle S_z \rangle = -S \cdot B_s \left[g_{Mn} \mu_B S H / (k_B T) \right] \quad (1.6)$$

where $S = 5/2$ for Mn^{2+} ion, H is the applied magnetic field, g_{Mn} is the g-factor of Mn ion, B_S is the standard Brillouin function for $S = 5/2$.

On the other hand, for a nonmagnetic semiconductor in the presence of an external magnetic field, the conduction and valence bands are split into Landau levels, each Landau level being further split into sublevels corresponding to the two spin orientations of the electron. That is the normal Zeeman splitting in the nonmagnetic semiconductors. In principle it can be used to create spin polarized carriers, however, the normal Zeeman splitting is usually too small compared to kT , so that it has no significant spin-polarizing effect on the band structure and on the carrier transport. With the Mn incorporated, the two sublevels of the two spin orientations of the electrons split strongly in a magnetic field due to the exchange interaction between the Mn ions and the carriers. Thus the giant Zeeman splitting leads to a large difference in the density of states of spin-up and spin-down electrons near the Fermi level. This modification can be described by an effective g factor of the carriers accounting for the sp-d exchange interaction between the Mn ions and the band states.

In a common non magnetic semiconductor the g-factor of the electrons and holes usually differs from that of the free electron of 2.0023. In wide-gap materials such as GaAs it is very small, e.g. for electrons $g_e = -0.41$. The theory of the electronic g-factor in semiconductors is rather complicated. It is strongly determined by the band structure of the semiconductor. Approximations based on $k.p$ models do not always yield satisfactory results.^[14] However, as a rule of thumb, the g-factor of the CB in zincblende crystals approaches, that of the free electron with increasing band gap. For example, the g-factor of the free electron in vacuum yields a Zeeman splitting of only a few meV at moderate fields. In magnetic semiconductors, the strong spin-orbit interaction may yield band splittings as big as hundreds of meV, which correspond to effective g-factors of the order of 100-200 yielding highly spin polarized-carriers at moderate fields.

1.3.3. Exchange integrals $N_0\alpha$ and $N_0\beta$ in II(Mn)-VI and III(Mn)-V DMS

According to the equation (1.2), (1.4) and (1.5), the exchange integrals $N_0\alpha$ and $N_0\beta$ are directly proportional to the coupling constants J_{s-d} and J_{p-d} , respectively as defined in (1.2). J_{s-d} and J_{p-d} describe the coupling between the electron spins in the conduction band and the Mn spins and the coupling between the hole spins in the valence band and the Mn spins, respectively. Therefore,

$$\alpha = \langle S | J_{s-d} | S \rangle; \beta = \langle X | J_{p-d} | X \rangle \quad (1.7)$$

where $|S\rangle$, $|X\rangle$ are the Bloch wave functions. There are two processes contributing to the sp-d exchange interaction: 1) the direct exchange interaction between the band states and d electrons. This process tends to align the spin of the electron parallel to that associated with the Mn^{2+} ion, and because of this may be referred to as ferromagnetic interaction leading to a positive contribution to the exchange integrals $N_0\alpha$ and $N_0\beta$. 2) the hybridization of $3d^5$ levels with the s and p band electrons. At the Γ point, the s - d hybridization is forbidden by symmetry. This contribution to $N_0\alpha$ is virtually zero. Therefore the exchange integral $N_0\alpha$ related with the CB is always positive and arises from the direct exchange. The sign of $N_0\alpha$ is the same in all II(Mn)-VI and III(Mn)-V DMS, i.e. $N_0\alpha > 0$, but about an order of magnitude smaller in the latter. On the other hand, the p-d hybridization is always allowed. So that the exchange integral $N_0\beta$ related with VB contains direct exchange and hybridization contribution. The latter of the two being larger. The value of $N_0\beta$ is thus dominated by hybridization, which depends strongly on the local electronic configuration of the Mn ion nature in DMS as discussed in 1.3.1.

In II(Mn)-VI DMS where Mn is incorporated as $3d^5$, (isoelectronically with the replaced group II cation), the AFM type coupling leads to a negative contribution to $N_0\beta$, i.e. $N_0\beta < 0$. It has been confirmed that $N_0\alpha \approx 0.2\text{eV}$ and $N_0\beta \approx -1.0\text{eV}$ for most II(Mn)-VI DMS measured by optical experiments^[15] and calculated from theory.^[16]

In III-V DMS, it is important to note that the Mn ions can be A^0 or A^- , i.e. $3d^5$ +hole (effective mass acceptors besides providing a local spins) or $3d^5$.^[9] The p-d exchange depends on the type of center, i.e., whether Mn forms an A^0 or A^- center. In the latter case, the electron can jump through the same exchange channels as they do for the Mn^{2+} in II-VI DMS, so antiferromagnetic exchange is expected, i.e. $N_0\beta < 0$. In turn for an A^0 , the weakly bound hole provides an additional exchange path. The hole is spin-polarized and can accommodate only VB electrons with the spin parallel to the total spin of d-shell, i.e. $N_0\beta > 0$. The p-d exchange integral $N_0\beta$ for the Mn centers results from the competition of ferromagnetic and antiferromagnetic channels. This complicated hybridization of Mn centers and hole spins, leads to different interaction contributing to the sign and magnitude of the average $N_0\beta$. On the other hand, the crystal field due to especially the position of the nearest-neighbor anions also strongly affects $N_0\beta$. Therefore, the key parameter $N_0\beta$ determined by the nature of Mn center and its environments, results in wide spread of experimentally observed average $N_0\beta$ parameters. This, for example, was shown experimentally for GaAs:Mn and GaAs:Mn,Te alloys as follows.^[17]

Te is doped into p-type GaAs:Mn with small Mn concentration, leading to a control of the carrier concentration and Mn concentration independently. With increasing Te concentrations, it induces the transition of the majority carrier type from p (the samples A to C) to n (the samples D and E) as shown in the left of Fig. 1.5. In the right graph of Fig. 1.5, MCD spectra taken in transmission geometry for the series of paramagnetic GaAs:Mn alloys with and without Te co-doping layers are depicted. All spectra (except for sample D) were recorded at a magnetic field of 1 Tesla. A positive (negative) MCD signal corresponds to dominant σ^- (σ^+) absorption in the layer.

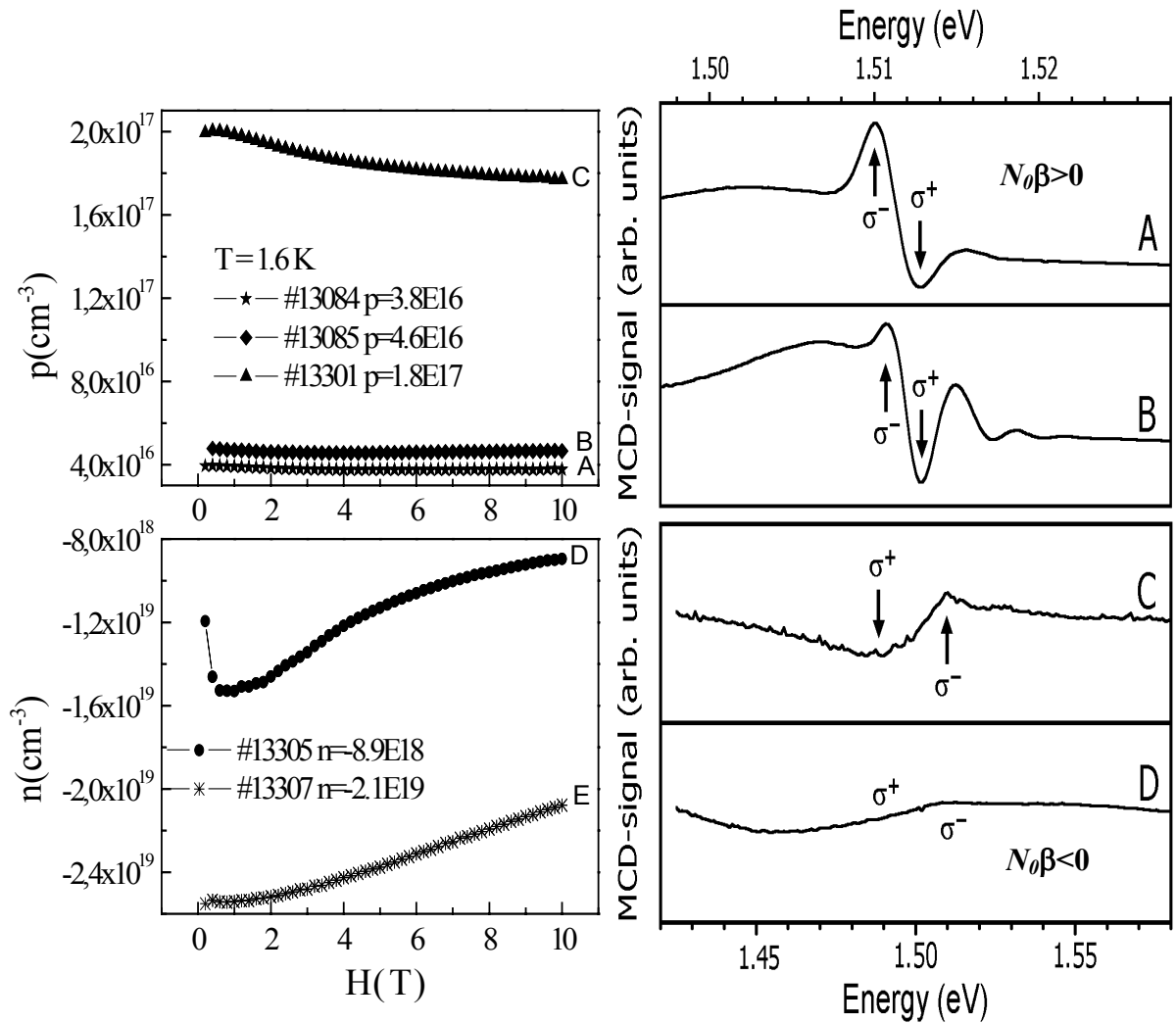


Fig. 1.5. (left) Hall-measurements of paramagnetic GaAs:Mn and GaAs:Mn,Te alloys at $T=1.6$ K. (right) MCD spectra at $T=1.8$ K and $B=1$ T for the samples A to C and $B=3$ T for sample D. A sign reversal of the valence band exchange integral $N_0\beta$ occurs.

As discussed above the p - d exchange integral $N_0\beta$ is much bigger than $N_0\alpha$, therefore, the Zeeman splitting energetic difference of the heavy-hole excitons in the Faraday geometry between σ^+ and σ^- is mainly determined by $N_0\beta$. i.e.,

$$\Delta E_{HH} = E_{HH}(\sigma^+) - E_{HH}(\sigma^-) \propto N_0(\beta - \alpha) \approx N_0\beta \quad (1.8)$$

As shown in the right figure of the Fig. 1.5, in the case of the p-type GaAs:Mn samples A and B without Te, the energy of the σ^+ transition is higher than that of the σ^- transition, $\Delta E_{HH} > 0$, i.e. $N_0\beta > 0$. Thus, the corresponding VB exchange integral $N_0\beta$ is positive, i.e., FM coupling. In case of the GaAs:Mn,Te samples C and D, the σ^+ transitions are red-shifted compared to the σ^- transition. $\Delta E_{HH} < 0$, indicates $N_0\beta < 0$, i.e., AFM coupling.

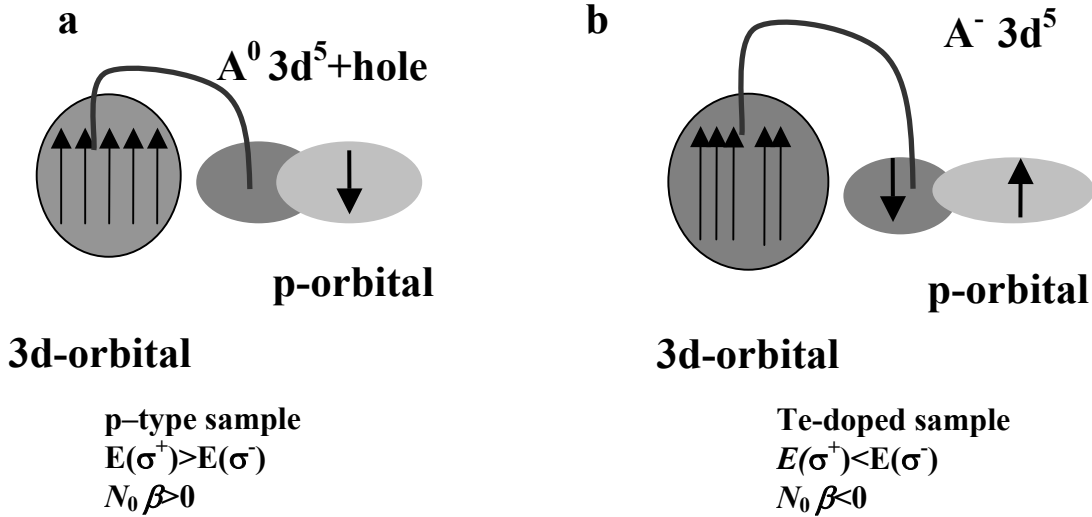


Fig. 1.6. Model of the electron-configuration in the 3d Mn-shell. (a) d^5+h complex in the case of p-type GaAs:Mn $\rightarrow N_0\beta$ is positive. (b) d^5 complex in the case of (II,Mn)VI or n-type GaAs:Mn,Te $\rightarrow N_0\beta$ is negative.

Schneider et al.^[12] demonstrated that Mn acts as $A^-(3d^5)$ center and $A^0(3d^5+h)$ can be distinguished in ESR due to their different g factor. The spin-flip Raman spectra and EPR experimental results^[17] showed the Mn in the samples A and B act as $A^0(3d^5+h)$ center, in contrast to C with A^- and A^0 centers, D with A^- center. Therefore, the FM-type coupling of samples A and B can be attributed to the dominant role of the FM channel provided by Mn acting as $A^0(3d^5+h)$ centers, as schematically depicted in Fig. 1.6.a. In case of the

GaAs:Mn,Te samples C and D, due to Te co-doping the VB is filled with electrons consequently leads to Mn acting as A^- centers and an AFM type coupling as depicted in Fig. 1.6.b. Thus, the sign and magnitude of exchange integral $N_0\beta$ indicating FM or AFM coupling can be tuned by the local electronic structure of the Mn ion. On the other hand, it can be found in the some parts of the following chapters, that $N_0\beta$ is also tuned by different growth procedures, i.e. MOVPE-grown and MBE-grown GaMnAs-based alloys and GaAs:Mn/MnAs hybrids, which strongly affects the spin-dependent transport in these studied materials.

1.3.4. Antiferromagnetic superexchange interaction between the Mn ions in II-Mn-VI DMS

The Mn-Mn or d-d exchange interaction is described by the spin-5/2 Heisenberg Hamiltonian

$$H = -\sum_{i \neq j} J^{dd}(R_{ij}) S_i \cdot S_j \quad (1.9)$$

where $J^{dd}(R_{ij})$ is the antiferromagnetic coupling between the local Mn moments S_i and S_j separated by $R_{ij} = |R_i - R_j|$ and depends strongly on R_{ij} . The overwhelming contribution is from the two-hole processes of the Anderson superexchange mechanism, which can be viewed as an indirect exchange interaction mediated by the anion^[18].

1.3.5. Origin of the ferromagnetism in III-V DMS

The ferromagnetism in III(Mn)-V DMS is mediated by carriers. In 1998, F. Matsukura et al^[19] explained a model to calculate Curie temperatures in semiconductors based on the Ruderman-Kittel-Kasuya-Yosida (RKKY) interaction. They demonstrated that the ferromagnetism of (Ga,Mn)As has its origin in the RKKY interaction mediated by holes. The RKKY exchange Hamiltonian between the Mn spins at site i and site j is expressed by

$$H = -J_{ij} \vec{S}_i \cdot \vec{S}_j \quad (1.10)$$

where J_{ij} is given by

$$J_{ij} = -\frac{2mk_F^4}{\pi h^2} J_{pd}^2 F(2k_F r_{ij}) \exp\left(-\frac{r_{ij}}{l}\right) \quad (1.11)$$

Here, S_i and S_j are the Mn spin at site i and site j ; k_F is Fermi wave vector of the hole gas, h is the Planck constant, J_{pd} is the p-d exchange interaction described above, r_{ij} is the distance between i and j , and $F(2k_F r_{ij})$ is an oscillating function, and l is the mean free path of carriers. The Curie temperature T_C is in approximation given by

$$T_C = \frac{1}{3} x S(S+1) \sum_r z_r J_{ij}(r) \quad (1.12)$$

where x is the effective Mn ions concentration, z_r is the number of r th nearest group-III sites and $S = 5/2$ is the Mn spin.

On the other hand, H. Akai^[20] reported the results of Korringa-Kohn-Rostoker coherent-potential and local density approximation (KKR-CPA-LDA) calculations of the electronic structure of doped (In,Mn)As alloys. He proposed a mechanism for the carrier-induced ferromagnetism based on these calculation. He pointed out that Zener's double exchange mechanism can describe the ferromagnetism in (In,Mn)As. In a band structure picture, double exchange essentially means the following: Near half filling, with the exchange splitting bigger than the bandwidth, the band energy of the ferromagnetic state is lower than that of the antiferromagnetic state when a sufficient number of carriers exists. In the case of (In,Mn)As, the exchange splitting is much bigger than the width of the VB, and a considerable number of holes is present. Therefore, the conditions mentioned for double exchange interaction are fulfilled. It is suggested that the ferromagnetic state occurs as a result of a competition between the double-exchange and superexchange.

In 2001, T. Dietl^[21] et al presented a mean-field model of ferromagnetism mediated by delocalized or weakly localized holes in zincblende and wurzite dilute magnetic semiconductor. They modified a Zener model to adopt the two-fluid model of electronic states near the metal-insulator transition (MIT). The central suggestion of this model is that the holes in extended or weakly localized states mediate the long-range interactions between the localized spins on both side of the MIT in the III-V and II-VI magnetic semiconductors. According to this model, the conversion of itinerant electrons into singly occupied impurity states with increasing disorder occurs gradually. This leads to a disorder-driven static phase separation into two types of regions, one populated by electrons in extended states, and another that is totally depleted of carriers or contains singly occupied impurity-like states. If there is an exchange coupling between the two fluids, the latter region controls the magnetic response of the doped magnetic semiconductor and gives rise to the presence of bound

magnetic polarons (BMP's) on both sides of the MIT in magnetic semiconductors. Furthermore, the coupling between the BMP's appears to be ferromagnetic in the Zener p-d exchange interaction model. The ferromagnetic transition Curie temperature is given by

$$T_C = x_{eff} N_0 S(S+1) \beta^2 A_F \rho_S(T_C) / 12k_B \quad (1.13)$$

where $x_{eff} N_0$ is the effective Mn spin concentration, β is the p-d exchange integral, ρ_S is the spin density of states related to the carrier magnetic susceptibility. Fig. 1.7. depicts the results calculated on the basis of this model, where the cation sublattice contains 5% of Mn^{2+} ions and 3.5×10^{20} holes per cm^3 . The calculated results provide valuable chemical trends for ferromagnetic transition temperatures in magnetic semiconductor compounds.

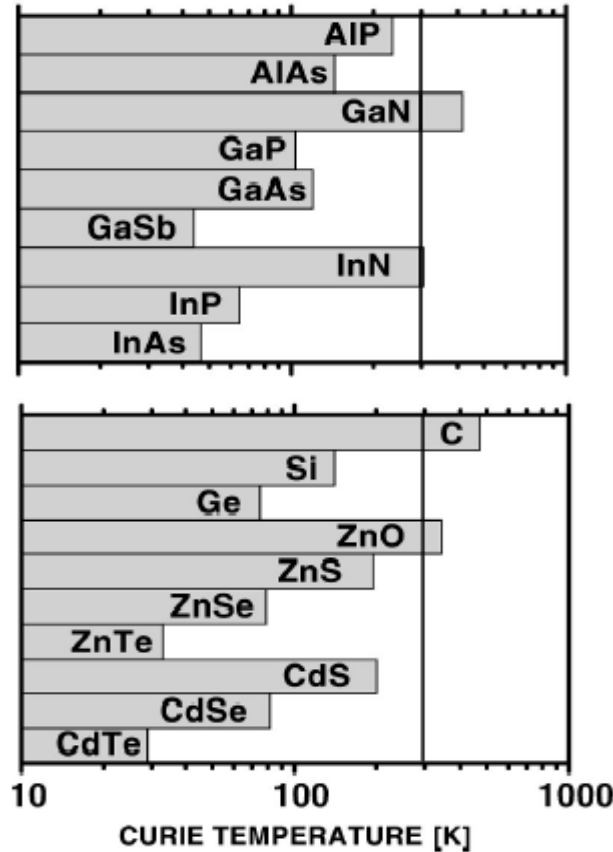


Fig. 1.7. Curie temperatures for various III-V (top panel) as well as for group IV and II-VI (lower panel) semiconductor compounds as calculated by T.Dietl.^[21]

P. Marvopoulos^[22] compared the two models of H. Akai and of T. Dietl, and concluded that the type of model applicable for describing the ferromagnetism in a DMS depends sensitively

on the position of Mn d-states in this compound. The double exchange interaction dominates when impurity bands in the gap are formed and the Curie temperature T_C increases proportional to the root of x , where x is the Mn concentration. A typical example for such a compound is (Ga,Mn)N. The host VB is lower in energy than the Mn d-states and a clear impurity band appear in the band gap. The p-d exchange mechanism dominates when the d-states of the impurity are nearly localized, as it is the case for (Ga,Mn)Sb, and a linear x -dependence of T_C is obtained. Thus, despite the fact that the origin of the ferromagnetism in DMS is still a controversial issue, many valuable studies already have been made in this field, and continuous progress is made.

In summary, the sp-d exchange interaction and the Mn-Mn exchange interaction lead to the paramagnetic, spin-glass and antiferromagnetic behaviors observed in traditional II(Mn)-VI DMS. In the case of III(Mn)-V DMS, an additional degree of freedom comes into play, the free carrier concentration. Due to the RKKY or Zener type exchange interaction between the Mn ions mediated by the free carriers, a ferromagnetic phase can be obtained.

1.4. Magneto-transport in DMS

1.4.1. MR effect in II(Mn)-VI DMS

Unusual negative and positive MR effects have been found in both of n and p type II(Mn)-VI DMS at low temperatures. They are related to the field-induced band splitting, due to the strong sp-d exchange between Mn ions and free carriers. For example, a strong negative MR has been observed in p-Hg_{1-x}Mn_xTe and n-Cd_{1-x}Mn_xSe, and a positive MR has been found in n-Cd_{1-x}Mn_xSe. The discussed mechanisms for the observed MR phenomena include:

- 1) The redistribution of carriers between spin-subbands of the conduction or valence band due to a tuning of the density of states by the sp-d exchange interaction.^[23]
- 2) The field-induced destruction of the magnetic polarons formed in zero-field.^[23]
- 3) Magnetic field induced insulator-metal transition.^[23]
- 4) Quantum corrections to the conductivity which arise from the destructive effect of the giant spin-splitting on the Hartree corrections^[24].
- 5) The increase of the Thomas-Fermi screening radius induced by the formation of spin clusters near Mn impurities, leading to a shift of the mobility edge^[25].

In summary, these complicated effects can be simply summarized as sp-d exchange interaction and disorder effects on the band structure and effects due to electron-electron interactions. Their interplay can lead to a competition of negative and positive contributions

to the MR effect in the II(Mn)-VI DMS discussed in detail in chapter 3. It seems that the strong negative MR dominates in the strongly localized regime. A pronounced competition of the two MR contributions takes place in the vicinity of the metal-insulator transition.

1.4.2. MR effects in III(Mn)-V DMS

In the ferromagnetic III(Mn)-V DMS, due to the cooperative interaction between the carriers and the fluctuation of the magnetization below the Curie temperature, the transport properties are even more complex than those in the II(Mn)-VI DMS. The behavior can also change from insulator to metal with increasing Mn concentration. At higher Mn-contents $x \approx 8\%$, a large fraction of the Mn is usually incorporated as interstitials which act as donors leading to a high degree of compensation. This is manifested by the occurrence of a reentrance into an insulating phase. Below the Curie temperature, a large negative MR effect accompanied by an anomalous Hall effect as shown in Fig. 1.8 is observed. In addition, a very large negative MR with a large anisotropy has been observed in ‘reentrant’ insulating sample at high x .

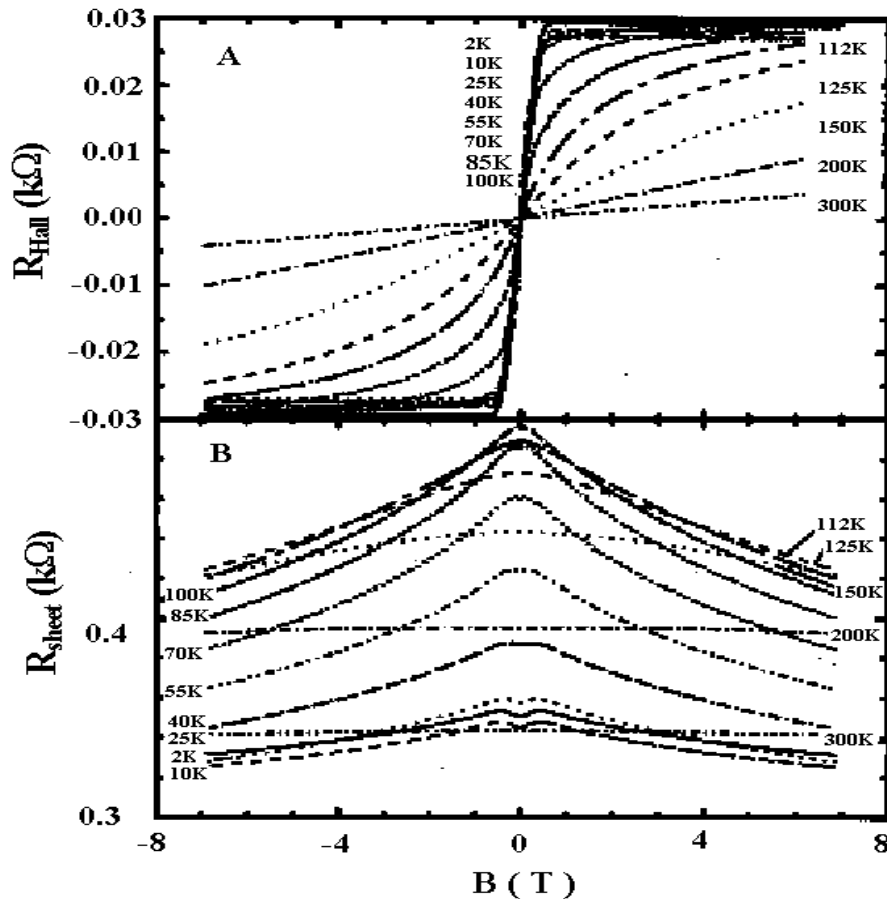


Fig. 1.8. (A) Magnetic field dependence of the Hall resistivity and (B) the sheet resistivity of GaMnAs with 5.3%Mn at various temperatures.

Below the Curie temperature, correlation effects should significantly contribute to the magnetic and transport properties. A lot of studies suggest that the negative MR mechanism in the ferromagnetic III(Mn)-V DMS is attributed to the destruction of bound magnetic polarons whose signatures have also been observed in magnetization measurements^[26,27]. On the other hand, an increasing Fermi energy in a spin split band reduces the localization length by reducing the energy difference between the mobility edge (the energy level separating the localized from the extended states) and the Fermi level, i.e., the relative position of the Fermi level towards the mobility edge changes and a decrease of the spin-disorder scattering due to the alignments of the magnetization^[28] occurs. This was also suggested for the explanation of the negative MR.

As to magnetic polarons, at least three kinds of magnetic polarons can be distinguished (i) bound magnetic polaron (BMP), i.e., electrons localized by a defect or impurity potential, the sp-d interaction supplying an additional binding energy. (ii) self-trapped magnetic polaron, i.e., electron localized in a region (fluctuation) of high Mn content, the sp-d coupling constituting the main binding force; (iii) free magnetic polaron, i.e., delocalized electron surrounded in its way through the crystal by a ferromagnetically aligned cloud of d-spins. However, such a self-trapped magnetic polaron requires a rather large sp-d coupling constant and effective mass to be thermally stable. Hence, such a complex can probably exist only in the form of the trapped heavy hole, particularly in systems of reduced dimensionality such as quantum wells or quantum dots. Bound magnetic polarons are likely to be formed in ferromagnetic DMS, with a high degree of compensation where only some of the Mn-ions act as acceptor. A. C. Durst et al, suggested that the bound magnetic polaron is formed by the exchange interaction between localized carriers and magnetic ions. Furthermore, they found a fit to the polaron part of susceptibility data in a Curie-Weiss form revealing a net ferromagnetic interaction between the polarons.^[29,30] Below the Curie temperature, the ferromagnetic interaction between the polarons dominates the direct antiferromagnetic interaction. On the other hand, the magnetic field contributes to the activation energy from the localized BMP state to the delocalised states above mobility edge, which can lead to the negative MR observed in ferromagnetic DMS.

1.4.3. MR in ferromagnet(FM)/semiconductor hybrids

Contemporary interest in the hybrid ferromagnet/semiconductor heterostructures is driven by their relevance to ‘spintronic’ semiconductor applications that rely on spin injection from a ferromagnet (or paramagnet) into a semiconductor, or the ferromagnet affecting the spin

orientation of the carriers in the semiconductor directly to produce spin-dependent transport. A granular ferromagnet/semiconductor hybrid consists of ferromagnetic clusters embedded in a semiconducting matrix. The ferromagnet can be a metal, half-metal, or semimetal, superconductor, or semiconductor. The semiconductor can be nonmagnetic, paramagnetic, ferromagnetic, or even antiferromagnetic. These various degree of freedom induce a very complicated situation in the hybrids because the spin-transport not only depends on the individual properties of the ferromagnet and semiconductor, but also on the interface and interaction between them. This leads to all kinds of advantages or disadvantages in the context of spin-dependent transport which have not been entirely assessed and understood until now. For examples, the negative tunneling magnetoresistance (TMR) and GMR effect in the ferromagnetic metal (Fe, Co, MnAs)/semiconductor hybrid can be explained by tunneling through a Schottky barrier at the interface,^[31] or magnetic-field induced suppression of the spin-dependent interface scattering.^[32] On the other hand, the positive extraordinary magnetoresistance (EMR) observed in nonmagnetic metal/semiconductor hybrid can be explained by the magnetic-field induced current redistribution between the two materials.^[33] In the chapters 4 and 5, we focus on the GaMnAs/MnAs paramagnetic-ferromagnetic hybrids, magneto-transport, Hall measurements, atomic force microscopy (AFM), transmission electron microscopy (TEM) and ferromagnetic resonance (FMR) measurements, and the magneto-transport under high hydrostatic pressure were used to characterize the influence of the different of magnetic interactions on the transport behaviour of this hybrid. The local inhomogeneous magnetic field and the spin-dependent (independent) barriers caused by the ferromagnetic MnAs clusters lead to an unusual large negative and positive MR effects. To understand these magnetic interaction effects and transport phenomena in the studied GaAs:Mn/MnAs paramagnetic-ferromagnetic hybrids is very useful for fabricating hybrid structures acting as spin filter and related spintronic devices based on DMS in the future.

References:

- [1] J. M. Kikkawa, I. P. Smorchkova, N. Samarth, and D. D. Awschalom, *Science*. **277**, 1284 (1997).
- [2] J. M. Kikkawa and D. D. Awschalom, *Phys. Rev. Lett.* **80**, 4313 (1998).
- [3] M. N. Baibich, J. M. Broto, A. Fert, F. N. Van Dau, and F. Petroff, P. Eitenne, G. Creuzet, A. Friederich, and J. Chazelas, *Phys. Rev. Lett.* **61**, 2472 (1988).
- [4] G. Binash, P. Grünberg, F. Saurenbach, and W. Zinn, *Phys. Rev. B*. **39**, 4828 (1989).
- [5] N. H. Mott, *Proc. Roy. Soc. A*. **153**, 699 (1936).
- [6] T. Kasuya, A. Yanase, *Rev. Mod. Phys.* **40**, 684 (1968).
- [7] A. Haury, A. Wasiela, A. Arnoult, J. Cibert, S. Tatarenko, T. Dietl, and Y. Merle d'Aubigné, *Phys. Rev. Lett.* **79**, 511 (1997).
- [8] D. Loss and D. P. DiVincenzo, *Phys. Rev. A*. **57**, 120 (1998).
- [9] A. Twardowski, *Mater. Sci. and Eng. B*. **63**, 96 (1999).
- [10] J. Binowski, P. Kacman, and T. Dietl, *Mat. Res. Soc. Symp. Proc. Vol.* **690**, F6.9 (2002).
- [11] M. Linnarsson, E. Janzen, B. Monemar, M. Kleverman, and A. Thilderkvist, *Phys. Rev. B*. **55**, 6939 (1997).
- [12] J. Schneider, U. Kaufmann, W. Wilkening, M. Baeumler, and F. Köhl, *Phys. Rev. Lett.* **59**, 240 (1987).
- [13] I. Vurgaftman, J.R. Meyer and L. R. Ram-Mohan, *J. Appl. Phys.* **89**, 5815 (2001).
- [14] M. Oestreich and W. W. Rühle, *Phys. Rev. Lett.* **74**, 2315 (1995).
- [15] R. L. Aggarwal, S. N. Jasperson, P. Becla, and R. R. Galazka, *Phys. Rev. B*. **32**, 5132 (1985).
- [16] B. E. Larson, K. C. Hass, H. Ehrenreich, and A. E. Carlsson, *Phys. Rev. B*. **37**, 4137 (1988).
- [17] Th. Hartmann, S. Ye, P.J. Klar, W. Heimbrod, M. Lampalzer, W. Stolz, T. Kurz, A. Loidl, H.-A. Krug von Nidda, D. Wolverson, J. J. Davies, and H. Overhof, *Phys. Rev. B*. **70**, 233201 (2004).
- [18] A. Lewicki, J. Spalek, J. K. Furdyna, and R. R. Galazka, *Phys. Rev. B*. **37**, 1860 (1988).
- [19] F. Matsukura, H. Ohno, A. Shen and Y. Sugawara, *Phys. Rev. B*. **57**, R2037 (1998).
- [20] H. Akai, *Phys. Rev. Lett.* **81**, 3002 (1998).
- [21] T. Dietl, H. Ohno and F. Masukura, *Phys. Rev. B*. **63**, 195205 (2001).
- [22] P. Mavropoulos, K. Sato, and S. Blügel, 34th IFF Spring school 2003, *Fundamentals of Nanoelectronics*. **A4** (Schriften des Forschungszentrums Jülich, Jülich 2003).

- [23] J. K. Furdyna, *J. Appl. Phys.* **64**, R29 (1988).
- [24] M. Sawicki, T. Dietl, J. Kossut, J. Igalson, T. Wojtowicz, and W. Plesiewicz, *Phys. Rev. Lett.* **56**, 508 (1986).
- [25] Y. Shapira, N. F. Oliveira, Jr., D. H. Ridgley, R. Kershaw, K. Dwight, and A. Wold, *Phys. Rev. B.* **34**, 4187 (1986).
- [26] H. Ohno, H. Munekata, T. Penney, S von Molnar, and L. L. Chang, *Phys. Rev. Lett.* **68**, 2664 (1992).
- [27] Adam C. Durst, R. N. Bhatt, and P.A. Wolff, *Phys. Rev. B.* **65**, 235205 (2002).
- [28] A. Van, Esch, L. Van Bockstal, J. De Boeck, G. Verbanck, A.S. Van Steenbergen, P. J. Wellmam, B. Grietens, R. Bogaerts and F. Herlach, G. Borghs, *Phys. Rev. B.* **56**, 13103 (1997).
- [29] Adam C. Durst, R. N. Bhatt, and P. A. Wolff, *Phys. Rev. B.* **65**, 235205 (2002).
- [30] R. N. Bhatt and P. A. Lee, *phys. Rev. Lett.* **48**, 344 (1982).
- [31] J.A.C. Bland, A. Hirohata, Y. B. Xu, C. M. Guertler and S. N. Holmes, *IEEE Trans. Mag.* **30**, 2827 (2000).
- [32] H. Akinaga, J. De Boeck, G. Borghs, S. Miyanishi, A. Asamitsu, W. Van Roy, Y. Tomioka, and L. H. Kuo, *Appl. Phys. Lett.* **25**, 3368 (1998).
- [33] M. Holz, O. Kronenwerth and D. Grundler, *Appl. Phys. Lett.* **86**, 072513 (2005).

2. Preparation and structural properties of the studied GaMnAs-based alloys and hybrids

2.1 MOVPE and MBE growth

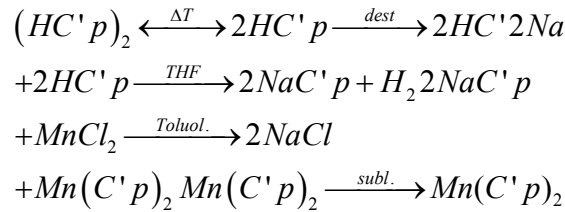
Here, we describe the six series of (Ga,Mn)As-based samples grown on (001) GaAs substrates by means of metal-organic vapour-phase epitaxy (MOVPE)^[1-3] or by molecular beam epitaxy (MBE), respectively. Most studies focus on the MOVPE-grown samples.^[4-6] However, in order to find the influence of the growth methods on the transport behaviour, MBE-grown samples are also studied. The MOVPE is a deposition method in which a thin solid film is synthesized by the chemical reaction of molecules from the gaseous phase on a heated surface. The precursors used for the MOVPE of compound semiconductors are conventional metal organic-compounds whereas in MBE usually elemental sources are used. Because the precursors do not have to be broken up to form the semiconductors in MBE, the growth temperatures in MBE can be considerably lower by 100-200°C than in MOVPE. For growing samples of the (Ga,Mn)As system MOVPE as well as MBE can be employed. Both techniques are non-equilibrium growth techniques. To a certain extent the sample quality is sacrificed for obtaining high Mn-contents. Therefore, it is important to compare samples based on both techniques to separate intrinsic from extrinsic effects.

Fig. 2.1 shows the comparison of phase diagrams of the (Ga,Mn)As system obtained by MBE-growth^[7] and MOVPE-growth. For the MBE samples, compared with ordinary GaAs grown at 600°C, the growth temperature of Ga_{1-x}Mn_xAs is much lower to avoid phase segregation. The limit lies between 200°C and 400°C, depending on the Mn concentration. When the growth temperature is too high, a second-phase forms. When the growth temperature is too low, the films tend to become insulating or polycrystalline. The maximum of the Mn solubility in the Ga_{1-x}Mn_xAs is below 10%, and beyond this concentration the second phase forms even at low growth temperature. For the MOVPE samples, it can be concluded as shown in the right figure of Fig. 2.1: For low Mn/Ga ratios, p-type GaAs:Mn in the range of 10¹⁹ cm⁻³ is formed; For high Mn/Ga ratios and deposition temperatures below 500°C, whisker growth is observed. Temperatures of 500°C and above in combination with high Mn/Ga ratios lead to hetero-epitaxial growth of MnAs-clusters defect free in a surrounding GaAs:Mn-matrix. The enrichment of Mn at the growth surface finally results in GaAs:Mn/MnAs hybrids formation.

For MOVPE samples, bis-(methylclopentadienyl) manganese (MeCp)₂Mn was selected as the source compound because of its thermal decomposition characteristics. The (MeCp)₂Mn

2. Preparation and structural properties of the studied GaMnAs-based alloys and hybrids

compound is in the solid phase with an estimated vapour pressure of about 10^2 hPa at room temperature. The following chemical synthesis of this compound has been chosen



Where $C'p$ is $CH_3-C_5-H_4$. MOVPE growth has been performed in a standard commercial horizontal reactor system (Aix 200-GFR, Aixtron Corp.) at a reduced reactor pressure of 50hPa using H_2 -carrier gas. Due to the intended MOVPE non-equilibrium growth conditions at reduced deposition temperatures ($400^\circ C$ to $600^\circ C$), the more efficient precursors triethylgallium (TEGa) and tertiarybutylarsine (TBAs) have been used. To investigate the suitable growth regime, the growth parameters (e.g. temperature, Mn/Ga ratio, growth rate and V/III-ratio) have been varied individually, and the various high structural quality samples are obtained.

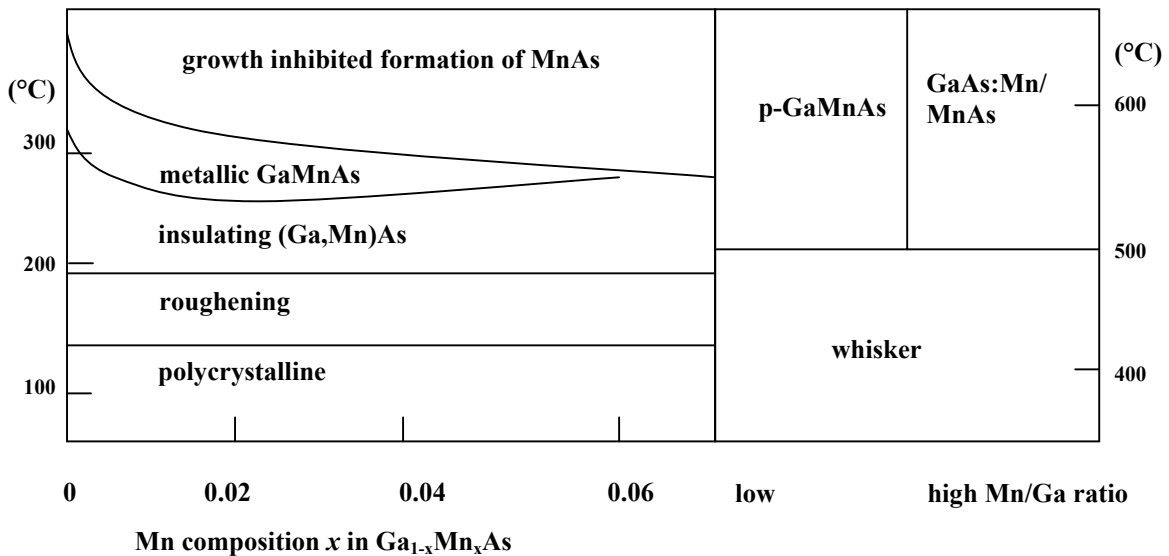


Fig. 2.1. Comparison of the growth phase diagram for MBE (left) and MOVPE (right) samples.

The surface of these samples has been investigated by scanning electron microscopy (SEM) as shown in the Fig. 2.2, from the left to right, a whisker sample, a $Ga_{1-x}Mn_xAs$ alloy and a GaAs:Mn/MnAs hybrid sample are presented.

As a rule, a ternary alloy formed by substituting Mn for the group-III element in the III-V lattice will retain ideally the crystal structure of the parent III-V compound. The lattice

2. Preparation and structural properties of the studied GaMnAs-based alloys and hybrids

parameters of all known DMS ternary alloys should obey Vegard's law very closely^[8]; applied to $\text{Ga}_{1-x}\text{Mn}_x\text{As}$

$$\alpha_{\text{GaMnAs}} = (1-x)\alpha_{\text{LT-GaAs}} + x\alpha_{\text{MnAs}}$$

where $\alpha_{\text{LT-GaAs}} = 5.66\text{\AA}$ and $\alpha_{\text{MnAs}} = 5.98\text{\AA}$ ^[8] are the lattice parameters of the zincblende GaAs and zincblende MnAs, x is the Mn composition. The validity of this law has been confirmed for $\text{Ga}_{1-x}\text{Mn}_x\text{As}$ by some studies.

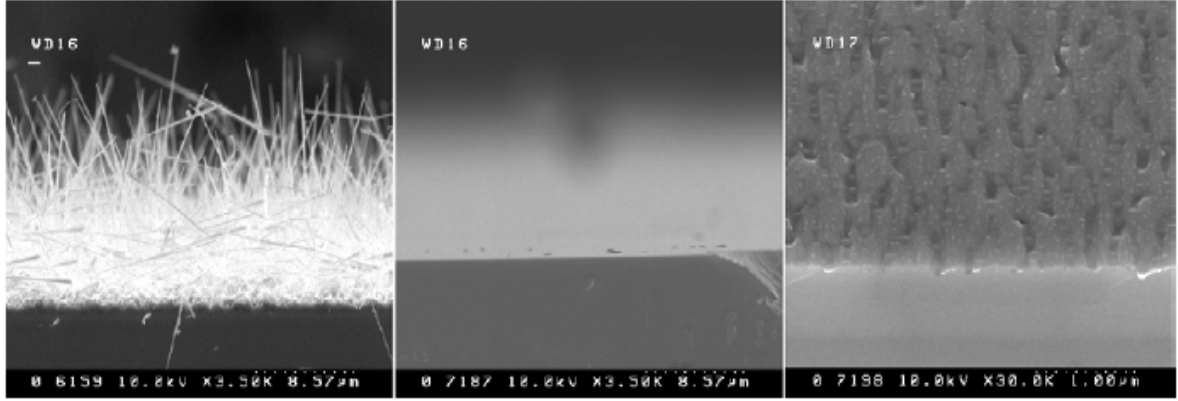


Fig. 2.2. SEM results of the MOVPE-grown samples.

2.2 Six studied series of (Ga,Mn)As-based samples

2.2.1 Paramagnetic GaAs:Mn alloys (MOVPE grown)

A series of $\text{Ga}_{1-x}\text{Mn}_x\text{As}$ alloy samples was grown by MOVPE, where x is varied from the doping regime to about 0.5 %. All these specimens are paramagnetic above 1.6 K and show p-type conductivity, indicating that the majority of the Mn atoms incorporated on

Tab. 2.1. paramagnetic-GaAs:Mn alloys

sample	Structure	Growth Temperature	V/III ratio	Mn/Ga	Thickn-ess(nm)	$V_{\text{growth}}(\mu\text{m/h})$
#12357	GaAs:Mn-bulk	550°C	10	0.5%	1000	2
#12352	GaAs:Mn-bulk	550°C	10	2%	1000	1
#12359	GaAs:Mn-bulk	550°C	10	8%	300	1
#12696	GaAs:Mn-bulk	500°C	5	4%	500	0.5
#12699	GaAs:Mn-bulk	500°C	10	4%	500	0.5
#12701	GaAs:Mn:bulk	500°C	5	8%	500	0.5
#13084	GaAs:Mn-bulk	550°C	5	8%	2000	0.5
#13085	GaAs:Mn-bulk	550°C	5	8%	2000	0.5

2. Preparation and structural properties of the studied GaMnAs-based alloys and hybrids

Ga sites and acting as acceptors. In these samples the growth parameters have been varied individually to control the Mn concentrations and the thickness of layers as shown in Tab. 2.1. These samples are used to study the influence of the Mn-concentration on the valence band magneto-transport.

2.2.2 Co-doped GaAs:Mn,Te alloys (MOVPE grown)

A series of $\text{Ga}_{1-x}\text{Mn}_x\text{As}$ alloys grown by MOVPE with $x \approx 0.1\%$ but with different co-doping levels of Te was grown. Such that the type of majority carriers changes (i.e., the conductivity changes from p to n-type) with increasing Te doping level. The #12357 is the reference paramagnetic p-GaAs:Mn sample without Te co-doping. The #13420 is n-GaAs:Te as another reference sample. Again, all samples exhibit paramagnetic behaviour at temperatures above 1.6 K. These samples are used to probe the influence of *p-d* exchange interaction on the valence band transport, and especially the *s-d* exchange interaction on the conduction band transport in the n-type sample.

Tab. 2.2 Co-doped GaAs:Mn,Te alloys

sample	structure	Gr-Temp	V/III	Mn/Ga	Th(nm)	$V_{\text{growth}}(\mu\text{m/h})$
#12357	GaAs:Mn-bulk	550 ⁰ C	10	0,5%	1000	2
	structure	Reference	Th(nm)	Te/Ga		
#13300	GaAs:Mn	#12357	500	0		
#13301	GaAs:Mn, Te	#12357	500	5E-5		
#13303	GaAs:Mn, Te	#12357	500	1E-4		
#13305	GaAs:Mn, Te	#12357	500	2E-4		
#13307	GaAs:Mn, Te	#12357	500	4E-4		
#13309	GaAs:Mn, Te	#12357	500	8E-4		
#13420	GaAs:Te	#12357	500	some		

2.2.3 p-GaAs:Mn/MnAs hybrids and their magnetic and structural properties (MOVPE grown)

This series consists of hybrid structures where MnAs clusters are formed within the $\text{Ga}_{1-x}\text{Mn}_x\text{As}$ alloy samples with $x \approx 0.1\%$ during the growth. All samples are p-type and exhibit ferromagnetism with a Curie-temperature of 325 K due to the MnAs clusters, but the surrounding GaAs:Mn matrix exhibits paramagnetic behaviour down to 1.6 K. By

2. Preparation and structural properties of the studied GaMnAs-based alloys and hybrids

varying the thickness of the layers from 150 nm to about 1000 nm (#13080 to #13072), the size of the MnAs cluster can be varied (see also Tab. 2.3). These samples were grown at a growth temperature 500°C on (001) or (111) GaAs substrates with 0.5 $\mu\text{m/h}$ growth rate and a nominal Mn/Ga ratio in the gas phase of 24%. The samples #13383# to #14077 were grown at different growth temperatures and V/III ratios to achieve different types of clusters. #14015(a) to #14016(b) are samples with the two different orientations between the hard axis of MnAs clusters and the GaAs (001) substrates, which is confirmed by TEM. These samples are used to investigate the influence of the interaction between the ferromagnetic MnAs clusters and paramagnetic GaAs:Mn matrix for various types of MnAs clusters and cluster densities.

Tab. 2.3. p-GaAs:Mn/MnAs hybrids

sample	structure	Gr-Temp	V/III	Mn/Ga	Th(nm)	$V_{\text{growth}}(\mu\text{m/h})$	substrat
#13080	GaAs:Mn/MnAs	500°C	5	24%	150	0.5	(001)
#13077	GaAs:Mn/MnAs	500°C	5	24%	300	0.5	(001)
#13076	GaAs:Mn/MnAs	500°C	5	24%	500	0.5	(001)
#13072	GaAs:Mn/MnAs	500°C	5	24%	1000	0.5	(001)
#13076 (A)	GaAs:Mn/MnAs	500°C	5	24%	500	0.5	(111)
#13883	GaAs: Mn/MnAs	12697# 600°C	5	24%	500	0.5	(111)
#12697 (no)	GaAs:Mn/MnAs	500°C	5	24%	500	0.5	(001)
#14069	GaAs:Mn/MnAs	600°C	8	24%	150	0.05	(001)
#14077	GaAs:Mn/MnAs	550°C	8	24%	150	0.1	(001)
#14015 (a)	#13076	500°C	120	24%	500	0.5	(001)
#14015 (b)	#13076	500°C	120	24%	500	0.5	(001)
#14061 (a)	#13076	500°C	5	24%	500	0.5	(001)
#14061 (b)	#13076	500°C	5	24%	500	0.5	(001)

2. Preparation and structural properties of the studied GaMnAs-based alloys and hybrids

For these GaAs:Mn/MnAs hybrids, it has been confirmed by TEM and FMR that the magnetic particles are α -MnAs clusters hexagonal with NiAs-type structure ($a=0.37$ nm, $c=0.57$ nm).^[9-10] The crystallographic orientation of the clusters with respect to the zincblende matrix is almost MnAs [0001] || GaAs [111] direction as shown in Fig. 2.3, which agrees with the crystal orientation reported for MnAs nanoclusters.

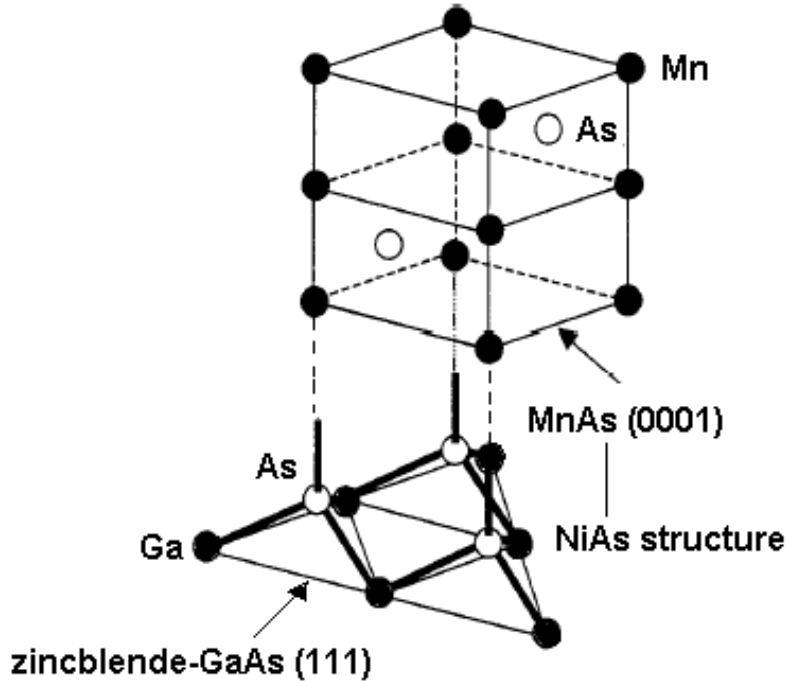


Fig. 2.3. The crystallographic orientation of NiAs-MnAs [0001] ||zinc-blende GaAs [111].

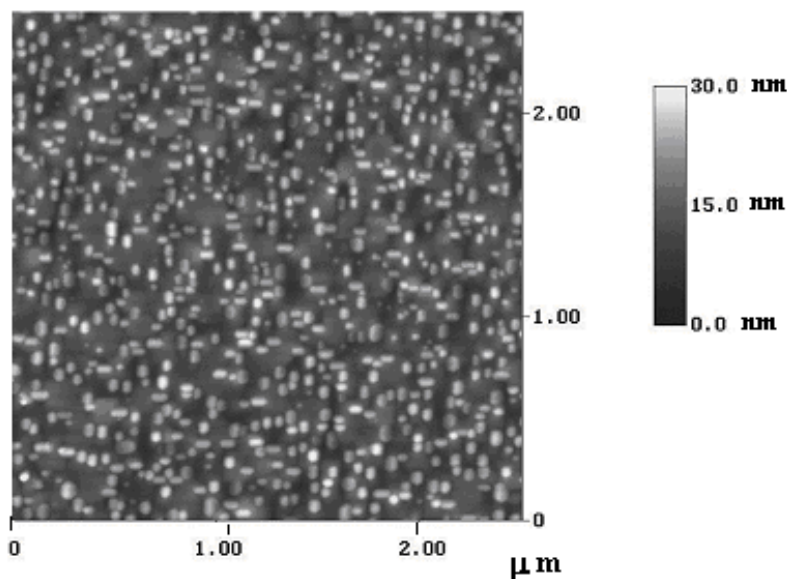


Fig. 2.4. AFM image of a GaAs:Mn/MnAs hybrid structure

2. Preparation and structural properties of the studied GaMnAs-based alloys and hybrids

The easy plane of the magnetization of MnAs clusters is perpendicular to the c-axis. However, there are four possible different orientations of clusters for the samples grown on (001) substrate and only one orientation for (111) substrate.

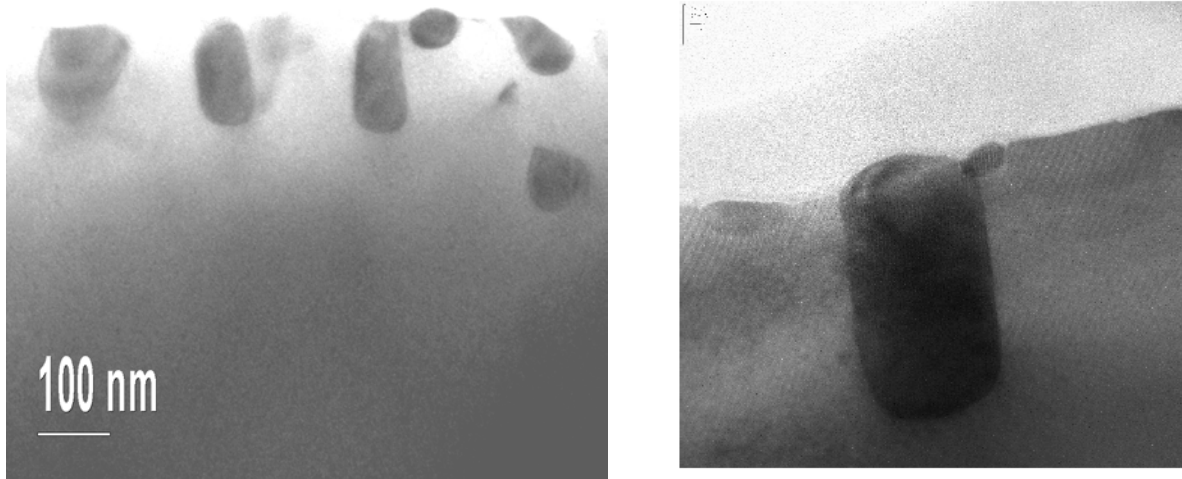


Fig. 2.5. (a) TEM micrograph (cross section) of the GaAs:Mn/MnAs hybrids, the clusters are located near the surface. (b) MnAs cluster at a higher magnification.

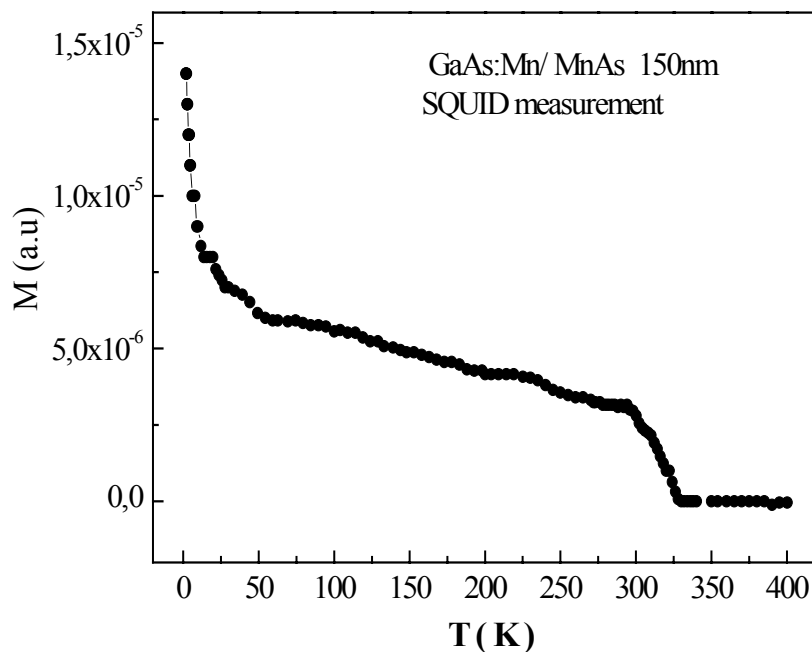


Fig. 2.6. SQUID measurement of the GaAs:Mn/MnAs hybrid with 150 nm thickness.

When the orientation of MnAs clusters is adjusted in a controlled way during the growth, the orientation relationship between the crystallographic MnAs and GaAs:Mn matrix can lead to

a magnetic anisotropy in the hybrids. This offers the opportunity to investigate the corresponding magnetic anisotropy on the interaction between the ferromagnetic MnAs nanoclusters and paramagnetic p-GaAs:Mn matrix. In this size regime, the magnetic properties i.e. Curie temperature as well as easy axis are unaffected.

The atomic force microscopy (AFM) measurement of a $2.5 \mu\text{m}^2$ area of the #13076 GaAs:Mn/MnAs hybrid with 500 nm thickness is shown in Fig. 2.4. It can be seen that the MnAs clusters are distributed homogeneously close to the surface and are of comparable size. The size and density of the MnAs clusters vary with the growth parameters. For example, the diameter of the MnAs clusters was varied from 35 nm to 120 nm and the height from 15 nm to 150 nm in samples with 150 nm to 1000 nm thickness (#13080 to #13072). The results were obtained by transmission electron microscopy (TEM) as shown in the Fig. 2.5. It was found that the MnAs clusters are situated close to the sample surface. Fig. 2.5(b) shows a cross-section at higher magnification of one bigger cluster. No evidence is known at present for any lattice defects.

The magnetic properties of the GaAs:Mn/MnAs hybrids were investigated by SQUID and FMR measurements. It was found that for all hybrid samples there exists a paramagnetic-ferromagnetic phase transition of the MnAs clusters at about $T = 325$ K when the temperature is decreased as shown in Fig. 2.6. The ferromagnetic transition temperature of the ferromagnetic MnAs clusters is similar to the Curie temperature of about 320 K for bulk MnAs. The little difference might be caused by the strain force in the films.

Fig. 2.7 gives the angular dependence of the FMR signal for the typical GaAs:Mn/MnAs hybrids grown on (001) and (111) GaAs substrate, respectively. Fig. 2.7(a) is the FMR signal of the (001) sample #13076 where the axis of rotation is perpendicular to applied field and parallel to the GaAs [110] direction as shown in the left of Fig. 2.7(a). The FMR signal indicates that the hard axis of the clusters is parallel to the c-axis of MnAs clusters with four equivalent GaAs [111] orientations of MnAs [0001] || GaAs [111] for the samples grown on (001) substrate. Fig. 2.7(b) is the FMR signal of the (111) sample #13076A with the axis of rotation perpendicular to applied field and perpendicular to the GaAs [111] direction as shown in the Fig. 2.7(b). The crystallographic orientation of the clusters with respect to the matrix is the same as sample (001) #13076. The FMR signal shows that the hard axis of the clusters is also parallel to the c-axis and that MnAs [0001] || GaAs [111] on (111) substrate. However, it is only found a single cluster orientation in sample #13076A grown on (111) substrate.

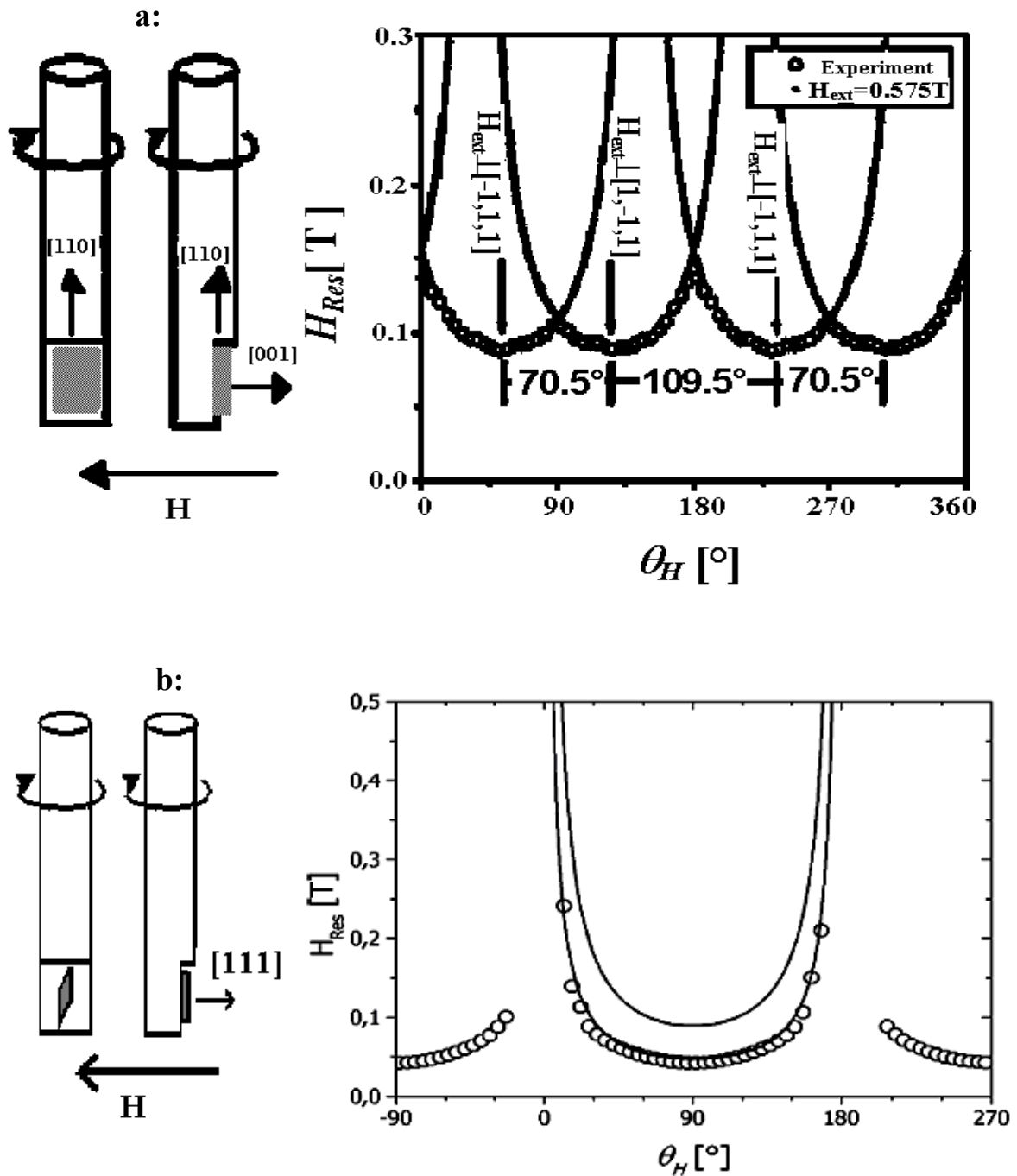


Fig. 2.7. Angular dependence of the FMR signal for GaAs:Mn/MnAs hybrid samples grown on (001) and (111) GaAs substrate, respectively.

2.2.4. p-GaInAs:Mn/MnAs hybrids (MOVPE grown)

A series GaInAs:Mn/MnAs hybrid structures was grown by a similar MOVPE growth procedure as the series discussed in 2.2.3. TEM as well as FMR investigations show that ferromagnetic α -MnAs clusters also form in the surrounding GaInAs:Mn matrix, which exhibits NiAs-type hexagonal structure. The ferromagnetic plane of the MnAs clusters is

perpendicular to the c-axis, and the magnetic easy axis of the clusters tends to be aligned in a direction parallel to [011]. All samples are p-type and exhibit a Curie-temperature of more than 300 K with the GaInAs:Mn matrix exhibiting paramagnetic behaviour down to 1.6 K. The thickness of all the samples is the same. By varying the growth temperature and V/(III+Mn) ratio as listed in Tab. 2.4, the density and type of MnAs clusters are varied.

Tab. 2.4. p-GaInAs:Mn/MnAs hybrids

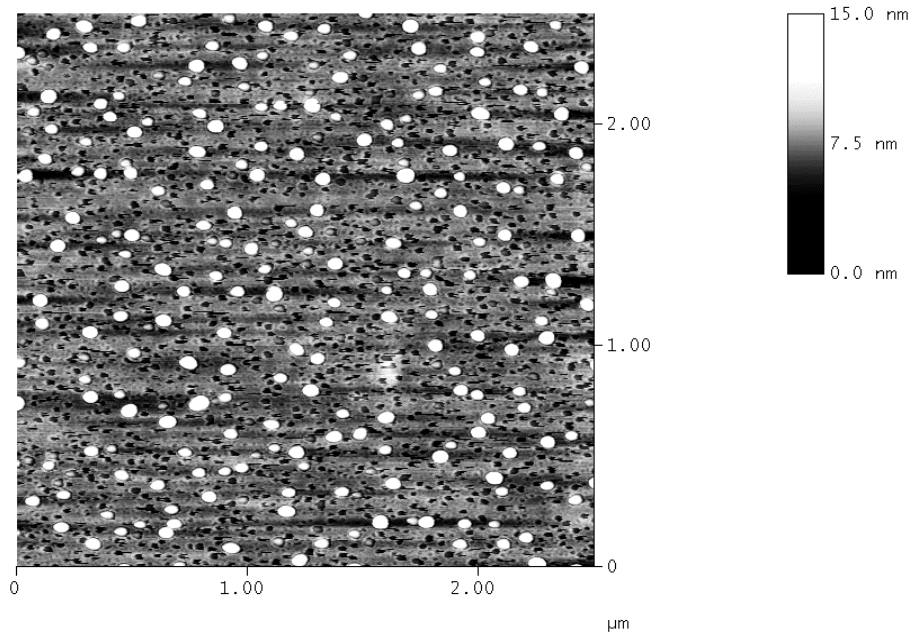
samples	Structure	Gr-Temp	V/(III+Mn).
#13985	GaInAs:Mn(160nm)/ InGaAs(10nm)InP(300nm)	500°C	24%
#13986	GaInAs:Mn (160nm)/ InGaAs(10nm)InP(300nm)	590°C	24%
#13996	GaInAs:Mn (160nm)/ InGaAs(10nm)InP(300nm)	500°C	4%
#13997	GaInAs:Mn (160nm)/ InGaAs(10nm)InP(300nm)	590°C	4%

2.2.5. p-Ga_{1-x}Mn_xAs alloys (MBE grown)

Three MBE-grown p-Ga_{1-x}Mn_xAs samples were studied for comparison with the MOVPE samples. #OM253 is a p-Ga_{1-x}Mn_xAs with 2% Mn with a Curie temperature T_C of about 25 K. The thickness of this sample is 300 nm. #40929A is a p-Ga_{1-x}Mn_xAs alloy with $x = 6.8\% \sim 7.4\%$. It consists of GaAs(2nm)/GaMnAs(600nm)/GaAs(150nm)/GaAs(001) SI substrate. #40929C is a p-Ga_{1-x}Mn_xAs alloy with $x = 7.0\% \sim 7.5\%$ and with a layer structure of GaAs(2nm)/GaMnAs(300nm)/GaAs(150nm)/GaAs(001) SI substrate. In these samples, the T_C values are far lower than these expected from the relationship $T_C = 2000x \pm 10$ K. This indicates a high degree of compensation probably due to the formation of interstitial Mn ions which act as donors. The effect of the interstitial Mn ions on the p-d exchange and the strong influence on the magneto-transport can be investigated in this system.

2.2.6. p-GaAs:Mn/MnAs hybrids (MBE growth followed by post-annealing)

a:



b:

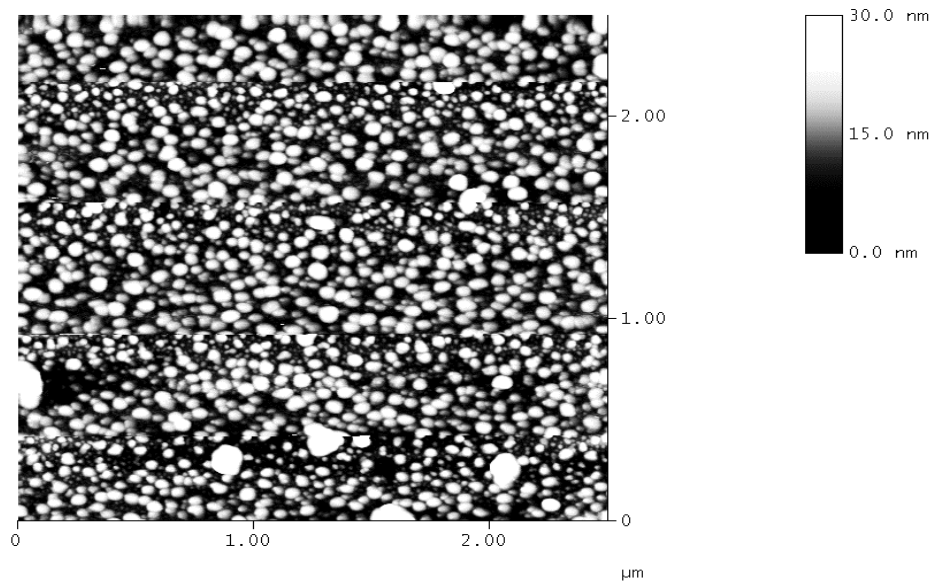


Fig. 2.8. AFM images of (a) at 450°C-annealed GaAs:Mn/MnAs hybrid and of (b) 500°C-annealed GaAs:Mn/MnAs hybrid.

A series of the GaAs:Mn/MnAs hybrids was obtained by annealing the MBE-grown #40929A at different temperatures in the range from 450°C to 650°C with steps of 50 degree in an arsenic atmosphere. Fig. 2.8 shows AFM results for the samples annealed at 450°C and 500°C, respectively. It shows clearly the formation of MnAs clusters, which are distributed homogeneously close to the sample surface. With increasing annealing temperature, the density of clusters increases as shown in the Fig. 2.8(a) and (b). It is found that the diameter and the density of MnAs clusters and the distance between them depend strongly on the growth and the annealing parameters (growth and annealing procedures, temperature and time of annealing, the Mn concentration, thickness of samples), which leads to different physical properties of the hybrids. Therefore, the GaAs:Mn/MnAs hybrids grown by MOVPE and MBE offer an good opportunity to investigate the relations between the effect of the type of MnAs clusters and the type of GaAs:Mn matrix on the transport properties, and in particular allow a distinction between intrinsic and extrinsic properties of the studied hybrids.

In summary, six series of GaAs:Mn-based alloys and hybrids were successful grown by MOVPE or MBE with high quality. The structural and magnetic properties of these samples have been studied by AFM, TEM, SQUID and FMR measurements. These GaAs:Mn-based alloys and hybrids exhibit different magneto-transport behaviour as will be discussed in the following chapters, which helps to understand the nature of the Mn ions in the GaAs:Mn DMS, and the interaction between the MnAs nanoclusters and paramagnetic GaAs:Mn matrix.

References:

- [1] M. Lampalzer, K. Volz, W. Treutmann, S. Nau, T. Torunski, K. Megges, J. Lorberth, and W. Stolz, *J. Cryst. Growth.* **248**, 474 (2003).
- [2] Th. Hartmann, M. Lampalzer, P. J. Klar, W. Stolz, W. Heimbrod, H. -A. Krug von Nidda, A. Loidl, and L. Svistov, *Physica E.* **13**, 572 (2002).
- [3] Th. Hartmann, M. Lampalzer, W. Stolz, K. Megges, J. Lorberth, P. J. Klar, W. Heimbrod, *Thin. Solid. Films.* **364**, 209 (2000).
- [4] S. Ye, P.J. Klar, T. Hartmann, W. Heimbrod, M. Lampalzer, S. Nau, T. Torunski, and W. Stolz, T. Kurz, H.-A. Krug von Nidda and A. Loidl, *Appl. Phys. Lett.* **83**, 3927 (2003).
- [5] S. Ye, P. J. Klar, T. Henning, M. Lampalzer, W. Stolz and W. Heimbrod, *J. Superconductivity: Incorporating Novel Magnetism.* **16**, 159 (2003).
- [6] T. Hartmann, S. Ye, T. Henning, P.J. Klar, M. Lampalzer, W. Stolz, and W. Heimbrod, *J. Superconductivity: Incorporating Novel Magnetism.* **16**, 423 (2003).
- [7] H. Ohno, *Science.* **281**, 951 (1998).
- [8] D. R. Yoder-Short, U. Debska, and J. K. Furdyna, *J. Appl. Phys.* **58**, 4056 (1985).
- [9] J. De Boeck, R. Oesterholt, A. Van Esch, H. Bender, C. Bruynseraede, C. Van Hoof, and G. Borghs, *Appl. Phys. Lett.* **68**, 2744, (1996).
- [10] H. Okamoto, *Bull. Alloy Phase Diagrams.* **10**, 549 (1989).

3. Transport properties of paramagnetic GaAs:Mn and co-doped GaAs:Mn,Te

Recently, most studies of the (Ga,Mn)As system focus on the physical properties of the ferromagnetic $\text{Ga}_{1-x}\text{Mn}_x\text{As}$ alloys,^[1-3] whereas only a few studies deal with the paramagnetic regime at small Mn concentrations or above the Curie temperature. Therefore, this research area still needs a lot of work to clarify the whole physical picture of the $\text{Ga}_{1-x}\text{Mn}_x\text{As}$ DMS system. In this chapter, we first discuss the MR effects in two series of paramagnetic p-type $\text{Ga}_{1-x}\text{Mn}_x\text{As}$ alloys grown by MOVPE and MBE, respectively. Unusual positive or negative MR effects observed at low temperatures have been found in these two series, which are similar to those observed in the II(Mn)-VI DMS in the earlier work.^[4-6] Moreover, the MR behavior such as the sign and the shape of the MR effect are very sensitive to the Mn concentration. This is proved by the different MR behavior of the MOVPE- and MBE- grown (Ga,Mn)As samples. We suggest that the interplay of two effects play an important role. One is the magnetic field-dependent spin splitting of the valence band caused by the *sp-d* exchange interaction and the corresponding shift of the position of the Fermi-level. The other is the disorder induced by the Mn incorporation. The competition of these two effects is responsible for the unusual positive and negative MR effects. The theoretical calculation by two models, a network model and a mobility model, confirm the important roles of these two effects in the III(Mn)-V magnetic semiconductor especially in the low Mn region. By adjusting the weighting of the effects of occupation of the four spin-subbands and disorder, negative and positive MR curves are obtained by these two models. Then, we discuss the series with different Te co-doping in p-GaAs:Mn with 0.1% Mn concentration, which can be changed to n-GaAs:Mn,Te by increasing the Te doping level. One of the important effects of Te co-doping is the valence band filled with electrons in the case of the GaAs:Mn,Te where Mn acts as A^- center only. The n-type samples allow one to probe the effect of s-d exchange interaction on the conduction band transport. Furthermore, the FM coupling with a positive $N_0\beta$ in p-GaAs:Mn attributed to the Mn acting as A^0 (d^5+h) centers changes to an AFM type coupling induced by Te co-doping.

3.1 Resistivity and Hall measurements

Resistance and Hall measurements were performed in the Van-der-Pauw geometry which is widely used to determine the resistivity of uniform samples. As originally suggested by Van

der Pauw, one uses an arbitrarily shaped thin-plate sample with four very small ohmic contacts placed on the periphery (preferably on the corners) of the plate. Resistance and Hall measurements were performed in a temperature range from 1.6 K to 300 K and in external magnetic fields (H) up to 10 Tesla. Four thin copper or gold leads were attached to the samples using indium as contacts. All contacts were ohmic. DC currents were used varying between $1 \mu\text{A}$ and 1mA , depending on the temperature and on the sample under study. The proportionality between the measured voltage and the current was always checked to ensure ohmic behaviour and the absence of self-heating. The magnetic field H was always perpendicular to the direction of the current in the sample. The standard procedure of reversing the direction of H was used to separate the resistance and Hall components of the voltage. The MR ratio is defined as $\Delta\rho(H)/\rho_0 = (\rho(H)-\rho_0)/\rho_0$, where ρ_0 and $\rho(H)$ are the resistivity in zero-field and at an applied H field, respectively.

3.2 MR effects of the paramagnetic GaAs:Mn alloys

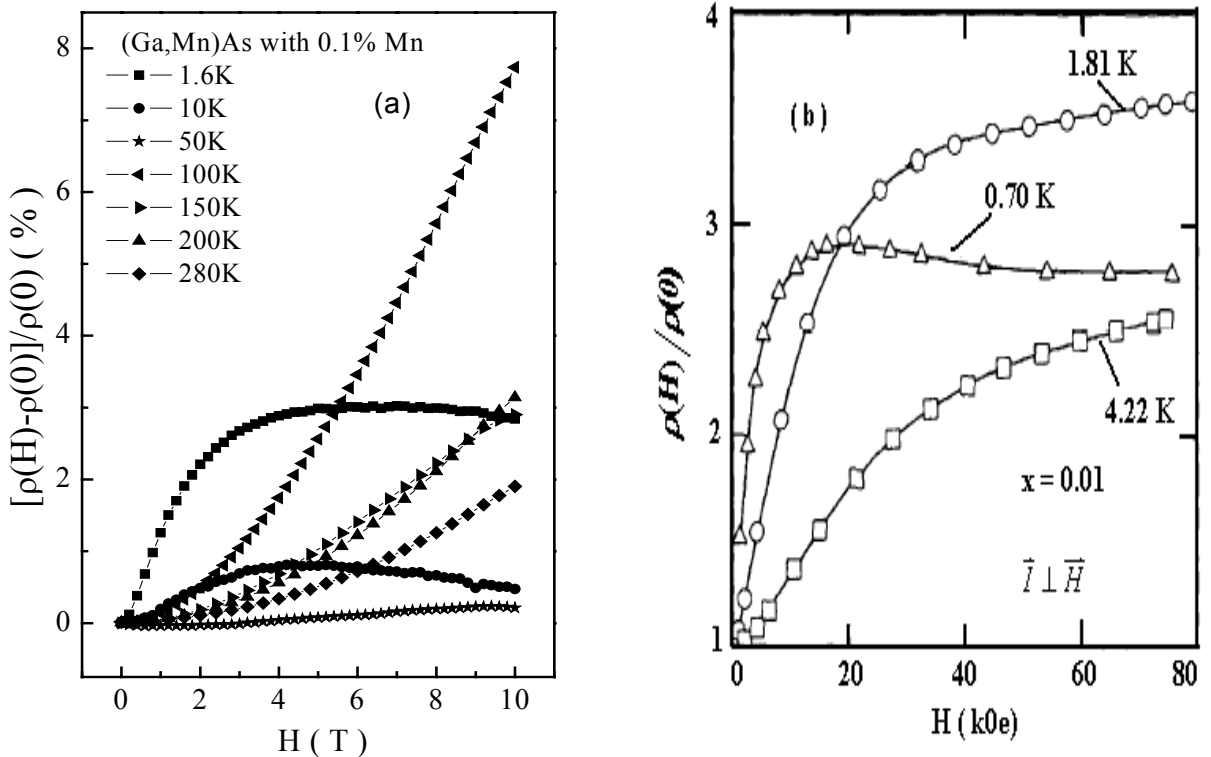


Fig. 3.1. p-type GaAs:Mn and n-type (II,Mn)VI DMS show similar MR effects. a) MR effect of p-type paramagnetic GaAs:Mn alloy with 0.1% Mn at various temperatures. (b) MR for n-Cd_{0.99}Mn_{0.01}Se at low temperatures.^[4]

Resistance measurements are a macroscopic way of studying the average microscopic character and behaviour of the carriers. An applied magnetic field means to amplify or induce the magnetic interaction effects in the material. Therefore, by MR measurements, one can obtain information about the magnitude of the spin interactions in the materials and their effects on the transport properties. Thus, MR measurements are an effective and comfortable method to study the influence of different spin interactions on the transport of free carriers, and may offer a suitable way of optimising spin polarization effects in the material and in corresponding devices.

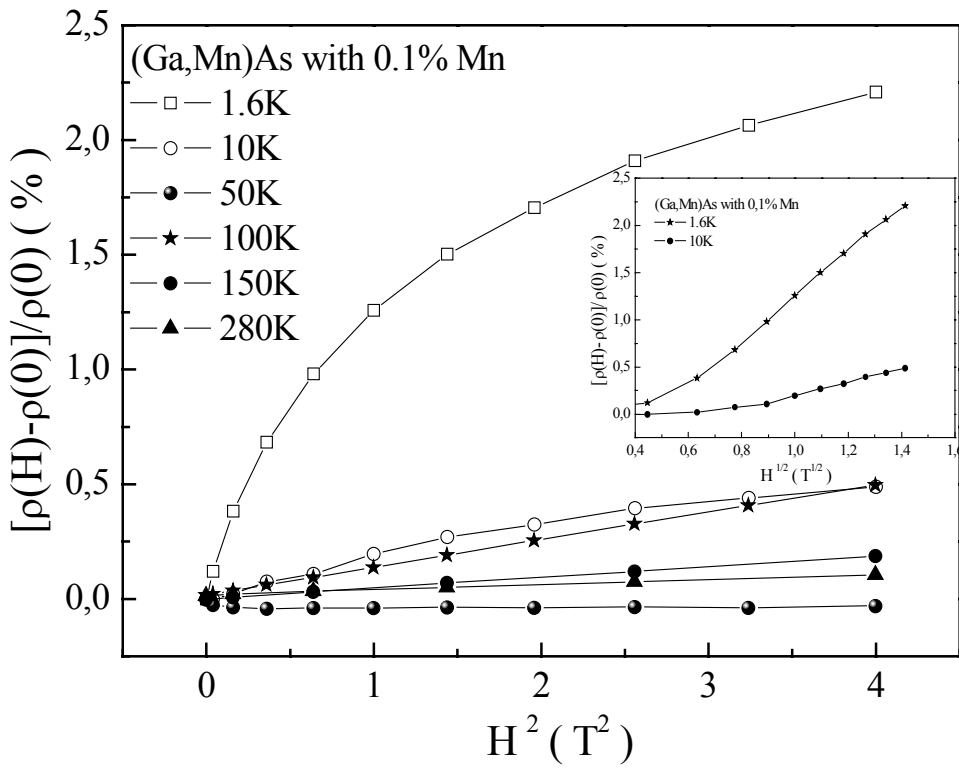


Fig. 3.2. Temperature dependence of MR as a function of H^2 for p-GaAs:Mn with 0.1% Mn; the inset shows plots of the MR as a function of $H^{1/2}$ for $T = 1.6$ K and $T = 10$ K.

Fig. 3.1(a) depicts the temperature dependence of the MR effect of a paramagnetic p-GaAs:Mn with about Mn~0.1% grown by MOVPE. It is found that in the whole temperature range, the MR effects are small but show a complicated field dependence, which differs from the normal parabolic MR behaviour. Especially at the lowest temperature $T = 1.6$ K, a positive MR effect seems similar to that observed in II(Mn)-VI DMS compounds such as $Cd_{0.99}Mn_{0.01}Se$ presented in Fig. 3.1(b). Firstly the MR increases steeply at low H -fields, then goes through a maximum

and finally decreases quite slowly at high fields. In case of $\text{Cd}_{0.99}\text{Mn}_{0.01}\text{Se}$, it was found that the intensity and the position of the maximum of the MR are very sensitive to temperature and Mn concentration. At $T = 10$ K, the positive MR becomes smaller, and decreases faster at high fields for II(Mn)-VI magnetic semiconductors. With increasing the temperature to 50 K, the whole MR curve almost flattens and eventually increases again. It exhibits a positive parabolic MR effect as that observed in normal semiconductors between $T = 100$ K and 280 K.

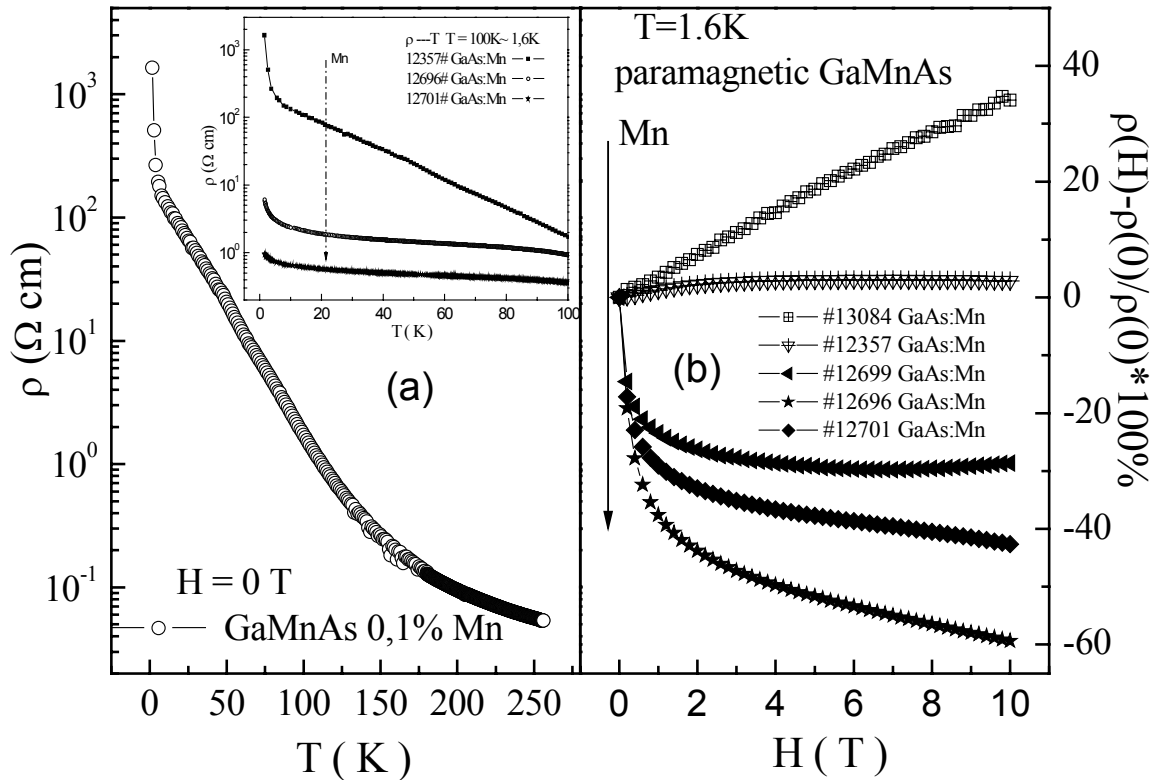


Fig. 3.3. (a) Temperature dependence of the resistivity of p-GaAs:Mn with 0.1% Mn; Inset in (a) and (b) are the temperature dependence of the resistivity and MR effect at 1.6 K for various Mn-contents up to 0.5%, respectively. The arrow indicates increasing Mn content.

Fig. 3.2 presents the temperature dependence of the MR for paramagnetic p-GaAs:Mn with 0.1% Mn as a function of H^2 . One expects a proportionality to H^2 for diamagnetic semiconductors. This prediction is clearly only obeyed at higher temperature for GaAs:Mn. At low temperatures, the data show that the initial rise of the resistivity becomes steeper with decreasing temperature, and at the lowest T the MR versus H^2 shows a marked curvature even in fields below 0.5 T. Presumably the field range over which the MR is proportional to H^2 is

quite narrow at these low temperatures. The inset of Fig. 3.2 shows the MR plotted against $H^{1/2}$ for low temperatures $T = 1.6$ K and $T = 10$ K. Here another linear behaviour is found at lower fields. The slope varies with increasing temperature. Therefore, in the low temperature region, the MR effect prefers to obey $H^{1/2}$.

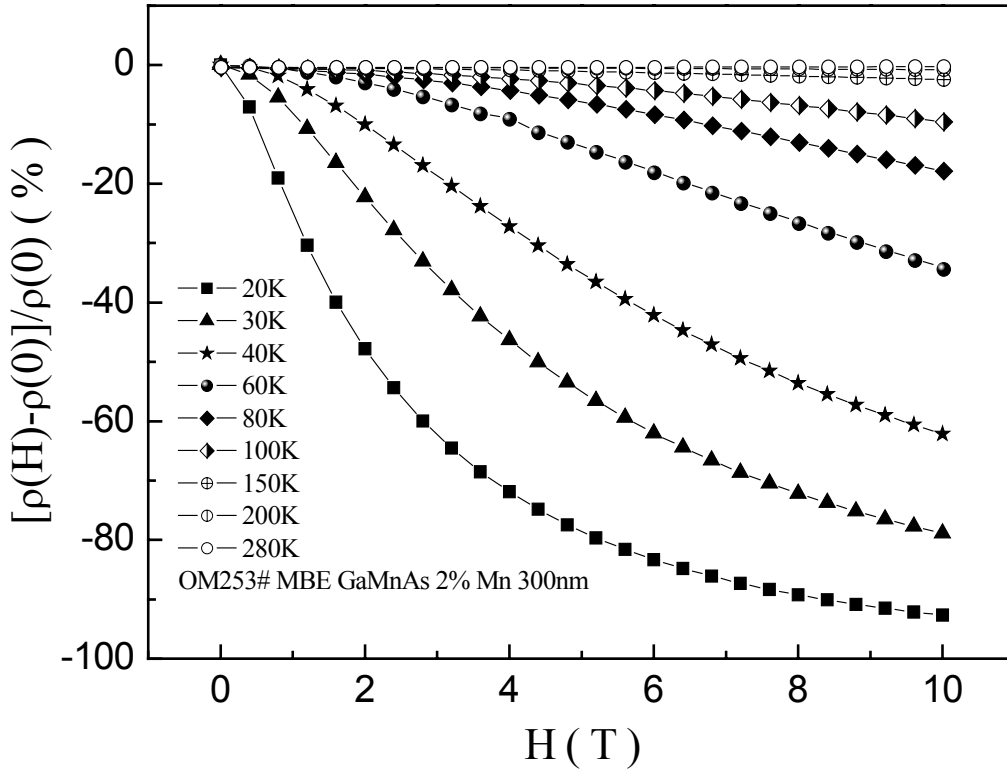


Fig. 3.4. MR effects of OM 253# MBE-grown Ga_{1-x}Mn_xAs with 2% Mn and *th* = 300 nm.

Furthermore, a series of Ga_{1-x}Mn_xAs alloy samples where *x* is varied from the doping regime to about 0.5% was measured. The temperature dependence of the resistivity at $H = 0$ T of the samples of this series is shown in Fig. 3.3(a). The paramagnetic GaAs:Mn alloy with about 0.1% Mn concentration exhibits semiconducting behavior which approaches the metal-insulator transition with increasing Mn concentration *x*; but up to $x \approx 0.5$ % all samples are still semiconducting as shown in the inset of Fig. 3.3(a). All these specimens are paramagnetic above 1.6 K and show p-type conductivity. Fig. 3.3(b) shows the MR curves at $T = 1.6$ K of five paramagnetic p-Ga_{1-x}Mn_xAs alloy samples of this series. By increasing the Mn concentration from doping levels to about 0.5%, the MR changes from a positive MR effect to a large negative MR effect which resembles that reported for MBE-grown Ga_{1-x}Mn_xAs alloys with $x > 1\%$ below and above T_C as shown in Fig. 3.4. For the sample with the highest Mn

concentration ($x \approx 0.5\%$), the MR decreases rapidly at low H -fields by about 30% up to 0.5 T. At higher fields the resistance decreases further but at a smaller rate of about -3% per Tesla for $H > 5$ T over the whole accessible field range. At 10 T the MR value is about -60%. The MBE-grown $\text{Ga}_{1-x}\text{Mn}_x\text{As}$ alloys with Curie temperature $T_C = 25$ K, shows similar behavior with large negative MR $\sim -90\%$ below T_C (see Fig. 3.4). Then the negative MR decreases with increasing temperature, and finally changes to a very small positive MR effect at room temperature. Therefore, it can be emphasized that the MR effect in the low temperature regime, where the MR effect can have positive as well as negative behaviour, depends strongly on the Mn concentration.

Early studies of magnetic semiconductors as well as the more recent investigations of II(Mn)-VI and III(Mn)-V DMS systems already have convincingly demonstrated that the presence of magnetic ions modifies dramatically the transport properties. The strong s-d (p-d) exchange interaction between the magnetic ions and conduction (valence) band states leads to a tuning of the density of states in the vicinity of the Fermi energy when an external magnetic field is applied. This interaction strongly affects the transport behavior. The essential difference between the II(Mn)-VI and III(Mn)-V DMS is: The Mn ions are electrically neutral in II(Mn)-VI DMS, neither introduce nor bind carriers and only provide the localized spins which give rise to the s,p-d exchange. In the III(Mn)-V DMS, the Mn ions act as effective mass acceptors d^5 +hole besides offering the localized spins, which can lead to a spontaneous magnetic phenomenon. Therefore, the situation in $\text{Ga}_{1-x}\text{Mn}_x\text{As}$ is more complicated than that in II(Mn)-VI DMS.

3.3. Experimental MR results in the context of theoretical models

As shown in the Fig. 3.1 and Fig. 3.2, abnormal positive and negative MR effects have been found in the both paramagnetic n- or p-type II(Mn)-VI and p-type III(Mn)-V DMS. Based on recent studies, it has been concluded that the strong spin splitting of the density of states which is associated with the s,p-d exchange interaction, with disorder effects as well as with electron-electron interactions plays an important role in the observed magnetic-field dependent transport properties of these two classes of DMS materials. One of the main consequences of the spin-splitting is a redistribution of carriers between spin-subbands. In degenerate semiconductors the redistribution starts when the spin-splitting energy becomes comparable to the Fermi energy, leading to an increase in the Fermi wave vector of majority-spin carriers. Since the scattering rate of the carriers depends usually on the Fermi wave vector, the redistribution affects the transport phenomena. Therefore, a negative MR effect can be caused by the

redistribution of the carriers in the spin subbands in an external magnetic field. On the other hand, in II(Mn)-VI DMS, M. Sawicki *et al*^[7] suggested that the positive MR observed in n-type CdMnSe is associated with quantum corrections to the conductivity which arise from the destructive effect of the giant spin-splitting on the Hartree corrections. Moreover, Y. Shapira^[4-6] *et al* suggested an increase of the Thomas-Fermi screening radius induced by the formation of spin clusters near impurities due to the spin splitting leading to a rise of the mobility edge causing the positive MR effect. However, no final agreement has been obtained on the explanation of the positive MR effect in II(Mn)-VI DMS. It only can be concluded is that positive as well as negative MR effects in DMS are dominated by the influence of the spin splitting effect.

On the other hand, the explanations mentioned above almost entirely ignore the importance of the disorder effect induced by the incorporation of the Mn ions,^[8] which can significantly affect the parameters related closely to the transport properties, i.e., the distribution of the occupied density of states near the Fermi level, the mobility etc. In fact, as far as disorder effects and their influences on the transport properties are concerned, there are already several successful theoretical models^[9-10] based on classical transport to explain many abnormal phenomena observed in disordered semiconductors with non-magnetic impurities. In the so called network model, the induced disorder can be described as following: the potential fluctuates due to the disorder on the length scale relevant for the transport, i.e., the potential is flat in the assigned length scale and a constant band mobility is assumed in cells of this scale; Alternatively, in the mobility model, one can work with flat bands throughout and a disorder dependent mobility. Then the mobilities depend on the change of the band edge with concentration of the impurity ions (e.g. Mn) and the magnetic field.

The basic idea of the network model is to divide the crystal into cubic cells of equal size (characterized by an edge length l) and to assign a local resistance which depends on the local disorder effect and the occupation of the local density of states in each cell. The Mn ions cause the giant Zeeman splitting, in addition to acting as impurities. Therefore, the disorder in the DMS system can be divided into a magnetic-field (H) dependent and a H -independent contribution. The resulting resistances are connected to a network forming the total resistance of the studied system. A two-dimensional $N \times N$ square array of cubic cells with index $m \in N^2$ is used to model the transport in an epitaxial layer. By solving Kirchhoff's equations for the network the macroscopic resistance is derived.

In the mobility model, the concept of treating the potential fluctuations is entirely different from the network model. The locally fluctuating electronic potential of each hole band of the

crystal is transformed into a flat potential characterized by a renormalized band edge, i.e., there is no dependence on a scaling length. Instead, an energy-dependent mobility fluctuation is introduced, which is determined by the characteristics of the potential fluctuation of the corresponding band.

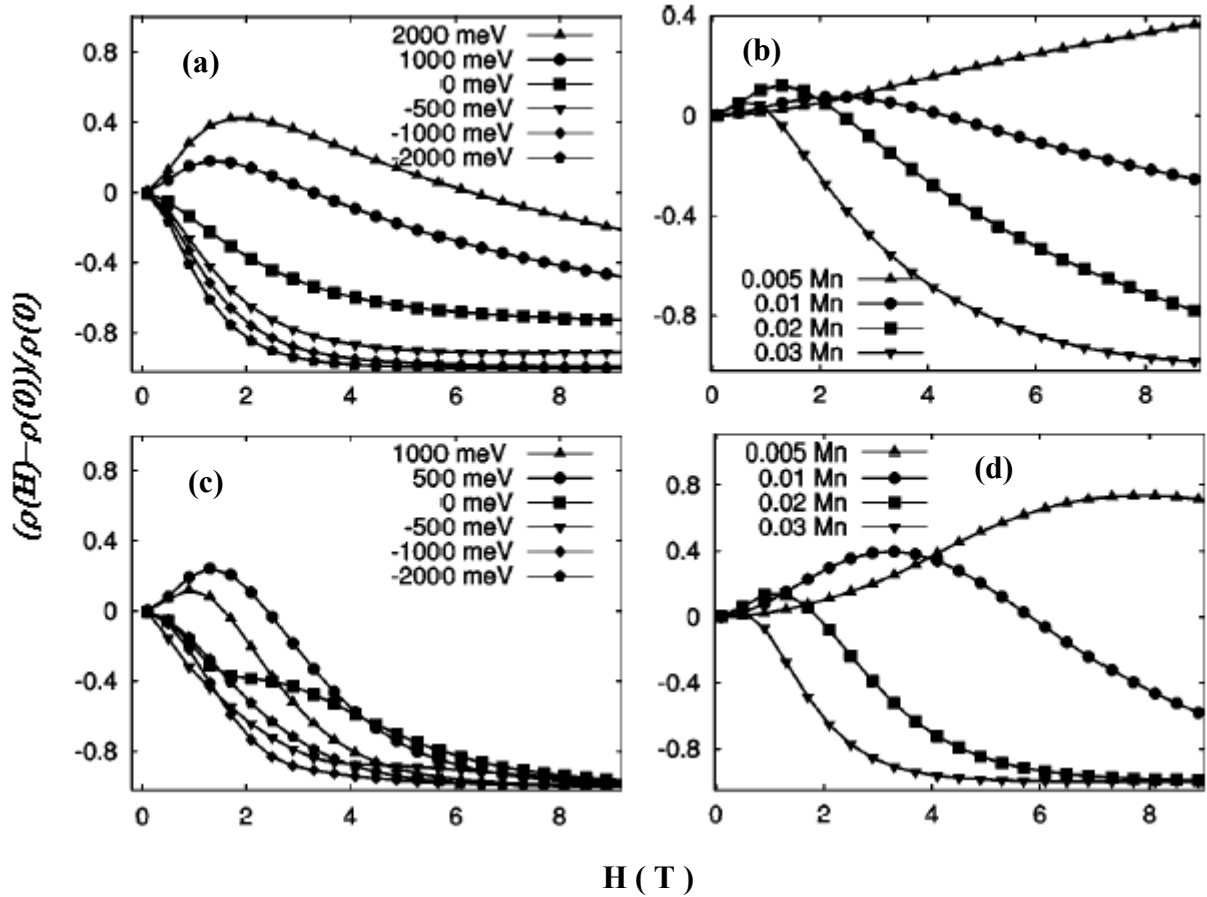


Fig. 3.5. (a) and (c) are MR for various disorder parameters with $T = 20\text{K}$, $E_A = 60\text{ meV}$, Mn concentration 0.01 calculated using network model and mobility model, respectively. (b) and (d) are MR for various Mn concentrations with fixing disorder parameters and $T = 30\text{ K}$, $E_A = 60\text{ meV}$, calculated using network model and mobility model, respectively.^[11]

Fig. 3.5 calculated from these two models shows a qualitative agreement with that observed in the II(Mn)-VI and III(Mn)-V DMS as described in Fig. 3.1. The results obtained from the network model and the mobility model can be summarized as follows: The obtained results depend on the applied magnetic field, on temperature, and on Mn concentration as shown in Fig. 3.5. Both models contain a free parameter, the edge length l in the network model and mobility cutoff factor in the mobility model. These two parameters determine strongly the

calculated MR behavior by weighting occupation and disorder effects. At low temperatures and in small magnetic fields, in the network model, the spin splitting effect of the valence band hardly changes the occupations of the four spin subbands. On the other hand, the field-induced disorder randomly modifies the resistances of the cells leading to an additional positive MR. This results in a plateau or positive MR curve. However, in the mobility model, the disorder-induced renormalization of the band gap enhances the occupation of all four bands which dominates the transport property, leading the local minimum in the MR curve.

In summary, negative and positive MR calculated by the network and mobility model show qualitative agreement with the experiments results on MR in II(Mn)-VI and III(Mn)-V DMS as shown in Fig. 3.1 and Fig. 3.4, more theoretical results can be found the paper from C. Michel et. al.^[11]

3.4. Hall measurements of paramagnetic GaAs:Mn alloy (MOVPE grown)

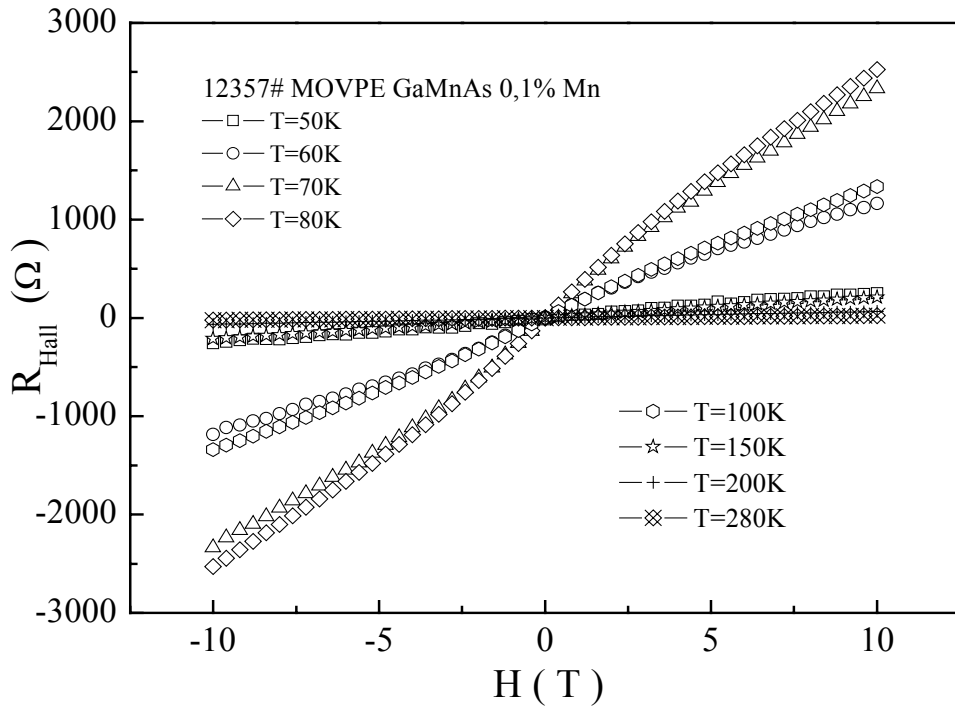


Fig. 3.6. Temperature dependence of the Hall resistance in GaAs:Mn alloy with a Mn concentration of 0.1%.

The Hall measurements were carried out on the GaAs:Mn sample with 0.1% Mn in the same T and H range as the MR measurements in Fig. 3.1. However, the Hall data can not be measured

at lower temperatures due to the strongly increased resistance. Therefore the temperature measurements only start from $T=50$ K as shown in Fig. 3.6.

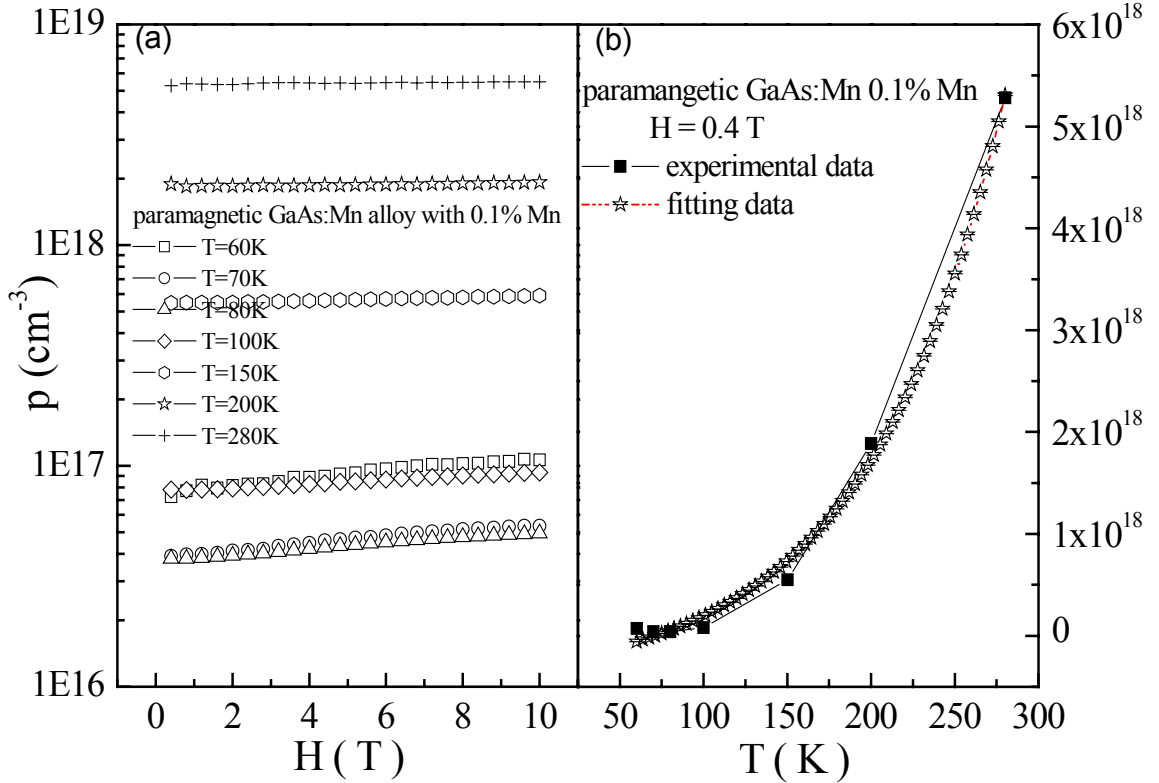


Fig. 3.7 (a) The magnetic field dependence of the carrier concentration at different temperatures. (b) The temperature dependence of the carrier concentration at $H = 0.4$ T of a GaAs:Mn sample with $x \sim 0.1\%$.

In diamagnetic semiconductors, the Hall resistance is usually proportional to the external magnetic field $R_H = \frac{1}{ne} \cdot H$, where the proportionality factor is basically one over the free carrier concentration. In contrast, the Hall resistance in ferromagnetic materials below the Curie temperature often shows magnetization-like behaviour, called anomalous Hall effect. In the paramagnetic samples studied here, the Hall resistance shows a little ‘S-shape’ behaviour as a result of the external magnetic fields at low temperatures ($T < 100$ K) region. With increasing temperatures, this unusual behaviour disappears and $R_{Hall}(H)$ shows a linear behaviour as function of the applied magnetic field, which is typical for normal semiconductor. The small variations of the Hall constants with field are due to the magnetic-field-induced tuning of the disorder and the density of states and respective carrier concentration. This is

well-known and typical for dilute magnetic semiconductors.^[12] For the whole measured temperature range, the Hall data are always analysed assuming that the anomalous Hall term is negligible compared to the ordinary Hall term. The reason is that the anomalous Hall voltage is proportional to the magnetization M of the Mn ions, but the susceptibility of this sample is much too small to cause a significant magnetization. According to the Hall measurements, we calculated the temperature dependence of the carrier concentration as a function of the applied magnetic field as shown in the Fig. 3.7. It confirms that the carrier concentrations depends on field. Moreover, it is confirmed that the sample is a p-type paramagnetic GaAs:Mn alloy, and the carrier concentration increases with increasing temperature, which obeys the $p = p_c e^{(-\Delta_c/2kT)}$ law for higher temperature.

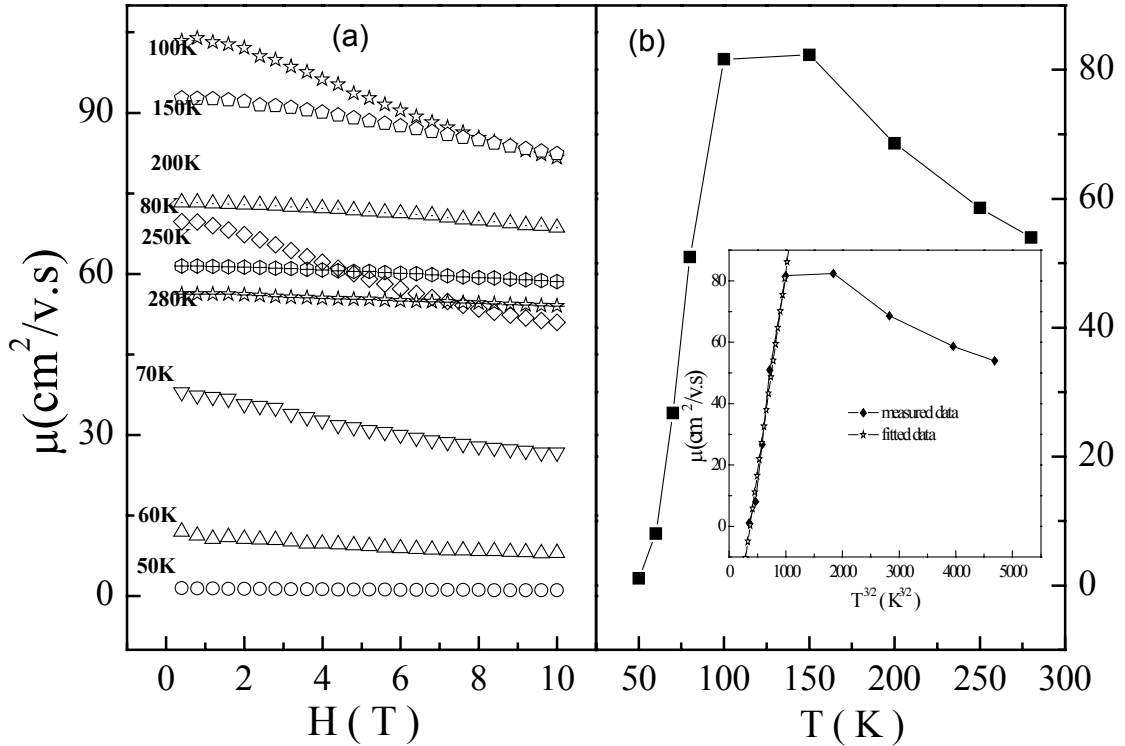


Fig. 3.8 (a) H -dependence of the mobility at different temperatures. (b) Temperature dependence of the mobility of a paramagnetic GaAs:Mn sample with $x \sim 0.1\%$.

The mobility of this sample at different temperatures was calculated using $\sigma = ne\mu$ at each field as shown in Fig. 3.8. It is found that the mobility decreases with increasing magnetic field and does not vary monotonously with temperature. Firstly the mobility increases with increasing temperature, but then reaches a maximum at about 100K, finally decreases again for

$T > 150$ K. On the other hand, it can be found the $\mu \propto T^{-3/2}$ in the low temperature region and $\mu \propto T^{-1/2}$ for high temperatures, as shown in the inset of Fig. 3.8(b), which shows the important influence of impurity scattering on the mobility at low temperatures. Moreover, when comparing with the MR effect, it is found that the parabolic MR effect is maximal at $T = 100$ K where the maximal mobility occurs.

In summary, the redistribution of the occupation of the four spin subbands and the H -dependent and H -independent disorder also play an important role in the Hall effect of DMS. The competition between occupation and disorder leads to the weighting of negative and positive MR effects and its strong dependence on the Mn concentration, temperature, and the growth conditions.

3.5 MR and Hall results of the paramagnetic GaAs:Mn,Te co-doped alloys

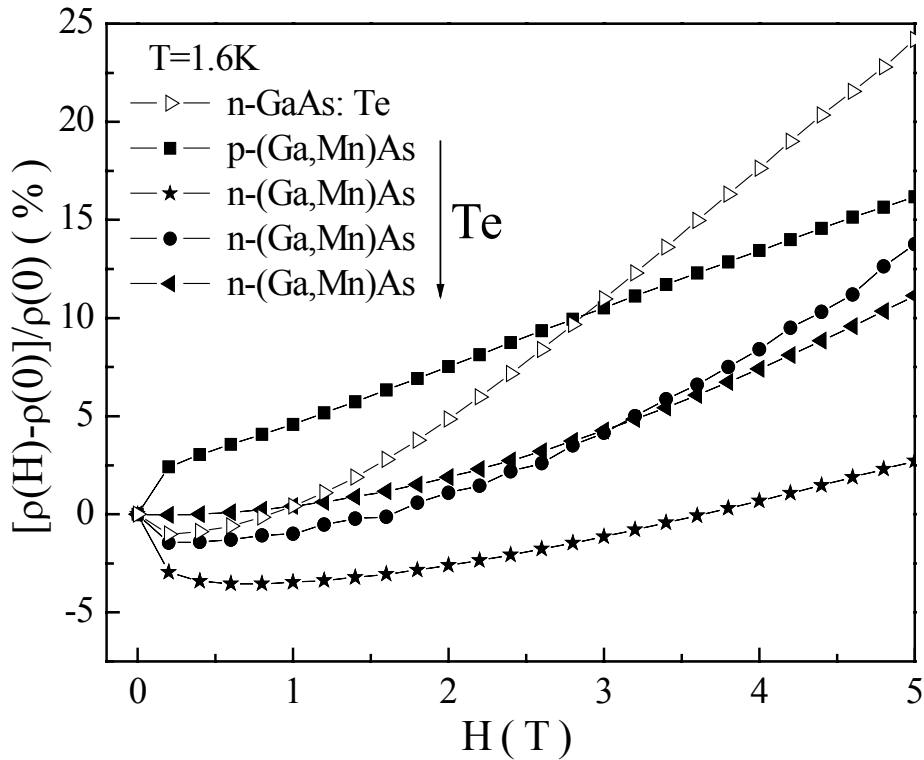


Fig. 3.9 MR effect at 1.6 K of GaAs:Mn alloy with 0.1% Mn and co-doped with different Te concentrations, and MR effect of a GaAs:Te reference sample. The arrow indicates increasing Te content.

In order to study the conduction band transport of paramagnetic GaAs:Mn DMS, Te is doped into p-GaAs:Mn with small Mn concentration, leading to a control of the carrier concentration by the Te incorporation which is almost independent of the Mn concentration. Fig. 3.9 depicts the variation of the MR effect at 1.6K due to co-doping with Te of paramagnetic GaAs:Mn layers. It is found that, at low temperatures, the p-type paramagnetic GaAs:Mn exhibits a positive MR effect due to the competition between the occupation effect and the disorder effect as discussed above. The n-type GaAs:Mn,Te samples on the other hand, show a negative MR effect at low fields and an almost positive parabolic behavior at higher fields. This is a typical curve known for highly n-doped GaAs^[13-14] as is also demonstrated by the MR curve of GaAs:Te without Mn doping (open triangles), which strongly resembles the MR curves of n-GaAs:Mn,Te. In other words, the positive MR effect due to the interplay between exchange effects and disorder vanishes and is replaced by a small negative MR related to weak localization effects. This change of the transport behavior with increasing Te concentration reflects the transition of the majority carrier type from p to n type confirmed by the Hall measurements as shown in the left graph of Fig. 1.5 in chapter 1. In case of conduction band transport, the *s-d* exchange interaction also induces a conduction band spin splitting. However, as the valence band exchange integral $|N_0\beta|$ is much larger than the corresponding $|N_0\alpha|$ of the conduction band, i.e. $|N_0\beta| \gg |N_0\alpha|$ in (Ga,Mn)As alloys as discussed in chapter 1, the *s-d* induced contribution to the MR in n-GaAs:Mn,Te is of minor importance and the weak Anderson localization effects dominate at the lowest temperature.

When the external field is zero, in the regime of Anderson localization induced by Te incorporation, the dominant scattering process is elastic (i.e., it holds $\tau_{elastic} \ll \tau_{inelastic}$ for the elastic and inelastic scattering times). Theoretically, weak localization^[15-17] originates from the Langer-Neal graph in the Kubo formalism, which deals with quantum corrections of several electronic properties of disordered systems. In a physical picture, it presents an interference with conduction electrons split into pairs of waves constructively interfering in the backscattering direction. This interference leads to an increase of the resistivity. When an external magnetic field is applied, the phase coherence of the two partial waves is destroyed, leading to a reduction of the backscattering amplitude, i.e., negative MR effect. Therefore, the transport property is considerably altered by the incorporation of Te into GaAs:Mn at the lowest temperature. The observed MR effects at the lowest temperature in GaAs:Mn,Te can be understood qualitatively as a superposition of a weak localization MR contribution and a classical transverse quadratic contribution. With increasing temperature, the inelastic scattering by longitudinal optical (LO) phonons becomes the dominant scattering process and

3. Transport properties of paramagnetic GaAs:Mn and co-doped GaAs:Mn,Te

$\tau_{elastic} \ll \tau_{inelastic}$ is no longer fulfilled, leading to a suppression of the weak localization effect. The decreasing weak localization leads to a smaller negative MR effect as confirmed in Fig. 3.10. On the other hand, it is found that the negative MR effect decreases with the Te concentration. This phenomenon can be due to the competition effects of the elastic scattering and the decreasing disordered potential by the Te incorporation.

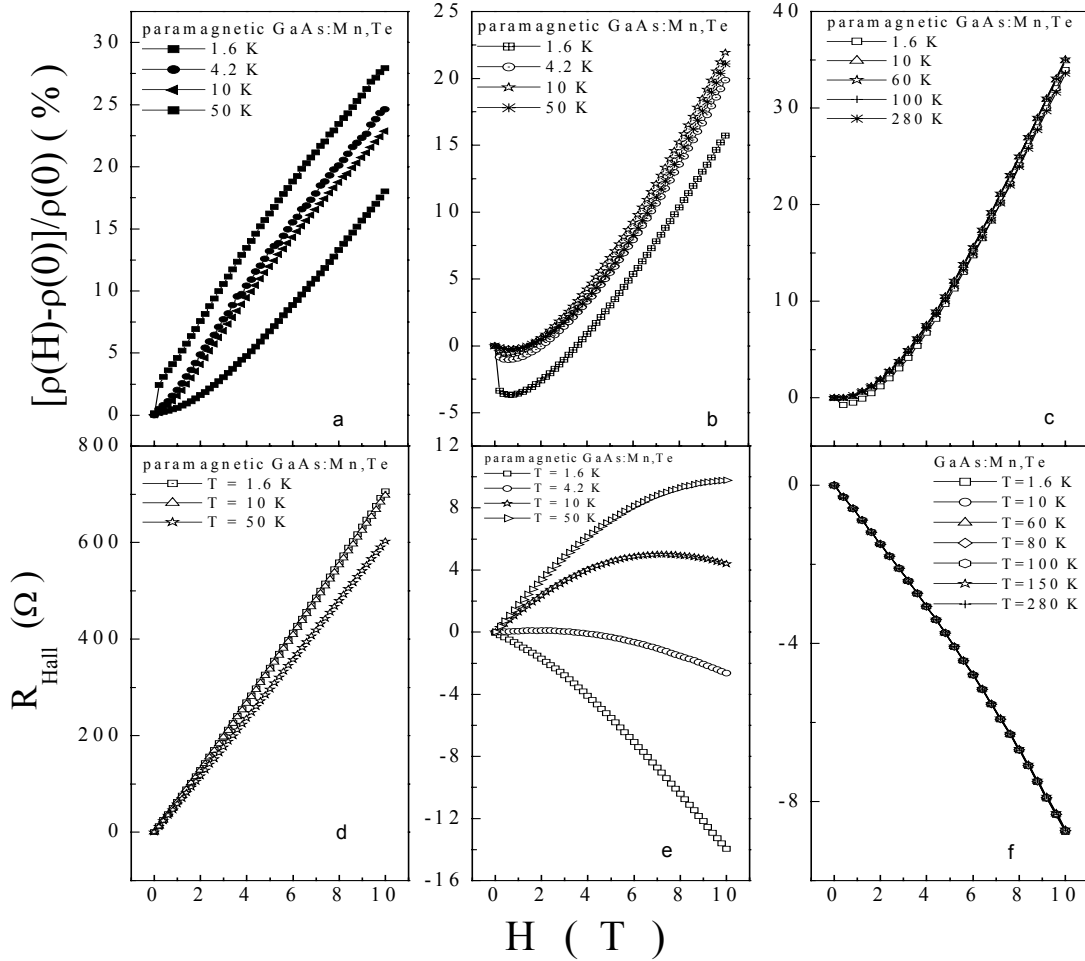


Fig. 3.10. MR and Hall resistance of GaAs:Mn,Te. The Te concentration increases from left to right.

Fig. 3.10 compares the magnetic field dependence of the magnetoresistance (MR) and the Hall resistance ($R_{xy}(H)$) at various temperatures for paramagnetic GaAs:Mn with different Te concentrations, from left side to right, the Te concentration increases. From Fig. 3.10(d)-(f), it is found that the slope of the $R_{xy}(H)$ changes from positive to negative indicating the p-type to n-type transition by the increasing Te concentrations. In Fig. 3.10(d) the magnetic field dependence of the $R_{xy}(H)$ shows an almost linear behavior and the positive slope of the $R_{xy}(H)$

indicates that the transport in the sample is dominated by holes at the lowest Te concentration. For the intermediate Te doping as shown in the Fig. 3.10(e), the curve of the $R_{xy}(H)$ is not linear any more, a bending with a increasing magnetic field indicates the combination of the two $R_{xy}(H)$ contributions with negative and positive slope, respectively. First, the negative slope of $R_{xy}(H)$ indicates electron-dominated transport at the lowest temperature, As the temperature increases, however, the slope switches sign to positive, indicating a transition from electron to hole-dominated transport. For the highest Te doping as shown in the Fig. 3.10(f), the negative slope of the $R_{xy}(H)$ is almost linear again and shows a weak dependence on the variation of the temperature, the sample is in the n-type region.

Correspondingly, the two band model for the Hall coefficient at low magnetic field can be expressed as follows:^[18]

$$R = \frac{p\mu_p^2 - n\mu_n^2}{(p\mu_p + n\mu_n)^2} \cdot e \quad (3.18)$$

where p and n are hole and electron concentration, μ_p and μ_n are the mobility of hole and electron, respectively.

However, at high magnetic field, the two band model for the Hall coefficient changes to:

$$R = \frac{1}{(p-n) \cdot e} \quad (3.19)$$

which indicates that the sign can be changed with increasing external magnetic field. The MR is modified by such transition from hole to electron-dominated transport as shown in Fig. 3.10(a)-(c), which can be attributed to the weak localization effect at low temperature as discussed above.

3.6. Summary

In summary, in the first part of this chapter we discussed the transport properties of the p-type paramagnetic GaAs:Mn with a small amount of Mn and $\text{Ga}_{1-x}\text{Mn}_x\text{As}$ alloys with x of a few percent. The magnetic field-dependent spin splitting of the valence band and disorder induced by Mn incorporation are responsible for the unusual positive and negative MR effects. The theoretical calculation by the network model and mobility model confirm the important roles of these two effects in the III(Mn)-V magnetic semiconductor especially in the low Mn region. By

adjusting the weighting of the effects of occupation and disorder, the negative and positive MR are obtained. The main difference between these two models is: In the network model, the fluctuation of potential induced by the disorder is regularized by the edge length of the cubes, i.e., the potential is flat on the assigned length scale. In the mobility model, the local fluctuating electronic potential of each hole band of the crystal is transformed into a flat potential characterized by a renormalized band edge and a distribution of mobilities determined by the disorder.

In the second part of this chapter, a series of GaAs:Mn,Te samples with different degrees of Te co-doping and with a small Mn concentration is discussed. The Hall measurements reveal the presence of both types of free carriers, electrons and holes. It is possible to change the majority carrier type from p to n type with Te co-doping. Te co-doping causes a transition from VB transport to CB transport. This allows one to probe the influence of p - d exchange interaction on the valence band transport and to probe the s - d exchange interaction on the conduction band transport, respectively. In the case of conduction band transport, the s - d exchange interaction inducing conduction band splitting and its contributions to the MR are of minor importance, confirms that the $|N_0\beta| \gg |N_0\alpha|$ in (Ga,Mn)As. Consequently, the contribution of the exchange interaction to the MR effect weakens and finally disappears with increasing Te concentration. In the regime of high Te doping, weak localization induced by Te incorporation dominates the transport properties.

References:

- [1] A. Van Esch, L. Van Bockstal, J. De Bock, G. Verbanck, A. S. Van Steenberghe, P. J. Wellmann, B. Grietens, R. Bogaerts, F. Herlach, and G. Borghs, Phys. Rev. B. **56**, 13103 (1997).
- [2] F. Matsukura, H. Ohno, A. Shen, and Y. Sugawara, Phys. Rev. B. **57**, R2037 (1998).
- [3] H. Ohno, J. Mag. Mag. Mat. **200**, 110 (1999).
- [4] Y. Shapira, D. H. Ridgley, K. Dwight, A. Wold, K. P. Martin, and J. S. Brooks, J. Appl. Phys. **57**, 3210 (1985).
- [5] Y. Shapira, N. F. Oliveira, Jr, D. H. Ridgley, R. Kershaw, K. Dwight, and A. Wold, Phys. Rev. B. **34**, 4187 (1986).
- [6] Y. Shapira, N. F. Oliveira, P. Becla, and T. Q. Vu, Phys. Rev. B. **41**, 5931 (1990).
- [7] M. Sawicki, T. Dietl, J. Kossut, J. Igalsen, T. Wojtowicz, and W. Plesiewicz, Phys. Rev. Lett. **56**, 508 (1986).
- [8] P. A. Lee and T. V. Ramakrishnan, Phys. Rev. B. **26**, 4009 (1982).

- [9] S. Fahy, and E. P. O'Reilly, *Appl. Phys. Lett.* **83**, 3731 (2003).
- [10] A. L. Efros and M. E. Raikh, chapter 3: effect of composition disorder on the electronic properties of semiconducting mixed crystal, in *Optical properties of Mixed Crystals*. Editors R. J. Elliott and I. P. Ipatova, (Elsevier, Amsterdam 1988).
- [11] C. Michel, P. J. Klar, S. D. Baranovskii and P. Thomas, *Phys. Rev. B.* **69**, 165211 (2004).
- [12] T. Omiya, F. Matsukura, T. Dietl, Y. Ohno, T. Sakon, M. Motokawa, and H. Ohno, *Physica E* **7**, 976 (2000).
- [13] M. Benzaquen, D. Walsh and K. Mazuruk, *Phys. Rev. B* **38**, 10933 (1988).
- [14] J.M. Monsterleet, B. Capoen and G. Biskupski, *J. Phys.: Condens. Matter.* **9**, 8657 (1997).
- [15] G. Bergmann, *Phys: Rev. B.* **28**, 2914 (1983).
- [16] V. K. Dugaev, P. Bruno, and J. Baranas, *Phys. Rev. B.* **64**, 144423 (2001).
- [17] A. Crepieux, J. Wunderlich, V. K. Dugaev, P. Bruno, *J. Mag. Mag. Mat.* **242**, 464 (2002).
- [18] D. K. Schroder, *Semiconductor material and device characterization*. (Wiley, New York 1990).

4. Magneto-transport in GaAs:Mn/MnAs-based paramagnetic-ferromagnetic hybrids prepared by MOVPE and post-growth annealing of MBE-grown $\text{Ga}_{1-x}\text{Mn}_x\text{As}$ alloys

MR and Hall effect of series GaAs:Mn/MnAs and GaInAs:Mn/MnAs paramagnetic-ferromagnetic hybrids prepared either by MOVPE directly or by post-growth annealing of $\text{Ga}_{1-x}\text{Mn}_x\text{As}$ alloys grown by low-temperature MBE are discussed in this chapter. The details about the fabrication methods have been given in chapter 2. It was concluded that the properties of the MnAs cluster and the GaAs:Mn matrix of the hybrids strongly depend on the growth procedures and annealing parameters. Magneto-transport measurements have been used to study the correlation between the magnetic properties and the spin transport behaviour of hybrids fabricated by different methods to be able to distinguish between the intrinsic and extrinsic effects in these samples. In case of MOVPE-grown GaAs:Mn/MnAs hybrids, the MnAs nanoclusters form in the hexagonal NiAs-structure (type I) and the Curie-temperature of 325 K is somewhat higher than that of bulk MnAs. The surrounding GaAs:Mn matrix exhibits paramagnetic behaviour down to 1.6 K. In chapter 3, we have discussed the MR results for paramagnetic GaAs:Mn matrix with Mn~0.1%, which shows a small positive MR effects dominated by the interplay of disorder effects and the p-d interaction between the localised spins of the magnetic ions and the free carriers spins. A hybrid consisting of the same paramagnetic matrix, but with ferromagnetic MnAs clusters, shows a very different MR behaviour. At low temperatures, a negative MR (-30% at $H = 10\text{ T}$) shows up independent of the MnAs cluster size, which is as well demonstrated in the following, caused by a localization process of the carriers around the clusters. With increasing temperatures, the negative MR changes to a large positive MR which is suggested to be due to a spin-filter effect within the cluster-matrix system. The magnitude of this filter effect can be tuned by the size and shape as well as by the density of the clusters. A somewhat similar MR behaviour as a function of field and temperature was also observed in GaAs:Mn/MnAs hybrids prepared by other methods^[1] and in $\text{Ge}_{1-y}\text{Mn}_y/\text{Mn}_{11}\text{Ge}_8$ ^[2] hybrids. Therefore, the coexistence of a negative and a positive MR effect seems to be a common feature of paramagnetic-ferromagnetic granular hybrids. Both the ferromagnetism of MnAs clusters and the paramagnetism of the matrix play important roles for the spin-dependent transport in such hybrids, leading to large unusual MR effects. In case of the GaAs:Mn/MnAs hybrids prepared by post-growth annealing of $\text{Ga}_{1-x}\text{Mn}_x\text{As}$ alloys grown by low-temperature MBE, two types of clusters are observed. Besides the type I clusters small zincblende-type clusters with a Curie temperature of about 80 K (type II) have been found. A positive MR takes over from the

negative MR with increasing annealing temperature. For the GaInAs:Mn/MnAs hybrids, a transition from negative to positive MR with temperature is not observable. The reason for that and possible microscopic origins behind this mechanism will be discussed in this chapter.

4.1. Unusual MR effects in MOVPE-grown GaAs:Mn/MnAs hybrids

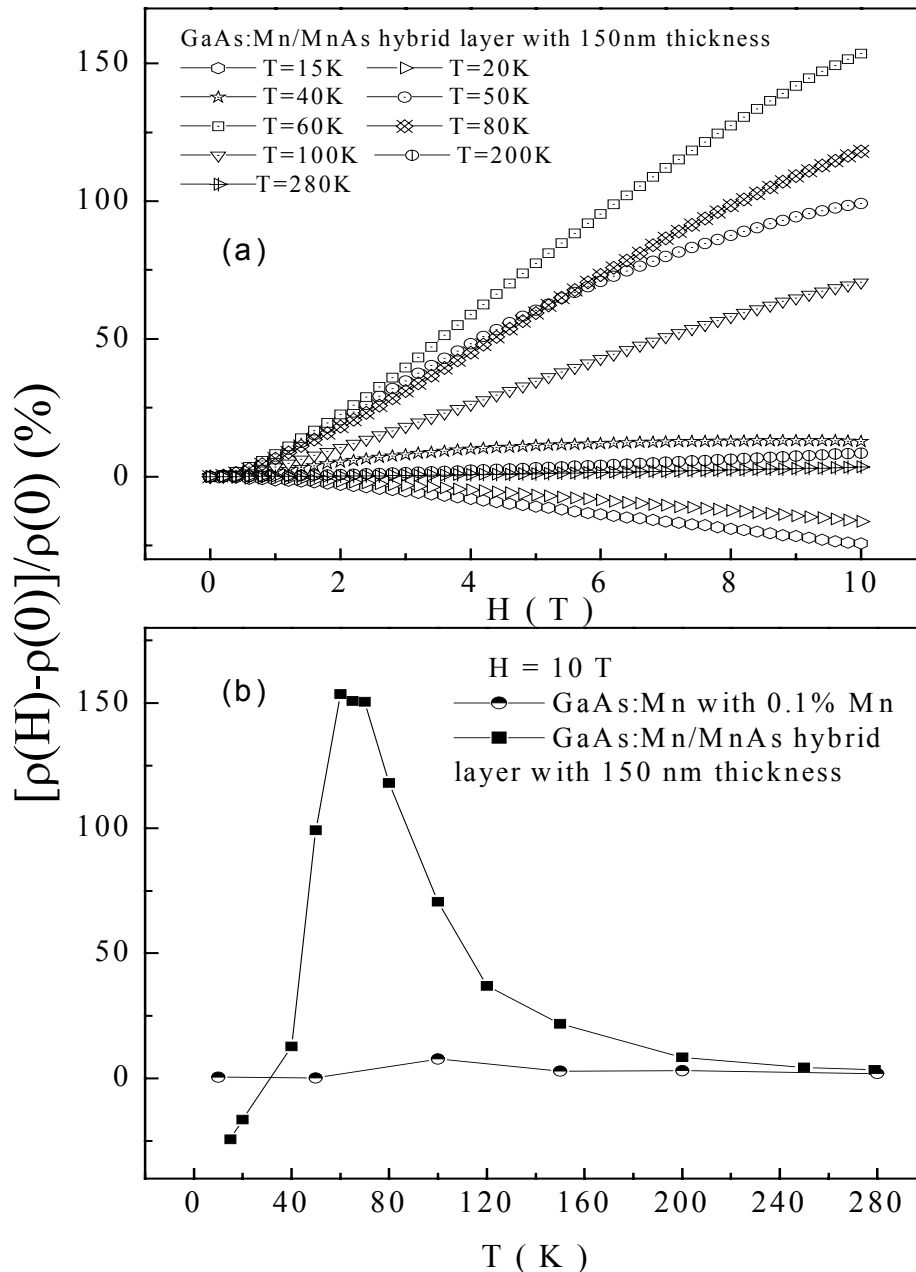


Fig. 4.1 (a) Temperature dependent MR results of a GaAs:Mn/MnAs hybrid with 150nm thickness in the temperature range between 15 K and 280 K. **(b)** Comparison of the temperature dependence of the MR value at $H = 10$ T for a paramagnetic GaAs:Mn matrix with and without ferromagnetic MnAs clusters.

Tab. 4.1 Carrier concentration at room temperature for the GaAs:Mn/MnAs hybrids of different thicknesses

Thickness (nm)	150	300	500	1000
Carrier concentration $p(\text{cm}^{-3})$	$2.9 \cdot 10^{18}$	$2.4 \cdot 10^{18}$	$2.0 \cdot 10^{18}$	$2.0 \cdot 10^{18}$

Fig. 4.1(a) depicts typical temperature dependent MR results for a GaAs:Mn/MnAs hybrid of 150 nm thickness between 15 K and 280 K. At low temperatures, one can observe a strong negative MR effect. As shown in Fig. 4.1(a), firstly the MR curve decreases slowly, and then decreases faster and monotonically without saturation with increasing the applied magnetic field H , and a MR ratio value of -30% is achieved at $H=10$ T. With increasing temperature, the negative MR effect is suppressed and then changes to a positive MR which increases quickly with temperature and reaches a maximum value of 160% at $H = 10$ T without saturation at 60 K. Then, the positive MR decreases and changes to a normal (quadratic) MR effect at room temperature as seen in the inset. Fig. 4.1(b) is a comparison of the temperature dependence of the MR value at $H = 10$ T for the paramagnetic GaAs:Mn with and without ferromagnetic MnAs clusters, which confirms that the magnitude of the MR effect is enhanced significantly by the presence of the MnAs clusters in the GaAs:Mn matrix.

Fig. 4.2 depicts the temperature dependent MR value at $H=10$ T for different GaAs:Mn/MnAs hybrids obtained by MOVPE growth. In this series the size and density of the ferromagnetic MnAs clusters within the samples were varied by varying the layer thickness between 150 nm and 1000 nm. The diameter of the clusters changes from 35 nm to 120 nm and the height from 15 nm to 150 nm with increasing layer thickness. These results were obtained by TEM as described in chapter 2. Furthermore, the clusters are always found in the vicinity of the surface, i.e., the fraction of the matrix not including clusters (the deeper layers) increases with increasing thickness of the hybrid. On the other hand, Hall measurements confirm that the carrier concentrations in this series of hybrids are comparable with each other indicating that the properties of the GaAs:Mn matrix are similar (Tab. 4.1). Similar trends for the temperature-dependent MR effects are observed throughout the series as shown in the Fig. 4.2(a). With increasing size of the clusters and fraction of the cluster-free matrix in the hybrid, it can be found that 1) The negative MR effect is the same for all samples; 2) The maximum value of positive MR effect decreases and the corresponding temperature shifts slightly to higher temperatures; 3) The transition temperature from a negative to a positive MR effect also shifts to higher temperatures.

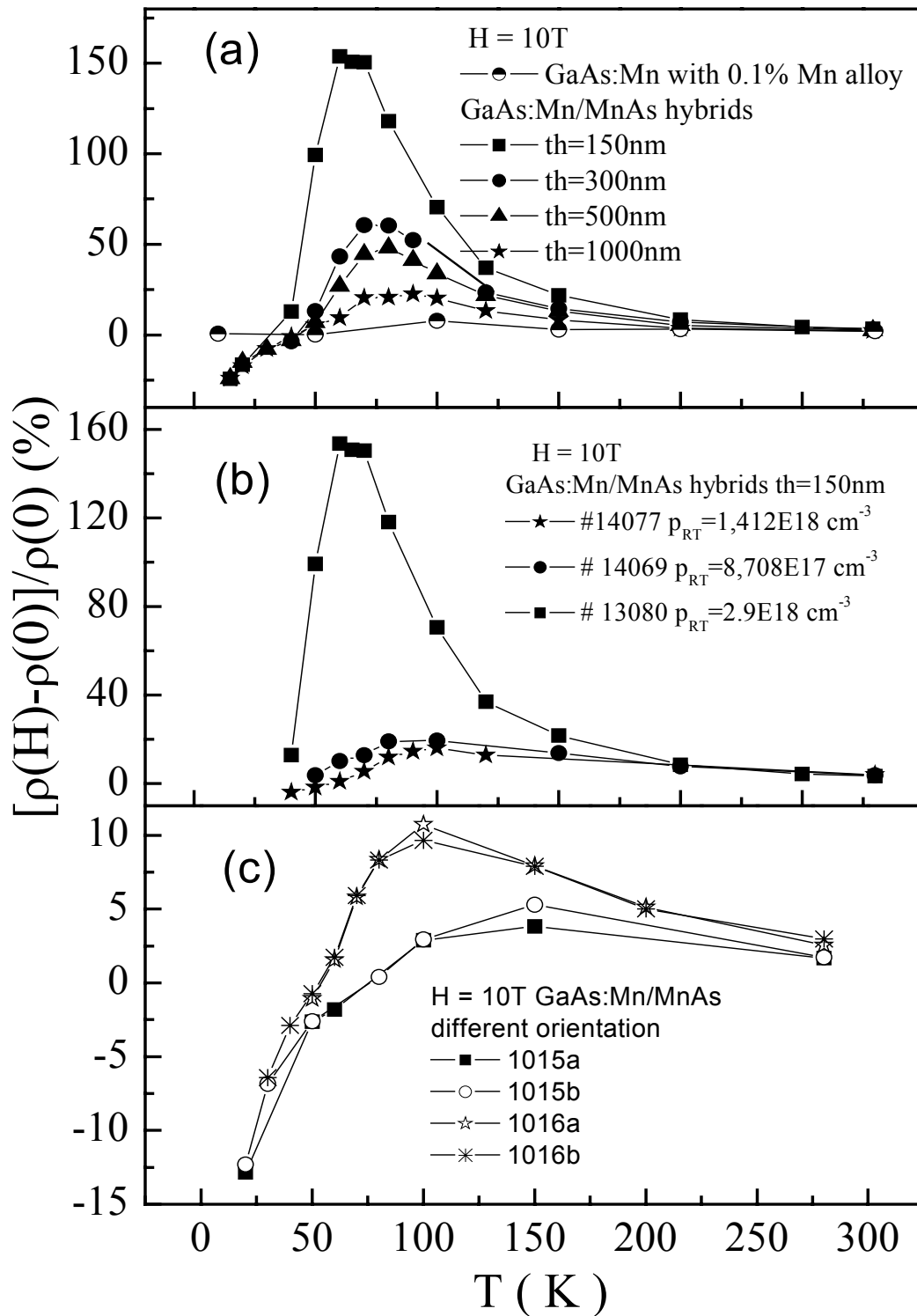


Fig. 4.2 Temperature dependence of MR at $H = 10$ T for Ga:As:Mn/MnAs hybrids (a) different thickness of the hybrids (b) Different growth temperatures and rates with the same thickness. (c) Different orientations of the MnAs clusters.

In a second series, the thickness of the layer is fixed at 150 nm whereas the size of clusters is increased as well as the Mn concentration in the paramagnetic matrix is decreased by varying the growth rate, V/III ratio, and growth temperature. This series also shows a transition from a negative to a positive MR, but generally much smaller effects with increasing growth temperature as shown in Fig. 4.2(b). In a third series, the preferred orientation of the c-axis of the ferromagnetic MnAs clusters was varied by adjusting the V/III ratio. It was found that this series also shows a negative to a positive MR transition, but the MR maximum shifts to higher temperature. Again, the MR effects are much smaller than for the first series effect as shown in Fig. 4.2(c). The observed positive MR is mainly due to the normal parabolic MR effect. Therefore, the MR effect of GaAs:Mn/MnAs hybrids strongly depends on the growth parameters.

4.2. Qualitative and quantitative discussion of the microscopic mechanism for the negative MR in MOVPE-grown GaAs:Mn/MnAs hybrids

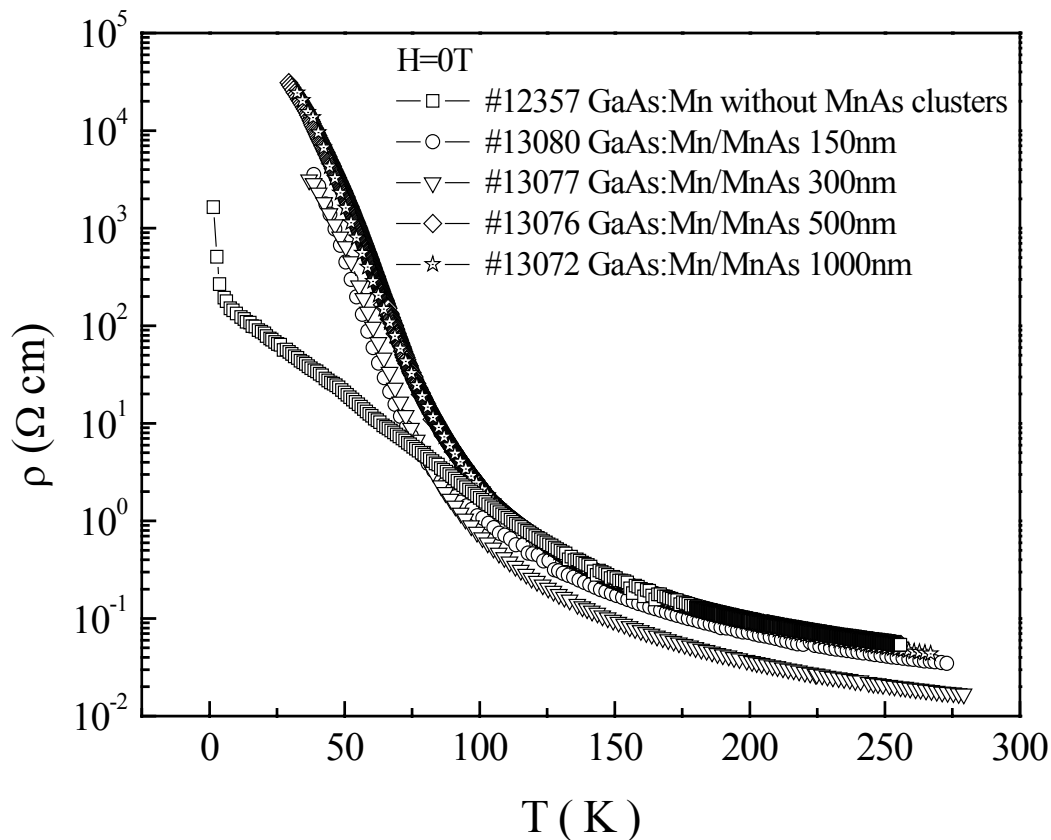


Fig. 4.3 Temperature dependence of the resistivity for GaAs:Mn with and without ferromagnetic MnAs clusters at $H=0$ T.

Fig. 4.3 gives the temperature dependence of the resistivity of GaAs:Mn with and without ferromagnetic MnAs cluster at zero external magnetic field. It is found that the resistivity is enhanced significantly at low temperatures by adding the ferromagnetic MnAs nanoclusters, and is almost independent on the thickness of the hybrids.

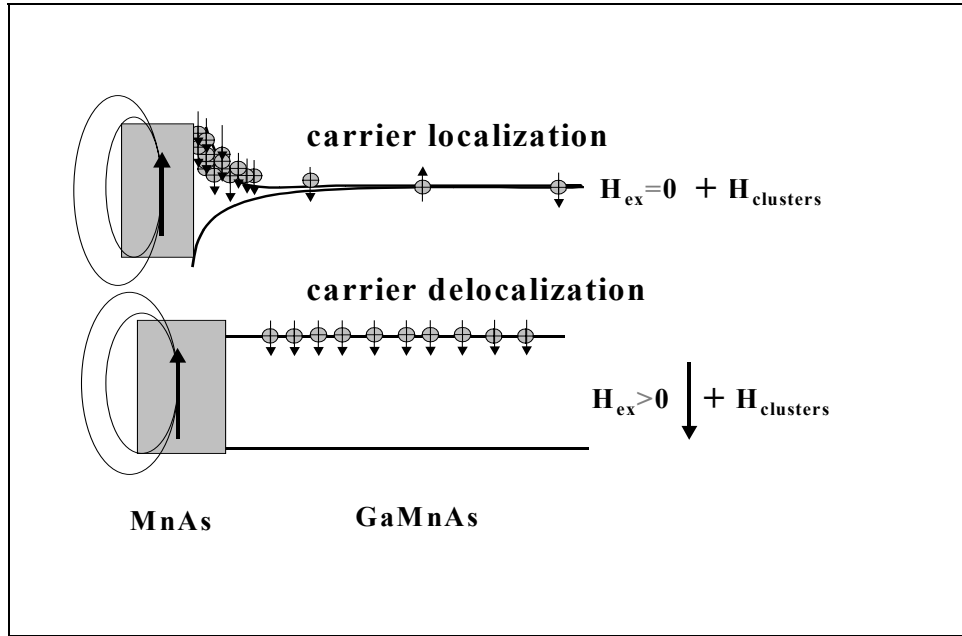


Fig. 4.4 A schematic representation of the mechanism yielding the negative MR effect.

For all the GaAs:Mn/MnAs hybrids studied, there are two important interactions between the ferromagnetic MnAs clusters and the paramagnetic GaAs:Mn matrix dominating the spin-dependent transport effects. One is the local giant Zeeman splitting occurring in the paramagnetic GaAs:Mn matrix in the vicinity of the cluster induced by the local magnetic field from the ferromagnetic MnAs clusters. This interaction can lead to the localization of the carriers in zero applied magnetic field in the region of high stray fields. Recently theoreticians have suggested that nanoscale Zeeman localization of carriers in paramagnetic semiconductors with ferromagnetic islands or permalloy hybrid structures might occur^[3,4]. In fact, even relatively small magnetic field 0.1-0.5 T can easily lead to 15 meV Zeeman splitting of the band states.^[5] Due to the giant Zeeman splitting, the inhomogeneous magnetic field produced by a ferromagnetic island or permalloy causes a local effective potential well that can efficiently trap spin-polarized carriers in the DMS at the interface to the ferromagnet. This interaction depends on the size and density of the ferromagnetic nano-particles, as well as on the effective g-factor determined by the concentration of the magnetic ions in the DMS and the magnitude of the exchange integrals. On the other hand, the interface between the metallic

or half-metallic MnAs clusters and GaAs:Mn paramagnetic semiconductor might act as a Schottky barrier producing another local potential due to the establishment of a single Fermi-level within the hybrid. Therefore, the combination of the two effects leads to a local spin dependent-band bending in the paramagnetic matrix near the ferromagnetic MnAs clusters.

Fig. 4.4 is a schematic representation of a possible mechanism yielding a negative MR based on a trapping of the free carriers at the cluster-matrix interface. Firstly, at zero applied magnetic field, the local magnetic field is not zero in the paramagnetic matrix due to the presence of the ferromagnetic clusters. An estimation of the dipolar field of a cluster with a density of the Mn-ions of $n_{\text{Mn}} \sim 3 \times 10^{28} \text{ m}^{-3}$ and a magnetic moment per Mn-ion of $3.4\mu_B$ ^[6] yields a magnetic field of about 1 T at the surface of the clusters. At low temperatures, this is almost sufficient to saturate the giant Zeeman splitting in the paramagnetic matrix close to the clusters, which induces a potential trap for the carriers with the spin orientation whose energy is lowered by the giant Zeeman splitting, i.e., traps spin-polarized carriers. Obviously, the trapping effect depends on 1) the temperature dependence of the Zeeman splitting given by the Brillouin function of the local average Mn-spin $\langle S_z \rangle$; 2) the density of the clusters. When an external magnetic field is applied, the giant Zeeman splitting occurs throughout the entire paramagnetic GaAs:Mn matrix, and the localized carriers of defined spin become delocalised, leading to a negative MR effect. With increasing temperature, the magnetic field of about 1 T induced by the clusters is no longer sufficient to saturate the Zeeman splitting and the trap depth decreases with increasing temperature following the Brillouin function. In addition, the thermal energy of the holes $k_B T$ increases with temperature. Therefore, this negative MR effect disappears with increasing temperatures.

A more quantitative insight into the negative MR effect can be gained by performing calculations using an extension of the network model developed previously for describing MR effects in chapter 3. The resistivities of the paramagnetic matrix are basically the same as in the case without clusters. To account for cluster effects in the model: 1) a single MnAs cluster is centered in a 25×25 network of cubic cell, with its size comprising 10% of the total system; 2) The cells representing the metallic cluster have a much lower resistance than the average cell of the semiconducting GaAs:Mn matrix; 3) The local band bending in the matrix near the cluster arises from the formation of a (spin- and H -field dependent) local Zeeman splitting and a spin and H -field independent Schottky barrier. It was assumed that the local magnetic field caused by the cluster decreases with d^3 . 4) The Schottky barrier was set to 20 meV (H -field and T -independent). As the electronic structure of MnAs is basically unknown, the Schottky barrier is assumed to decrease with d^5 . The corresponding energy shifts are added in

each cell. This way, in addition to the H -dependent spin splitting of the valence band and disorder effect by Mn incorporation in the paramagnetic matrix, the effects of the local Zeeman splitting and Schottky barriers induced by the MnAs clusters are included in the model. The following results have been obtained. The large negative MR effect at low temperatures caused by the release of the localized holes by applying a magnetic field are successfully modelled as shown in Fig. 4.5, which is in agreement with the experimental results.^[7] Furthermore, it can be seen that the temperature dependence of the resistivity of the samples changes after incorporating the clusters. The resistivity of the hybrids is significantly larger at low temperatures than that of a GaAs:Mn matrix without clusters due to the trapping of the carriers. At higher temperatures this effect is less significant. The magnitude of the trapping depends on the choice of the Schottky barrier and that of the cluster-induced local magnetic field.

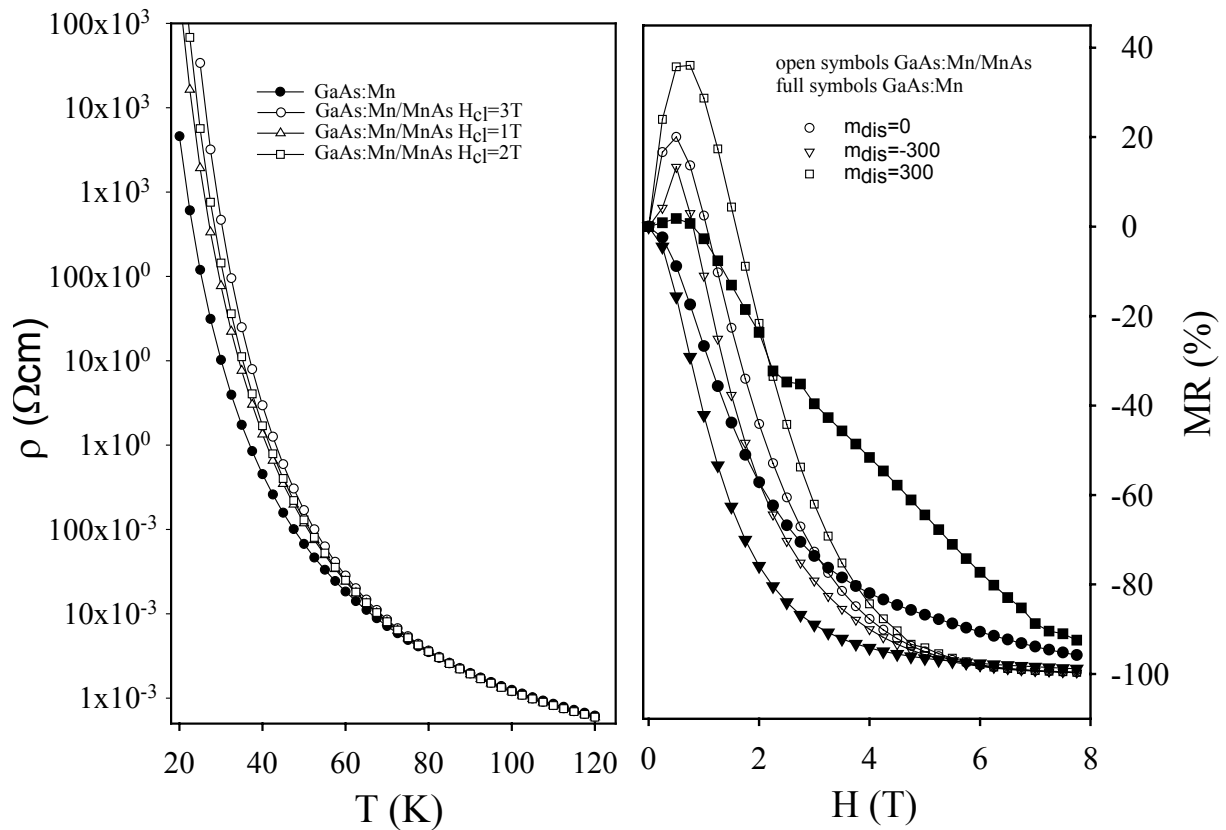


Fig. 4.5. Left: Calculated temperature dependence of the resistivity of paramagnetic GaAs:Mn and GaAs:Mn/MnAs hybrids at $H = 0\text{ T}$. Right: calculated MR curves for paramagnetic GaAs:Mn and GaAs:Mn/MnAs hybrids for various field-independent disorder parameters at $T = 30\text{ K}$.

At zero magnetic field and at low temperatures; a dramatic increase of the resistivity of the hybrid samples is observed in the experiment as show Fig. 4.6(a). Such strong increase is not observed in the paramagnetic GaAs:Mn alloy without MnAs. Therefore, the calculations are in good qualitative agreement with experimental results.

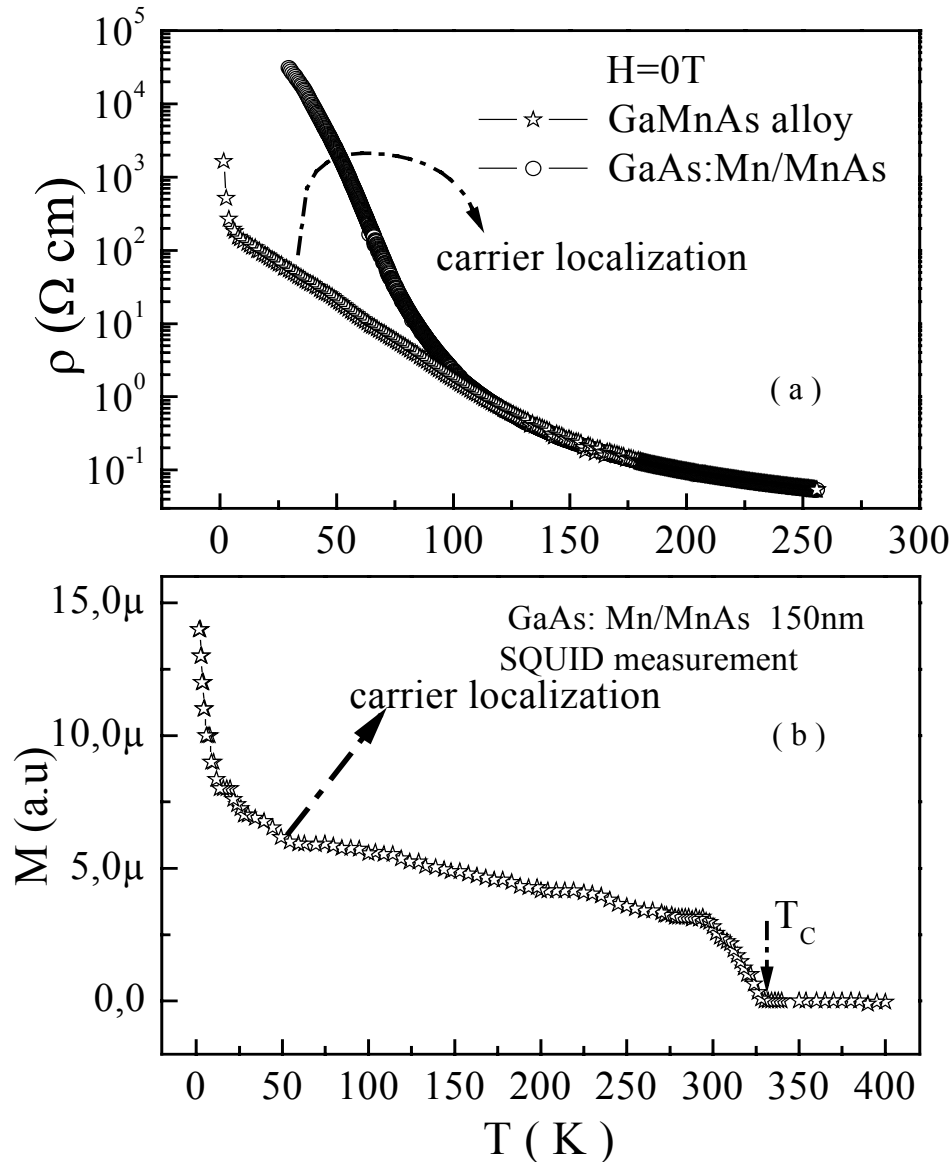


Fig. 4.6. Experimental evidence for a localization of carriers at low temperatures. (a) Comparison of the temperature dependence of the resistivity of samples with and without MnAs clusters at zero field. (b) Temperature dependence of the magnetization obtained by SQUID measurements for a GaAs:Mn/MnAs hybrid.

Fig. 4.6(b) presents the temperature dependence of the magnetization of a GaAs:Mn/MnAs hybrid obtained by a SQUID measurement. It is found that in addition to the magnetization of

the ferromagnetic MnAs clusters, which disappears on approaching the paramagnetic to ferromagnetic transition at 325 K, an abnormal enhanced magnetization is observed at low temperatures $T < 50$ K. This enhanced magnetization is caused by the trapping of spin-polarized carriers at the cluster-matrix interface, at low temperatures, due to the stray fields of the ferromagnetic MnAs clusters.

4.3. Qualitative description of the microscopic mechanism for the positive MR in MOVPE-grown GaAs:Mn/MnAs hybrids

In this section, the possible reason for the observed positive MR will be discussed. At a first glance it might be caused by the so called extraordinary magneto-resistance (EMR) effect, which has been observed in hybrids consisting of a high-mobility diamagnetic semiconductor with diamagnetic metal inclusions. The basic idea of the EMR effects is the following. If the conductivity contrast between the semiconductor and the metal is large (i.e., $\sigma_S \ll \sigma_M$), the current path through the hybrid changes when a magnetic field is applied. With no magnetic field, the current density \vec{j} is parallel to the local electric field \vec{E}_{loc} . The current flow through the material is focused into the metallic region, i.e., the metal inclusion act as short circuits. At high magnetic fields, the Lorentz force results in a directional difference between the \vec{j} and \vec{E}_{loc} . The angle between them being the Hall angle θ_H which is given by

$$\theta_H = \arctan(\mu_H H_{ext}) = \arctan\left(\frac{R_H H_{ext}}{\rho_0}\right) \quad (4.1)$$

where μ_H is the Hall mobility, R_H is the Hall constant and ρ_0 is the resistivity at $H_{ext}=0$. Due to the conductivity contrast, the local electric field \vec{E}_{loc} is perpendicular to the metal cluster surface. The Hall angle approaches 90° , leading to a current deflection at the metal clusters which then act as open circuits. The transition of the metal inclusions from a short circuit in zero-field to an open circuit at high field gives rise to the positive MR effect in such diamagnetic hybrids. To obtain a Hall angle close to 90° at fields below 10 T, a high mobility in the semiconductor is required. However, our GaAs:Mn reference sample has a rather small mobility of about 80 Vs/cm² which corresponds to a Hall angle at $H=10$ T of about 5° only. Therefore, the large positive MR effect observed in GaAs:Mn/MnAs hybrid can't be due to the EMR effect.

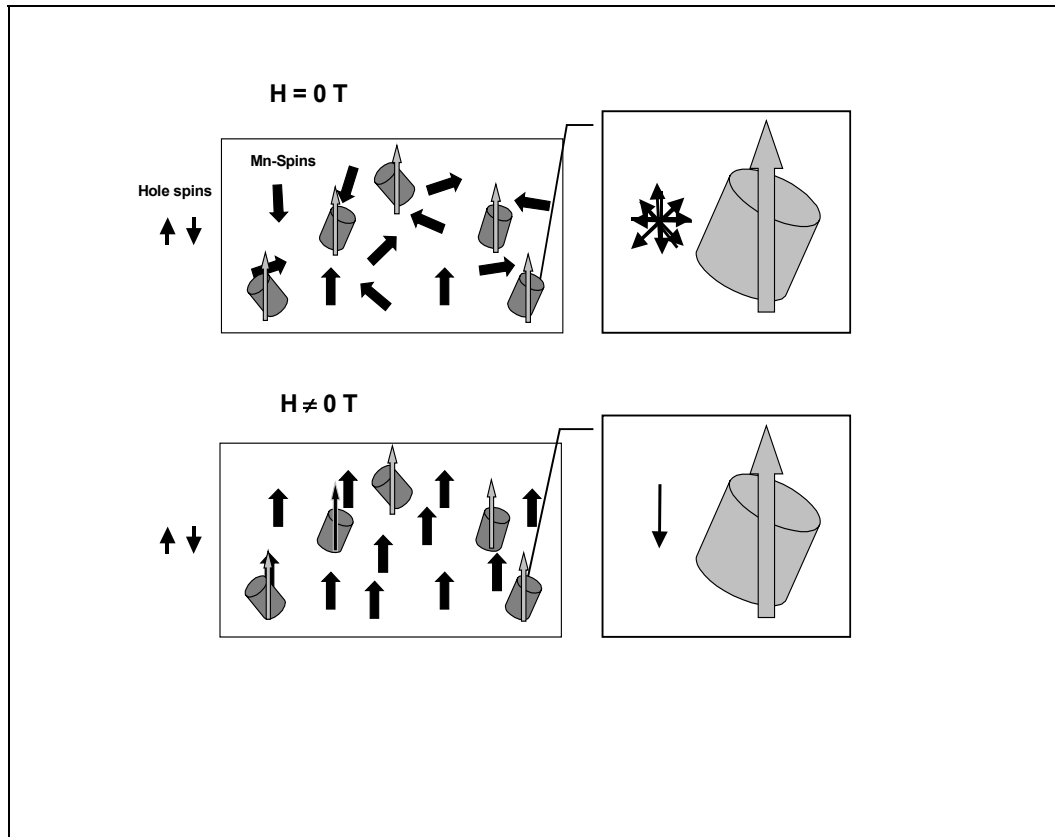


Fig. 4.7. A schematic representation of a possible mechanism due to the spin-dependent scattering yielding a positive MR effect.

The MR mechanism depicted in Fig. 4.7 is suggested to cause the positive MR effect in the GaAs:Mn/MnAs hybrid studied. This positive MR arises due to spin-dependent scattering. At zero magnetic field, the spin information of a single carrier is immediately lost due to scattering with the randomly oriented Mn $S=5/2$ spins. The spin-flip length is much smaller than the mean distance (50-200 nm, according to AFM measurements of the 500°C sample, 140 clusters/ μm^2 , the average diameter is about 80 nm) between the ferromagnetic clusters. Two independent effects are induced by switching on the magnetic field 1) the Mn $S=5/2$ ions become aligned and via the p-d exchange interaction align in turn the hole spins, which results in a preferential orientation of the carrier spins; 2) The magnetization of the MnAs clusters will be aligned along the field direction. This alignment of the MnAs cluster magnetization favours one carrier spin orientation at the Fermi edge within the clusters. Therefore, if the spin orientation favoured by the matrix is opposite to that favoured by the clusters, scattering of the carriers by the cluster leads to a change of its spin orientation. This change induces an enhancement of the spin disorder scattering between the carriers themselves as well as between carriers and the clusters, yielding a positive MR effect. The ability of the paramagnetic matrix to preferentially align the carrier spins decreases with

increasing temperature, i.e. the thermal disorder destroys the preferential orientation of the Mn-ions, leading to the decreasing of the large positive MR with increasing temperature as found in the experiments. As shown in Fig. 4.2, the magnitude of the positive MR effect is very sensitive to the properties of the paramagnetic GaAs:Mn matrix as well as the density, size, and orientation of the MnAs clusters.

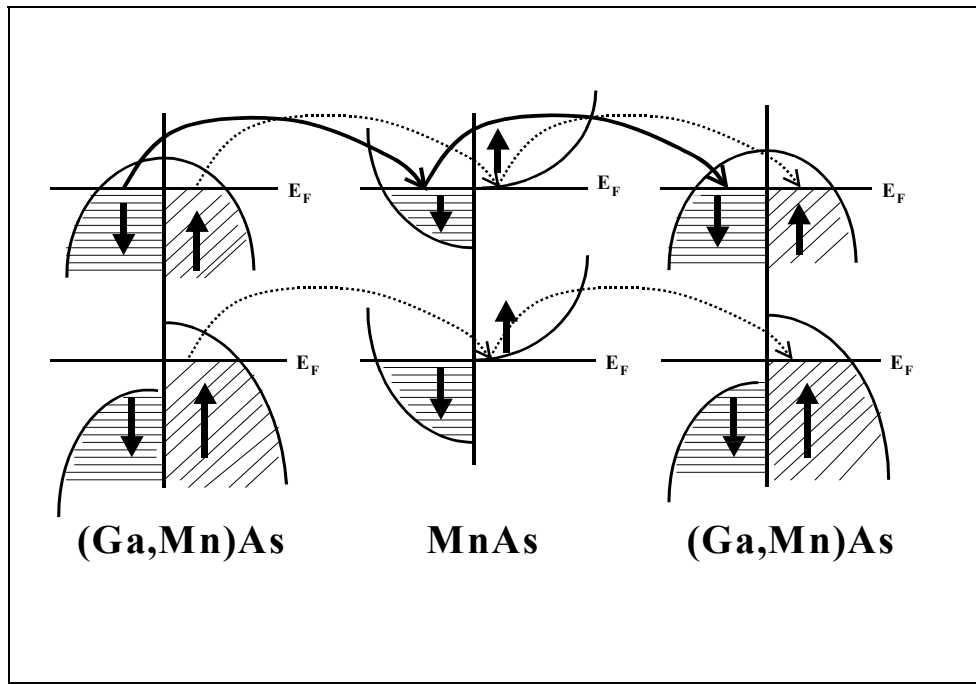


Fig. 4.8. A schematic representation the positive MR caused by the spin-filter effect of the clusters yielding a positive MR.

Alternatively to the spin scattering picture, the large positive MR can be also understood in a density of states picture. The underlying model is the two current-channel model where the ferromagnetic MnAs clusters act as spin-filters as shown in the Fig. 4.8. When no magnetic field is applied, the density of spin-up and spin-down states is the same in the paramagnetic GaAs:Mn matrix. Therefore, carriers of each orientation can pass through the MnAs clusters acting as a short circuit. With an applied magnetic field, the Zeeman splitting in the paramagnetic matrix causes an imbalance of the density of states for the spin-up and spin-down carriers, i.e., majority and minority spins. If the majority spins of the clusters are different to those in the matrix for $H \neq 0$, the possibility of carriers to pass through MnAs clusters is suppressed due to the MnAs clusters acting as open circuits in such case. Then a positive MR effect occurs.

4.4. Unusual Hall effects in MOVPE-grown GaAs:Mn/MnAs hybrid

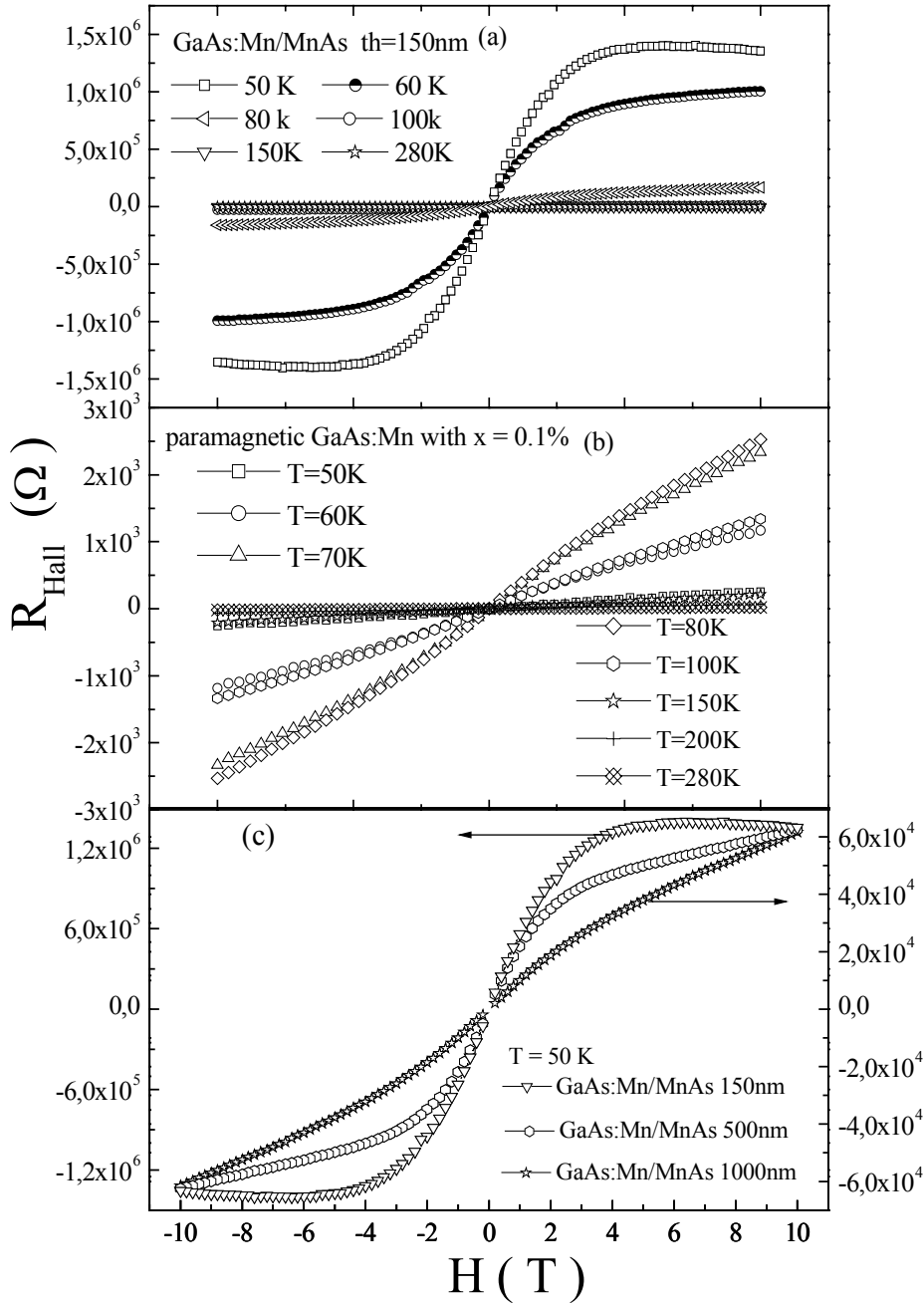


Fig. 4.9(a) Temperature dependence of the Hall resistance in a GaAs:Mn/MnAs hybrid with the film thickness $th = 150$ nm. **(b)** Temperature dependence of the Hall resistance in a paramagnetic GaAs:Mn sample without MnAs clusters. **(c)** Hall resistances of hybrids with different film thickness from 150 nm to 1000 nm at $T = 50$ K.

An associated phenomenon is the unusual behaviour of the Hall resistance observed in GaAs:Mn/MnAs hybrids. As shown in Fig. 4.9(a), at $T = 50$ K, the Hall resistance (R_{Hall}) of a GaAs:Mn/MnAs hybrid with small clusters increases quickly at low magnetic fields, and kind

of saturates at a magnetic field $H=4$ T, then almost keeps constant up to $H=10$ T. This Hall effect is quite different from that in paramagnetic GaAs:Mn samples where R_{Hall} shows an almost linear behaviour with the magnetic field as shown in Fig. 4.9(b). It is suggested that the observed unusual Hall curves in these hybrid structures can be attributed to a spin-dependent effect.

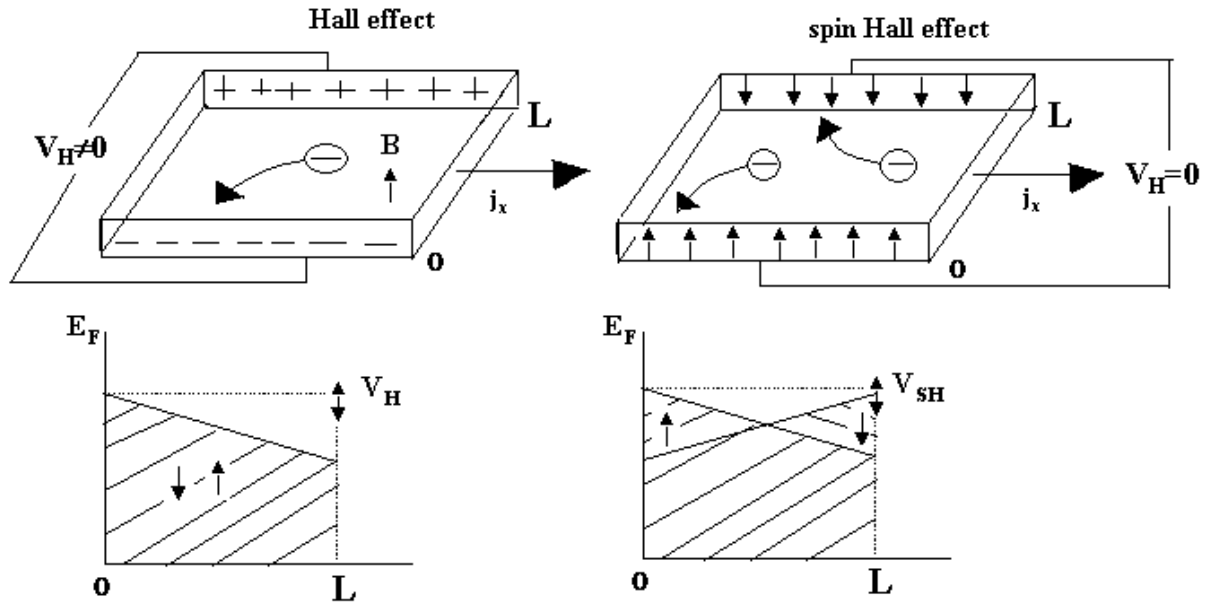


Fig. 4.10 Schematic representation of comparison of normal Hall effect (left figure) and spin-Hall effect (right figure).^[9]

Until now, the spin-dependent Hall contributions discussed in the literatures focus on two effects. One is observed in the ferromagnetic semiconductors, ferromagnetic metal, or ferromagnetic metal-normal metal hybrid, named as ‘spontaneous’ or ‘anomalous’ Hall effect. The anomalous Hall resistivity (transverse electric field per unit longitudinal current density) is found to be empirically fitted by the formula^[8],

$$R_H = R_0 H + 4\pi R_s M \quad (4.2)$$

where H is the applied magnetic field and M is the magnetization per unit volume. R_0 is the ordinary Hall coefficient and R_s is the anomalous Hall coefficient. Recently it was suggested that the anomalous Hall coefficient in ferromagnetic metals and DMS is determined by the modified spin-orbit coupling and spin-dependent scattering mechanisms.^[9-11]

The other contribution to the Hall effect is observed in two-dimensional electron gases (2DEG), usually referred as ‘spin-Hall effect’ and is shown in the right figure of Fig. 4.10. [12-13] In this case, when a spin-unpolarized current is injected, electrons experience an effective torque caused by a modified spin-orbit interaction, which tilts the spin up and spin down into two different directions. That means, the electrons which carry one spin direction are accumulated on one side of the sample whereas those of the other spin orientation are accumulated on the other side. If there is an imbalance of the densities of the two spin orientations in the sample, an unusual additional contribution to the Hall effect will arise. It should be noted that, even without magnetic field, which leads to zero Hall voltage, a spin Hall effect still can be observed due to the different Fermi levels for spin up and spin down electrons at both edges of the sample. Fig. 4.10 depicts the schematic representation of comparison of normal Hall effect and spin-Hall effect.

In our case, the paramagnetic-ferromagnetic GaAs:Mn/MnAs hybrid is a quite complicated system. First of all, the spin density of states in the paramagnetic matrix can be tuned by the applied magnetic field. Secondly, both the magnetic Mn ions in the paramagnetic matrix and the ferromagnetic MnAs clusters can act as inner magnetic fields and magnetic impurities. As we have discussed for the positive MR effect, a preferential spin orientation of the free carriers can be produced by the aligned Mn-ions via the p-d exchange interaction. On the other hand, the magnetizations of the Mn ions and MnAs clusters are aligned along the field direction. The aligned magnetizations can enhance the magnetic field and have a different effect on the carriers with spin-up and spin-down. Therefore, the interaction of the carriers oriented by the Mn-ions in the matrix with the aligned Mn ions in the matrix and the MnAs ferromagnetic clusters might lead to the unusual spin-dependent transport in the paramagnetic-ferromagnetic GaAs:Mn/MnAs hybrids.

Three important parts contributing to the observed unusual spin-dependent Hall effect in the studied GaAs:Mn/MnAs hybrid are suggested:

$$V_H^{meas} = \underbrace{V_H^{com}}_{\text{Giant-Zeeman-splitting contribution}} + \underbrace{V_H^{magnetization}}_{\text{Mn}^{2+} \text{ and MnAs}} + \underbrace{V_H^{spin-scattering}}_{\text{Mn}^{2+} \text{ and MnAs}} \quad (4.3)$$

The first term in this equation is the ordinary spin-independent Hall effect and arises from the Lorentz force acting on the free holes. However, instead of being linear with applied magnetic field, this ordinary term in the paramagnetic semiconductor depends on the magnetic field-

dependent tuning of the density of states due to the strong sp-d exchange interaction as discussed in the chapter 3. In other words, $V_H^{com} \propto \frac{1}{n(H)}$ where $n(H)$ is the carrier density and depends on the applied magnetic field. The second and the third term are the effects from Mn ions and MnAs clusters. Firstly, only their magnetization contribution to the alignment of the carriers is taken into account, i.e., the second term in the equation. Here, the magnetization of the sample is simply considered as an enhancement of the external magnetic field. The third term accounts for asymmetric spin scattering effects. The carriers incident on the magnetic impurities experience a potential which leads to a separation of the up and down spins. This effect on the carriers can occur when they are scattered by the Mn ions in the matrix, as well as when they are scattered by the MnAs clusters. On the other hand, the interaction between the carriers and the magnetic impurities can modify the spin-orbit interaction in the semiconductors.^[12] The modified spin-orbit interaction can lead to different changes of vector and velocity of the up and down spin carriers.

Therefore, the spin-dependent Hall effect depends strongly on the degree of spin orientation of the carriers in the paramagnetic matrix and the interaction between the oriented carriers and the Mn ions and the MnAs clusters. With an applied magnetic field, these effects lead to an accumulation of carriers with preferential spin orientation on opposite sides of sample, which cause a spin orientation-dependent Hall effect. However, a hysteresis can't be observed, which might be due to the paramagnetic matrix, i.e., the paramagnetic magnetization-like spin-dependent Hall effect as shown in Fig. 4.9.

With increasing temperatures, as seen from the Fig. 4.9(a), the saturation of the Hall resistance disappears, and it tends to a linear behaviour similar to that in the paramagnetic samples. The reason should be the decreasing ability of the paramagnetic matrix to align the carrier spins with increasing temperature, i.e., the thermal disorder destroys the preferential orientation of the Mn-ions, leading to the decrease of spin orientation of the carriers. In Fig. 4.9(c), the Hall resistances of GaAs:Mn/MnAs hybrid with the different thickness are compared at the same temperature $T = 50$ K. It can be seen that with increasing size of the MnAs ferromagnetic clusters and increasing thickness of the hybrid film, the Hall resistance at high fields becomes unsaturated which is similar to the behaviour with increasing temperature. The magnitude of the unusual Hall effect depends similar to the MR effect in the hybrids on temperature and cluster size/density. It can be concluded that increasing the MnAs cluster size or the effective density by increasing the thickness of hybrids decreases the unusual MR and Hall effects.

The distance between the clusters, the surface to volume ratio of the clusters, or the density of clusters will strongly affect the magnitude of the observed effects. (e.g., the smaller the clusters, the higher the clusters density, the closer distance between the clusters). For example, the spin transport depends strongly on the current path, the spin orientation of carriers can be easily lost when they move a too long distance between MnAs clusters (i.e., much larger than the spin-flip length), more details need to be studied.

In conclusion, the MR and Hall effects of GaAs:Mn/MnAs paramagnetic-ferromagnetic hybrids have been investigated. An unusual coexistence of large negative and giant positive MR effects in the same samples is observed. Accompanying the unusual MR effects, the Hall effect shows an unusual spin-dependent behaviour. Both the MR and the Hall effect depend strongly on the temperature and the properties of MnAs clusters. It is suggested that carrier localization induced by the giant Zeeman splitting at low temperatures is responsible for the negative MR effect and a spin-dependent scattering mechanisms are the possible origin of the large positive MR effect and the unusual Hall effect in such paramagnetic-ferromagnetic hybrids. It confirms that the interaction between MnAs ferromagnetic clusters and itinerant carriers and (Ga,Mn)As paramagnetic matrix plays an important role for the MR and Hall effect in such paramagnetic-ferromagnetic hybrids.

4.5. MR and Hall effects in MOVPE-grown GaInAs:Mn/MnAs hybrids

In order to compare the matrix effect on the spin-dependent transport property, the MR and Hall effect of MOVPE-grown GaInAs:Mn/MnAs hybrids with type I clusters prepared by a similar procedure are investigated as shown in Fig. 4.11. It can be found that at the lowest temperature $T=1.6$ K, the MR effect first is negative at low magnetic fields and then turns to a positive MR at high fields. This effect seems to be due to the weak localization effect induced by disorder as discussed in the chapter 3 for paramagnetic n-GaAs:Mn,Te samples. The magnetic field dependence of the Hall resistance also shows an unusual ‘S’-like behaviour at the lowest temperature, which is similar to that observed in heterogeneous ferromagnetic systems, multi-layers and granular mixtures.^[14] This spin-dependent Hall effect can be attributed to the influence by the strong s,p-d exchange interaction in the matrix. However, the unusual MR and Hall effect disappear rapidly with increasing temperature.

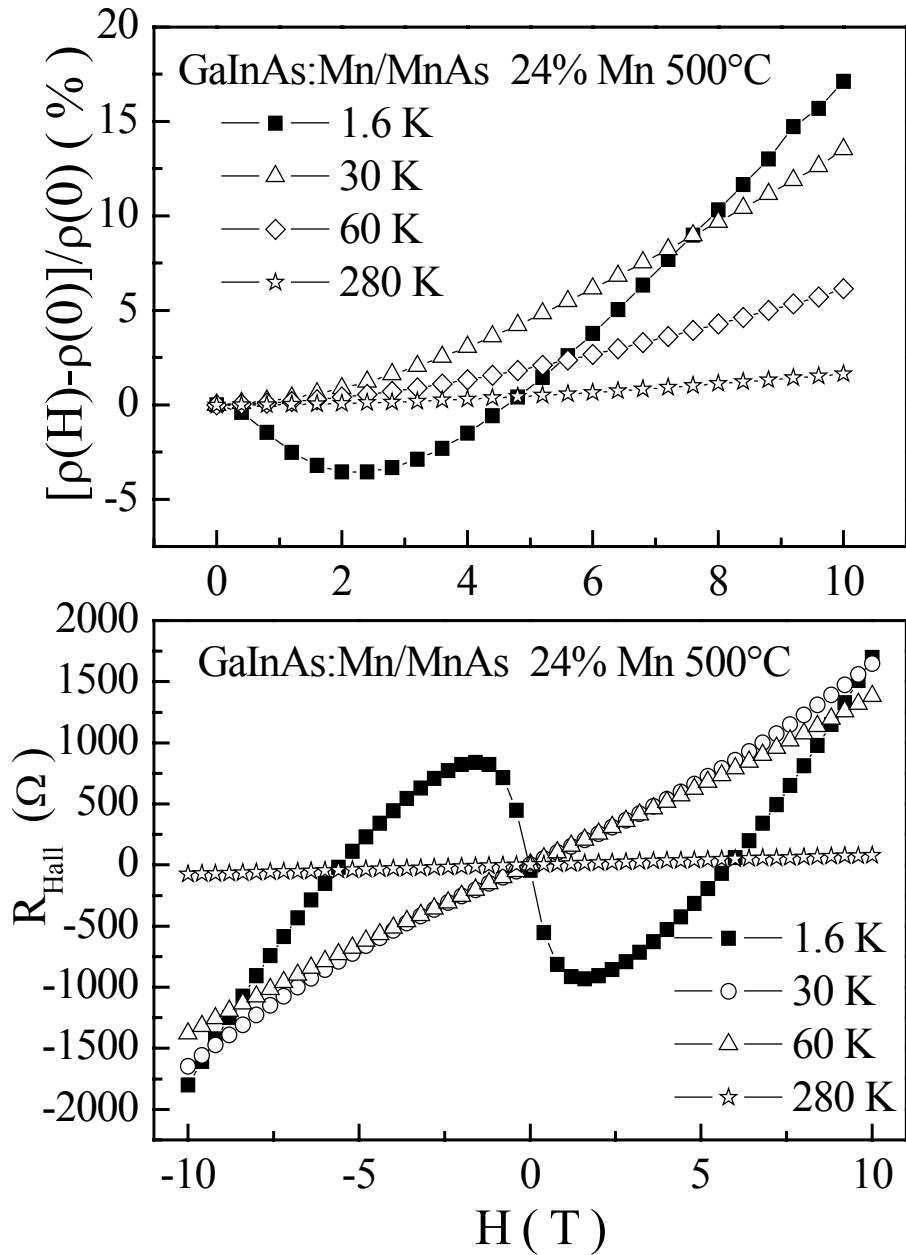


Fig. 4.11. The MR and Hall effect at different temperatures for a MOVPE-grown GaInAs:Mn/MnAs hybrid.

Therefore, the whole temperature and magnetic field dependence of MR and Hall effect appear, at first sight, totally different from those observed in a typical GaAs:Mn/MnAs hybrids. It seems that the ferromagnetic MnAs clusters have only minor effect on the spin-dependent transport in GaInAs:Mn/MnAs hybrid. The MR and Hall effect are almost entirely determined by the transport properties of the paramagnetic matrix. However, this is in

agreement with AFM results which suggest that the density of the MnAs clusters is very low in this sample. The competition of the occupation effects of the valence band due to the strong sp-d exchange interaction and the disorder effect for the MR in paramagnetic GaAs:Mn is suggested to be responsible for the unusual MR and Hall effect of GaInAs:Mn/MnAs at the lowest temperature. The results indicate that a strong magnetic-field independent disorder effects occur in the matrix and compete with the sp-d exchange interaction, leading to a weak localization dominating at the lowest temperature and the total positive MR effect at higher fields.

As the MnAs clusters almost do not play a role, the unusual MR and Hall effect disappear rapidly with increasing temperature, i.e., the Hall resistance shows a linear behaviour with applied magnetic field and the MR effect shows a parabolic behaviour at high temperature, due to the decreasing ability of the paramagnetic matrix to align the carrier spins with increasing temperature.

4.6. MR effects in GaAs:Mn/MnAs obtained by post-growth annealing of MBE-grown $\text{Ga}_{1-x}\text{Mn}_x\text{As}$ alloys

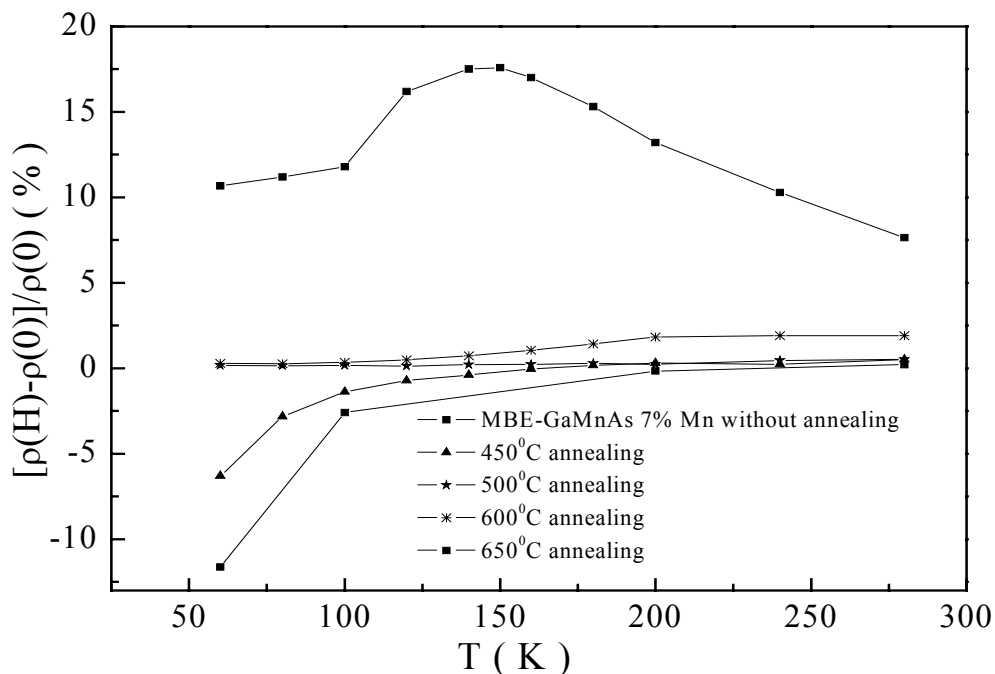


Fig. 4.12. Temperature dependence of the MR effect at $H = 10$ T of GaAs:Mn /MnAs paramagnetic-ferromagnetic hybrids prepared by post-growth annealing of MBE-grown $\text{Ga}_{1-x}\text{Mn}_x\text{As}$ alloys at different temperatures.

The temperature dependence of the MR effect at $H = 10$ T of GaAs:Mn/MnAs paramagnetic-ferromagnetic hybrids prepared by post-growth annealing of MBE-grown $\text{Ga}_{1-x}\text{Mn}_x\text{As}$ alloys at different temperatures is shown in the Fig. 4.12. It is found that:

1) At low annealing temperatures, the MR still shows a negative effect at low temperatures, which decreases with increasing temperatures without exhibiting a maximum. This phenomenon is similar to that observed in the as grown ferromagnetic $\text{Ga}_{1-x}\text{Mn}_x\text{As}$ with $x = 0.07$ alloy before annealing, which can be seen from the Fig. 4.13(a) and (b).

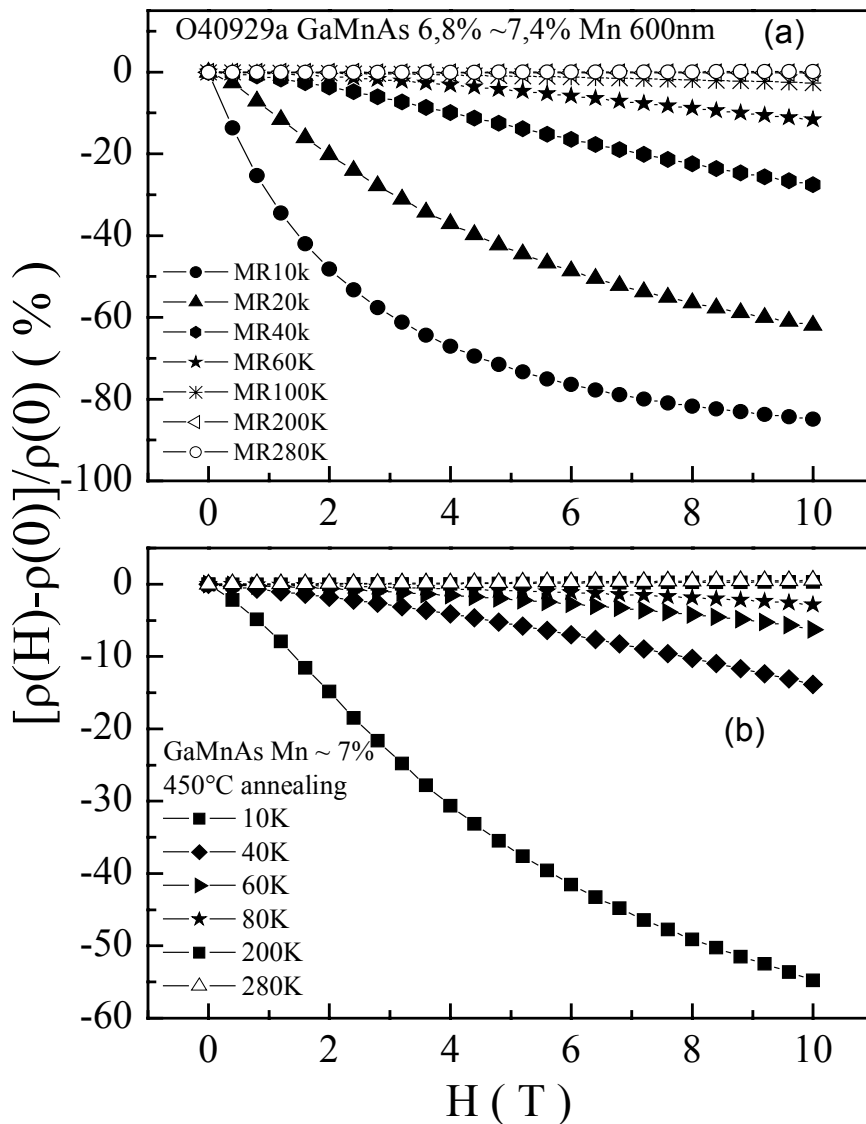


Fig. 4.13. Temperature dependence of the MR curves of GaAs:Mn/MnAs paramagnetic-ferromagnetic hybrids prepared by post-growth annealing of MBE-grown $\text{Ga}_{1-x}\text{Mn}_x\text{As}$ alloys with $\sim 7\%$ Mn (a) as grown and (b) annealed at 450°C .

2) A positive MR effect takes over from the negative MR with increasing annealing temperatures.

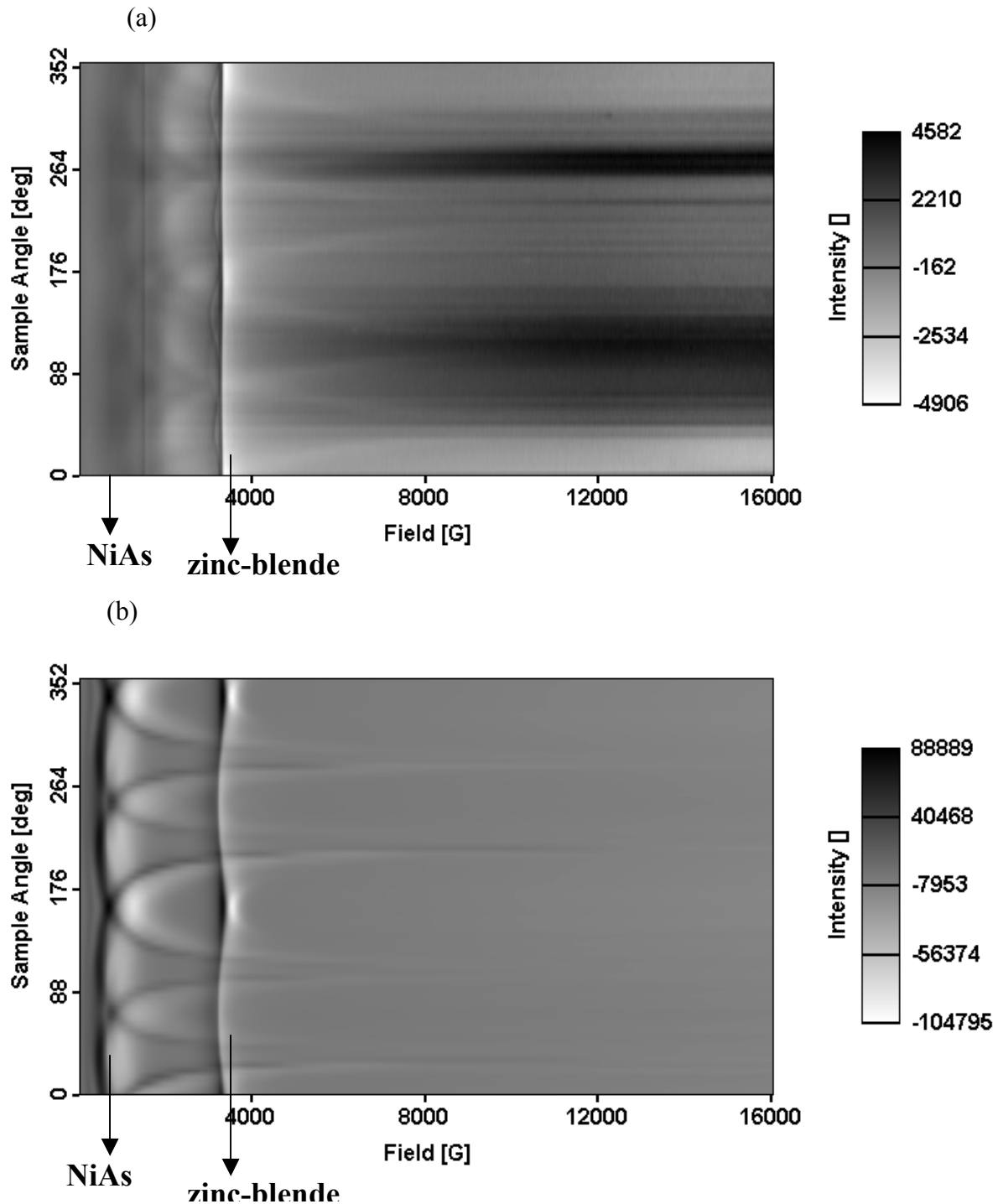


Fig. 4.14. The angle dependence of the FMR effect at $T = 150$ K of the GaAs:Mn/MnAs paramagnetic-ferromagnetic hybrids prepared by post-growth annealing at (a) 450°C (b) 650°C of $\text{Ga}_{1-x}\text{Mn}_x\text{As}$ alloys grown by low-temperature MBE.

3) For the GaAs:Mn/MnAs hybrid annealed at the highest temperature, The temperature dependence of the MR curves is depicted in Fig. 4.15. It was found that the MR shows a positive effect at all temperatures with a maximum MR at 150 K, which is similar to that have been found in the MOVPE-grown hybrids as seen in Fig. 4.12. However, the changes of the MR behaviour of the 650°C-annealed sample may be due to the too high annealing temperature and long annealing time leading to almost all Mn ions forming the MnAs clusters.

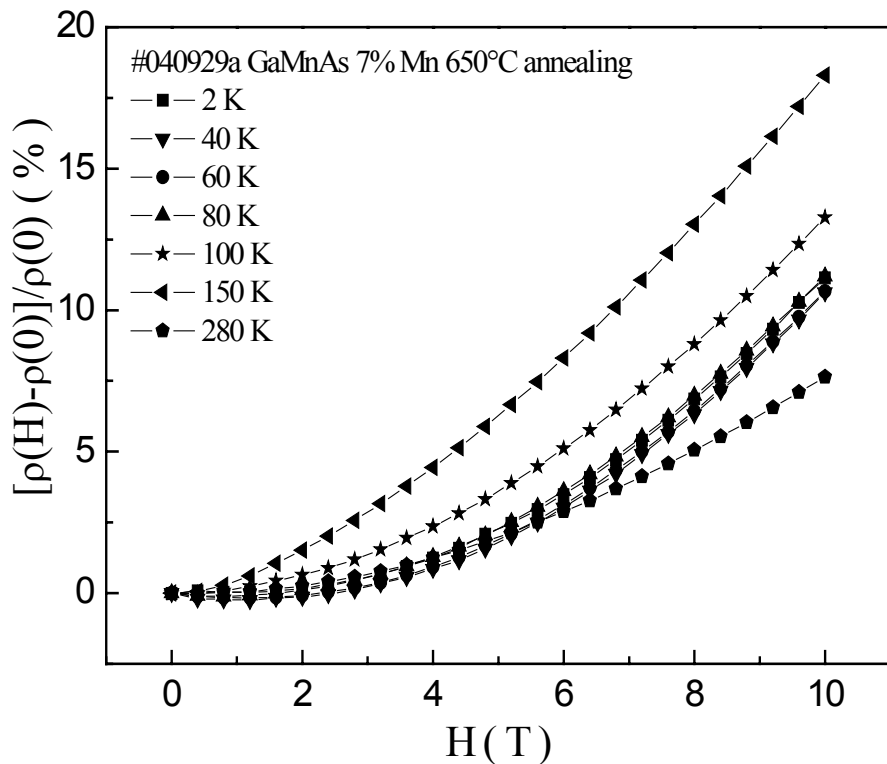


Fig. 4.15. Temperature dependence of the MR curves of GaAs:Mn/MnAs paramagnetic-ferromagnetic hybrids prepared by post-growth annealing of MBE-grown $\text{Ga}_{1-x}\text{Mn}_x\text{As}$ alloys with $\sim 7\%$ Mn annealed at 650°C.

The annealing procedure produces two effects: 1) The Mn ions are removed from the ordered lattice sites and interstitial sites of the matrix to form clusters and thus modify the properties of the matrix. 2) A precipitation takes place and MnAs clusters are formed. Therefore, both the properties of the matrix and the MnAs clusters strongly depend on the annealing temperature, which is also reflected by the MR behaviour which depends strongly on the interaction between the matrix and clusters.

According to the AFM measurement, the MnAs clusters already form at the lowest annealing temperature $T = 450^\circ\text{C}$. The magnetic properties of MnAs clusters can be obtained from ferromagnetic resonance (FMR) measurement as shown in the Fig. 4.14. The typical angle dependent-FMR signal of hexagonal (NiAs structure) MnAs clusters (type I) is observed. The temperature dependence of the FMR with the magnetic field perpendicular to the sample shows the FMR signal up to 325 K.

In addition, another FMR signal is observed with a resonance field of about 0.4 T which is almost independent of the field orientation. The temperature dependence of the FMR shows that this signal persists only up to 80 K. Therefore, besides the type I clusters of NiAs structure with $T_C \approx 325$ K, small zincblende clusters (type II) with a Curie temperature of about 80 K are also formed during post-growth annealing. The relative intensities of the two FMR signals vary with increasing annealing temperatures. The relative strength of the type I signal increases compared to the type II signal. Therefore, type II clusters are preferentially formed at low annealing temperatures. With increasing the annealing temperature, the type I clusters are formed which are similar to those obtained in GaAs:Mn/MnAs hybrids directly grown by MOVPE. It is also found that the density of the clusters increases with increasing annealing temperature. However, the question whether the different types of clusters lead to a different MR behaviour for MOVPE and for post-growth annealed MBE samples need more investigations. The size as well as the density of the formed clusters need to be studied in more detail and need to be compared with the results on MOVPE-grown samples.

Tab. 4.2 Carrier concentration at room temperature for the GaAs:Mn/MnAs annealed at different temperatures

Annealing temperature($^\circ\text{C}$)	0	450	500	650
Carrier concentration $p(\text{cm}^{-3})$		$4.1 \cdot 10^{18}$	$3.6 \cdot 10^{18}$	$1.4 \cdot 10^{18}$
Resistivity($\Omega \text{ cm}$)	0.23	0.20	0.18	0.21

The carrier concentration and resistivity at room temperature are shown in Tab. 4.2. It is found that the carrier concentration decreases with increasing annealing temperatures. The resistivity of the hybrid firstly decreases with increasing annealing temperatures and then increases again. The results indicate that the properties of the matrix associated with the concentration of Mn on lattice sites and interstitial Mn ions, are also strongly affected by the

annealing procedure. Moreover, in the first chapter, we have discussed that the average exchange integral $N_0\beta$ depends strongly on the ratio of Mn ions on lattice sites and Mn ions on interstitial sites.^[15, 16] The annealing procedure is likely to first remove the interstitial Mn ions, favouring a positive $N_0\beta$. Therefore it might cause a reduction of the Mn concentration in the matrix as well as a change of $N_0\beta$.

4.7. Summary

Thus, both the properties of the matrix and of the MnAs clusters strongly depend on the preparation procedure, which induces different interactions between the matrix and clusters. The MR and Hall effect investigated in these GaAs:Mn/MnAs and GaInAs:Mn/MnAs hybrids confirm that the interaction between the matrix and clusters produce a strong effect on the spin-dependent transport in these paramagnetic-ferromagnetic hybrids.

References:

- [1] P. J. Wellman, J. M. Garcia, J. L. Feng, and P. M. Petroff, *Appl. Phys. Lett.* **73**, 3291 (1998).
- [2] Y. D. Park, A. Wilson, A. T. Hanbicki, J. E. Mattson, T. Ambrose, G. Spano, and B. T. Jonker, *Appl. Phys. Lett.* **78**, 2739 (2001).
- [3] M. Berciu and B. Janko, *Phys. Rev. Lett.* **90**, 246804 (2004).
- [4] P. Redlinski, T.G. Rappoport, A. Libal, J. K. Furdyna, B. Janko, and T. Wojtowicz, *Appl Phys. Lett.* **86**, 113103 (2005).
- [5] J. Furdyna, *J. Appl. Phys.* **64**, R29 (1988).
- [6] J. E. Park, L. H. Yang, C. Y. Fong, W. E. Pickett, and S. Dag, *Phys. Rev. B.* **67**, 224420 (2003).
- [7] C. Michel, C.H. Thien, S. Ye, P.J. Klar, W. Heimbrodt, S.D. Baranovskii, P. Thomas, M. Lampalzer, K. Volz, W. Stolz, B. Goldlücke, *Superlattices and Microstructures.* **37**, 321 (2005).
- [8] H. Ohno, A. Shen, F. Matsukura, A. Oiwa, A. Endo, S. Katsumoto, and Y. Iye, *Appl. Phys. Lett.* **69**, 363 (1996).
- [9] J. E. Hirsch, *Phys. Rev. Lett.* **83**, 1834 (1999).
- [10] E. N. Bulgakov, K. N. Pichugin, A. F. Sadreev, P. Streda, and P. Seba, *Phys. Rev. Lett.* **83**, 376 (1999).

- [11] V. K. Dugaev, P. Bruno, and J. Barnas, Phys. Rev. B. **64**, 144423 (2001).
- [12] J. E. Hirsch, Phys. Rev. Lett. **83**, 1834 (1999).
- [13] J. Sinova, D. Culcer, Q. Niu, N. A. Sinitsyn, T. Jungwirth, and A. H. MacDonald, Phys. Rev. Lett. **92**, 126603 (2004).
- [14] A. Gerber, A. Milner, M. Karpovsky, B. Lemke, H. -U. Habermeier, J. Tuaille-Combes, M. Negrier, O. Boisron, P. Melinon, A. Perez, J. Mag. Mat. **242**, 90 (2002).
- [15] J. Blinowski and P. Kacman, Phys. Rev. B **67**, 12120 (R) (2003).
- [16] K. M. Yu, W. Walukiewicz, I. Kuryliszyn, X. Liu, Y. Sasaki, and J. K. Furdyna, Phys. Rev. B **65**, 201303(R) (2002).

5. Studies of the geometry and hydrostatic pressure dependence of the MR effects and of local transport in GaAs:Mn/MnAs hybrids

5.1 Geometry dependence of MR effects in GaAs:Mn/MnAs hybrids

The geometry dependence of the MR and Hall effect of the GaAs:Mn/MnAs hybrid has been investigated in the temperature range from $T = 15$ K to room temperature. It has been found that the MR and Hall effect depend strongly on the angles between the external magnetic field, the sample normal, and the current direction. In the geometry where the external magnetic field is perpendicular to the sample plane a large MR effect is observed as discussed in chapter 4. The MR effect decreases when the external magnetic field changes to an in-plane geometry, especially in the cases where the magnetic field is either parallel or perpendicular to the current direction. On the other hand, the angular dependence of the FMR signal in the GaAs:Mn/MnAs hybrid has also been investigated. The relation of the angular-dependent magnetism and MR in GaAs:Mn/MnAs hybrid structures are discussed in this part. The results indicate an anisotropic behavior of the interaction between the paramagnetic GaAs:Mn matrix and ferromagnetic MnAs nano-clusters.

Fig. 5.1. depicts the angular and the temperature dependence of the MR effects in the GaAs:Mn/MnAs hybrid structures. Fig. 5.1(a) is the temperature dependence of the MR in the geometry where the external magnetic field is perpendicular to the sample plane and to the current direction. As it has been discussed in the chapter 4, a negative MR as high as -30% achieved at $H = 10$ T without saturation with increasing magnetic field H at $T = 15$ K is observed. With increasing temperature, the negative MR effect is suppressed and then changes to a positive MR at a temperature $T_1 = 40$ K, which increases quickly and reaches the maximum value as high as 160% without saturation under an applied magnetic field $H = 10$ T at a temperature $T_2 = 60$ K. Above T_2 it drops again, but remains positive up to room temperature. Both temperatures T_1 and T_2 increase whereas the magnitude of the MR effect decreases with increasing MnAs cluster size. The considerable difference between the MR effect in the GaAs:Mn/MnAs hybrid structures and those of paramagnetic GaAs:Mn without MnAs clusters has been attributed to the appearance the ferromagnetic MnAs nano-clusters in the paramagnetic GaAs:Mn matrix. The interaction between the ferromagnetic MnAs clusters and the free carriers in the paramagnetic (Ga,Mn)As matrix is responsible for the temperature dependence of the unusual MR effect.

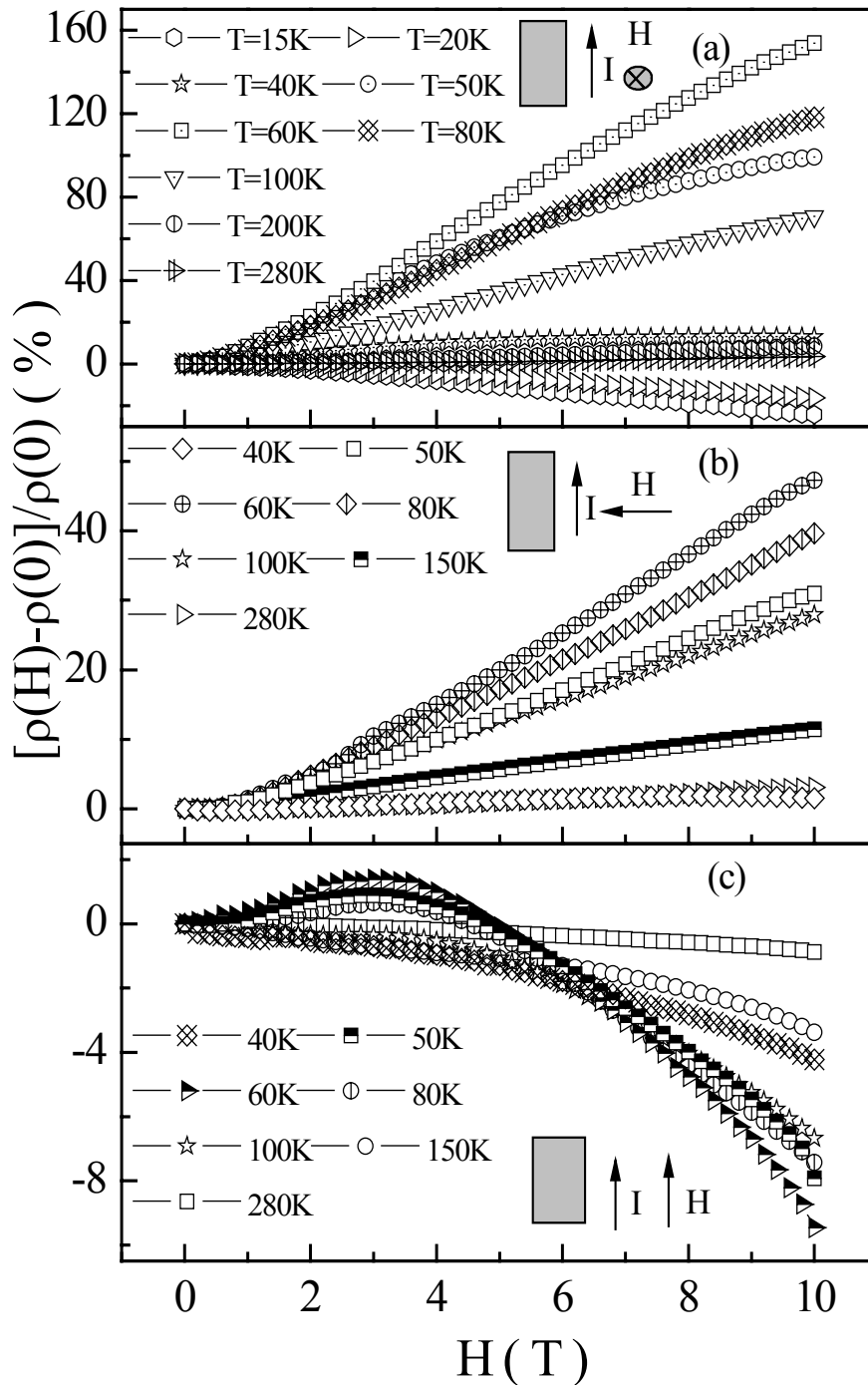


Fig. 5.1. Angular and temperature-dependent MR effects in a MOVPE-grown GaAs:Mn/MnAs hybrid with 150 nm thickness. (a) MR in the geometry where the external magnetic field is perpendicular to the sample surface. (b) MR in the geometry where the external magnetic field is in the plane and perpendicular to the current. (c) MR in the geometry where the external magnetic field is in the plane and parallel to the current.

Fig. 5.1(b) shows the temperature dependence of the MR in the geometry where the external magnetic field is parallel to the sample plane and perpendicular to the current direction. The MR behavior in this orientation still shows large MR effect. However, compared with that in the first geometry, it becomes smaller and shows different curve shapes. The maximum positive MR effect is only about 50% without saturation under an applied magnetic field $H = 10$ T at a temperature $T_2 = 60$ K.

When the applied external magnetic field is in the plane and parallel to the current as shown in Fig. 5.1(c), at low field below $H = 5$ T, firstly the MR effect changes very slowly with the external magnetic field as that in the other two geometry; and then it changes from negative to positive MR with the temperature increasing and reaches to the maximum at $T_2 = 60$ K. With increasing the applied external magnetic field, the MR decreases monotonically without saturation again, and at high magnetic field the maximum of the negative MR effect is also at $T_2 = 60$ K. However, the magnitude of MR effect in this orientation is comparable to that in the paramagnetic GaAs:Mn sample without MnAs ferromagnetic clusters.

Based on these different experimental results, it can be concluded that the MR effects of the GaAs:Mn/MnAs hybrid structures depend strongly on the orientation of the sample with respect to the external magnetic field. With the applied external magnetic field changing from perpendicular to the sample surface to in-plane and parallel to the current, the unusual MR effect decreases, and the MR behavior becomes similar to the MR effect of the paramagnetic sample without ferromagnetic MnAs clusters. These phenomena indicate that the degree of the interactions between the ferromagnetic MnAs clusters and the free carriers in the paramagnetic GaAs:Mn matrix is also angle dependent, i.e., depends on the current path through the sample.

Fig. 5.2 summarizes the temperature dependence of the MR effects for the three transport geometries. In all three graphs the MR values at $H = 10$ T are depicted as a function of temperature for the GaAs:Mn/MnAs hybrid and for the GaAs:Mn paramagnetic sample without MnAs clusters. With the applied external magnetic field changing from perpendicular to parallel to the current as shown in Fig. 5.2(b) and Fig. 5.2(c), the temperature dependence of MR effect at $H = 10$ T shows similar trends, but the magnitude decreases. For all three geometries the magnitude of the MR effect is the biggest at the characteristic temperature T_2 and approaches that of the sample without clusters at the highest temperatures. The MR effect due to the clusters is enhanced strongly in the GaAs:Mn/MnAs hybrid compared with the (Ga,Mn)As without MnAs clusters, when $I \perp H$ (Fig. 5.2(a) and (b)). When $I \parallel H$, the MR effects are comparable in magnitude in both samples indicating that the effect of the clusters

is weaker in this geometry (Fig. 5.2(c)). However, for the high temperatures, the effect decays with the temperature increasing for all three orientations as seen from Fig. 5.2.

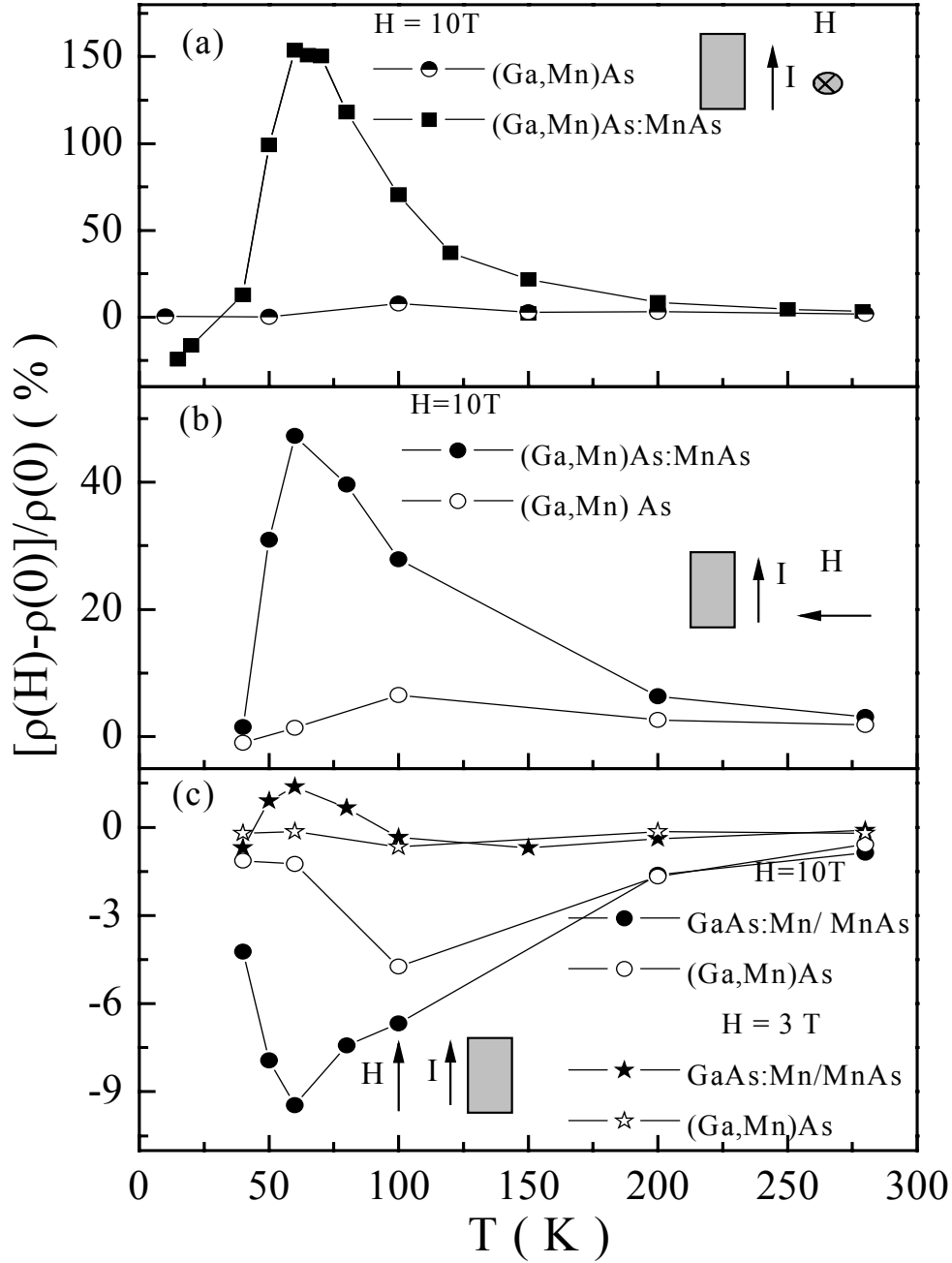


Fig. 5.2 Angle and temperature dependence of maximum MR value at $H = 10$ T and $H = 3$ T for a MOVPE-grown GaAs:Mn/MnAs hybrid and a MOVPE-grown paramagnetic sample GaAs:Mn without MnAs clusters. (a) the external magnetic field perpendicular to the sample surface. (b) The external magnetic field in the plane and perpendicular to the current. (c) The external magnetic field in the plane and parallel to the current.

In order to investigate the correlation of magnetism and MR in GaAs:Mn/MnAs hybrids, the angular dependence of the FMR of the 150 nm thickness sample was also investigated as shown in Fig. 5.3. The axis of rotation (perpendicular to H) was chosen parallel to the GaAs [011] direction. The positions (1) and (2) in the figure correspond to field geometries where $H \parallel [100]$ and $H \parallel [0 -11]$. Two distinct quasi-parabolic resonance curves are observed and assigned to sub-ensembles of clusters of similar orientation. A detailed analysis of the FMR data reveals that the c -axis of the hexagonal MnAs clusters is close to the four equivalent (111) directions of GaAs. The easy axis of magnetization of the MnAs clusters is always found in the basal plane perpendicular to the c -axis. In particular, the behavior of the total magnetization of the MnAs clusters is comparable for the two field geometries. Furthermore, FMR and magnetization measurements reveal that there is also virtually no difference in the magnetization behavior for the two in-plane geometries where $H \parallel [011]$ and $H \parallel [0-11]$, respectively, for samples grown at 500°C.

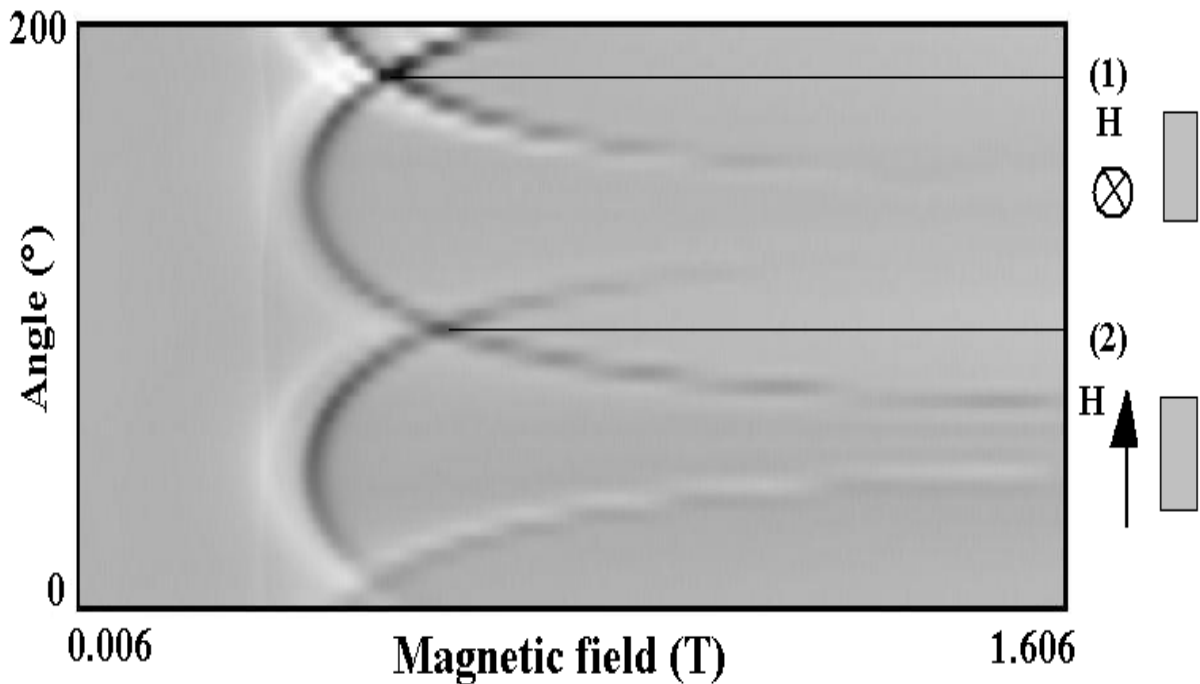


Fig. 5.3. Angular dependence of the FMR signal in a MOVPE-grown GaAs:Mn/MnAs hybrid. (1) The external magnetic field is perpendicular to the sample surface (2) The external magnetic field is in plane and parallel to the current.

The magnetic properties of the ensemble of ferromagnetic MnAs nano-clusters are very similar for the two magnetic field orientations studied by FMR. Therefore, the observed

anisotropy of the MR effects for current direction $I \parallel H$ and $I \perp H$ mainly reflects the difference in current path through the sample. This leads to a variation of the degree of interaction between the free carriers in the paramagnetic matrix and the ferromagnetic MnAs nano-clusters. For $I \perp H$ the current path through the sample is extended due to the circular movement between two scattering events and the number of interactions between the free carriers and the ferromagnetic clusters is enhanced. For $I \parallel H$ the current path through the sample is mainly in the paramagnetic GaAs:Mn matrix, the scattering and the interaction between the free carriers and the MnAs clusters become smaller. Despite the same interaction the weaker scattering leads to the observed MR effect similar to that in the paramagnetic sample.

Therefore, the MR effects in the GaAs:Mn/MnAs hybrids not only depend on the microscopic interaction mechanism between the free carriers in the paramagnetic semiconductor host and the ferromagnetic MnAs clusters, but also strongly on the transport geometry and the resulting current path through the sample.

5.2. Hydrostatic pressure dependence of MR and Hall effects in GaAs:Mn/MnAs hybrids

Based on the previous discussion, it was shown that the transport behavior of GaAs:Mn DMS is very sensible to the p-d exchange integral $N_0\beta$ which is dominated by the hybridization between the p-like valence band and the Mn ions. It was also shown that the local electronic structure of the Mn-centers leads to different contributions to the sign and magnitude of the average $N_0\beta$. Moreover, the crystal field, especially the positions of the nearest-neighbor anions also strongly affects $N_0\beta$.^[1,2] Therefore, the key parameter $N_0\beta$ is determined by the nature of Mn center and its environments. Applying an external hydrostatic pressure, one can exert an influence on the chemical bonds directly to modify the electronic structure as well as the crystal structure. In particular, in the GaAs:Mn samples studied hydrostatic pressure will have two effects. Firstly, it decreases the Mn-As bond-length (keeping the tetrahedral symmetry) which should increase the degree of p-d hybridization. Secondly, it should affect the acceptor depth, i.e., leads to a decrease at the number of free holes with increasing pressure. There are several reports where the pressure dependence of the exchange integral $N_0\beta$ was investigated in various DMS.^[3-5] Indeed, for the II-VI DMS, it has been found that the compression of the lattice induced by an applied hydrostatic pressure leads to an increase of the s,p-d exchange interaction. The magnitude of the pressure dependent exchange interaction is determined by the Mn concentration. For ferromagnetic III-V DMS, it was also

reported that the enhanced s,p-d exchange interaction under an external hydrostatic pressure leads to an increase of the Curie temperature of $\text{In}_{1-x}\text{Mn}_x\text{As}$ DMS.

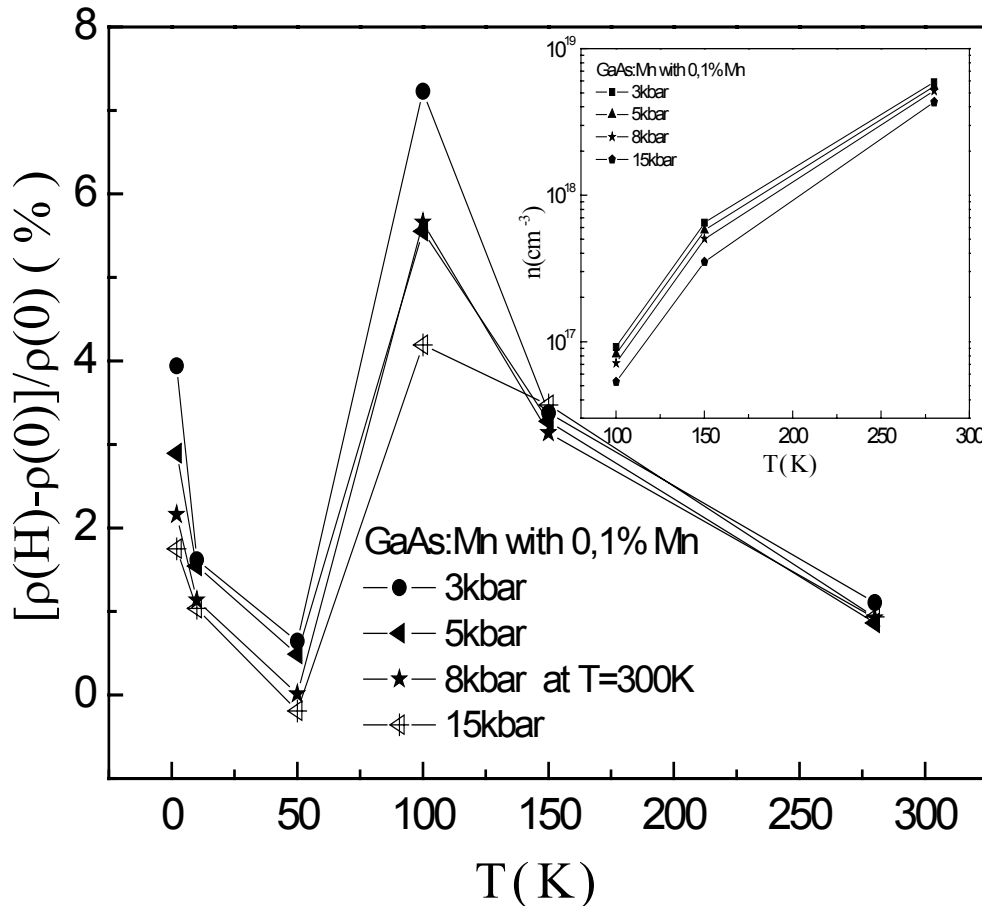


Fig. 5.4. Comparison of the temperature dependence of the MR value at $H = 10$ T for different hydrostatic pressures for a paramagnetic GaAs:Mn with 0.1% Mn. The inset is a comparison of the temperature dependence of the carrier concentration under different hydrostatic pressures for the same sample.

Here, the pressure dependence of the MR in the paramagnetic GaAs:Mn-based alloys and hybrids is investigated. In Fig. 5.4, the temperature dependence of the MR at $H = 10$ T for different applied hydrostatic pressure ranging from 3 kbar to 15 kbar for the paramagnetic GaAs:Mn with 0.1% Mn is presented. It is found that the positive MR effect at low temperature decreases with increasing applied hydrostatic pressure. As it was discussed in the chapter 3, the competition of occupation effects of the spin-subbands induced by the magnetic field-dependent spin splitting of the valence band and magnetic-field tuning of the disorder

induced by Mn incorporation is largely responsible for the observation of the negative as well as positive MR effects in the paramagnetic II-VI and III-V DMS.

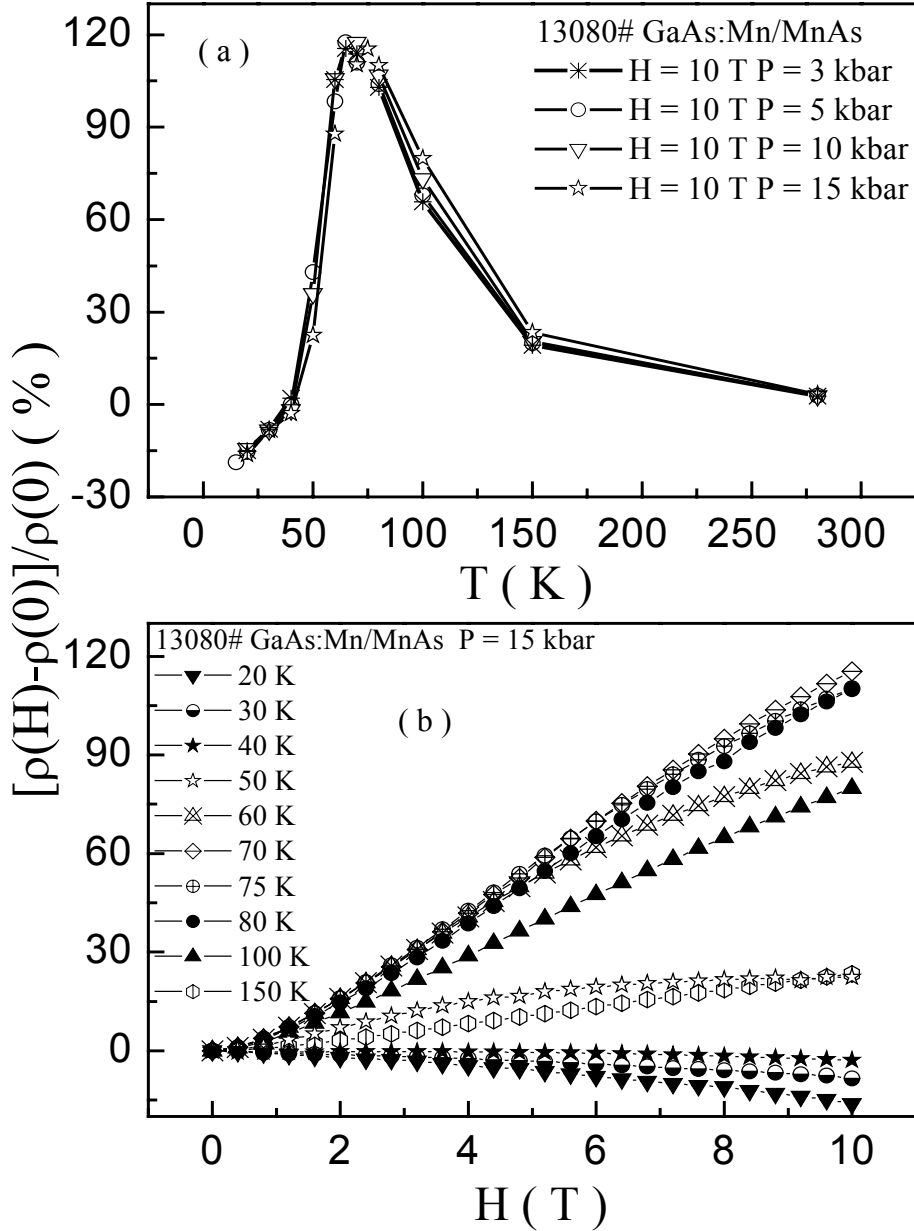


Fig. 5.5. (a) Comparison of the temperature dependence of the MR value at $H = 10$ T under different hydrostatic pressures for the GaAs:Mn/MnAs hybrid with 150 nm thickness. (b) Temperature dependent MR results of GaAs:Mn/MnAs hybrid at $P = 15$ kbar.

This discussion has been supported theoretically by the network model and mobility model. The occupation of the spin-subbands contributing to the negative MR effect plays a more

important role at high magnetic fields than at low fields. Therefore, the enhanced p-d exchange interaction confirmed in II-VI DMS under the applied hydrostatic pressure is also suggested to happen in the paramagnetic GaAs:Mn alloy with 0.1% Mn, which is in agreement with the increasing occupation effect leading to the decreasing positive MR effect at low temperature as shown in the Fig. 5.4.

On the other hand, the carrier concentration of the paramagnetic GaAs:Mn with 0.1% Mn decreases with increasing applied pressure as shown in the inset of Fig. 5.4. However, it has been reported in ferromagnetic $\text{In}_{1-x}\text{Mn}_x\text{As}$ DMS, that the external hydrostatic pressure hardly affects the carrier concentration. More investigations especially pressure dependent-optical measurements are needed, e.g. low temperature photoluminescence measurements.

Fig. 5.5 is a comparison of the temperature dependence of the MR value at $H=10\text{ T}$ under different hydrostatic pressures for the GaAs:Mn/MnAs hybrid with 150 nm thickness. With the increasing applied hydrostatic pressure, it is observed that

1) The shape of the MR curve at $P=15\text{ kbar}$ is similar to that observed at ambient pressure discussed in chapter 3, as shown in Fig. 5.5(b);

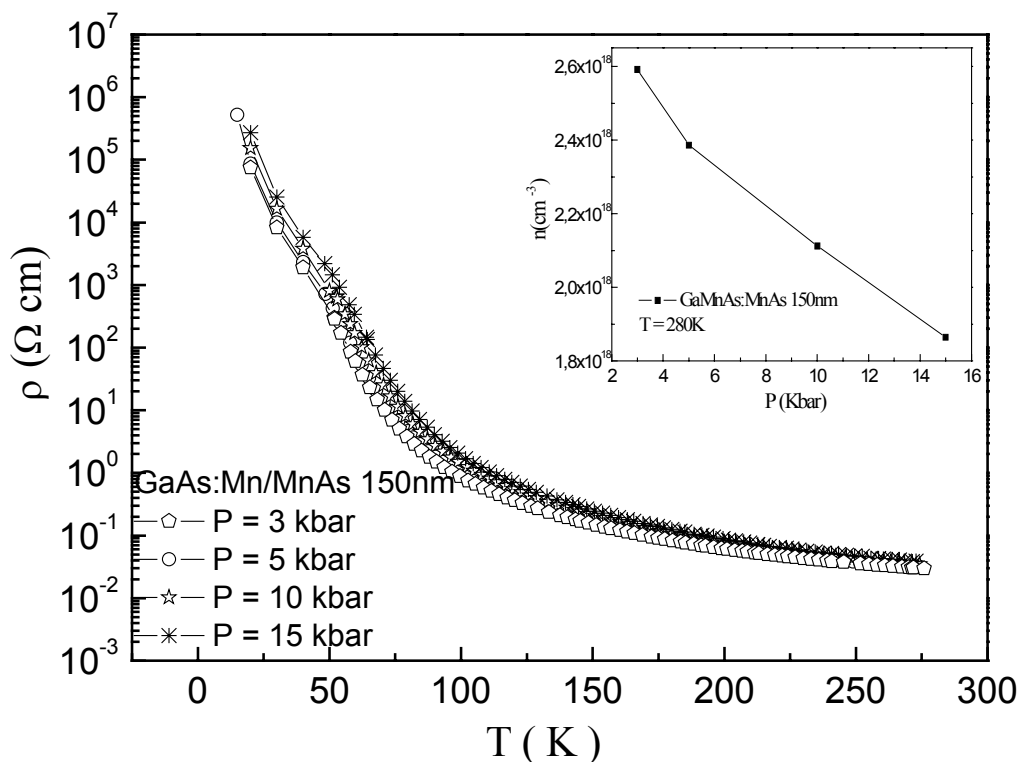


Fig. 5.6. Temperature dependence of the resistivity at $H=0\text{ T}$ under different hydrostatic pressures for the GaAs:Mn/MnAs hybrid with 150 nm thickness. The inset is the pressure dependence of the carrier concentration at room temperature.

2) The magnitude of the observed negative MR at low temperature is almost independent of the external hydrostatic pressure;

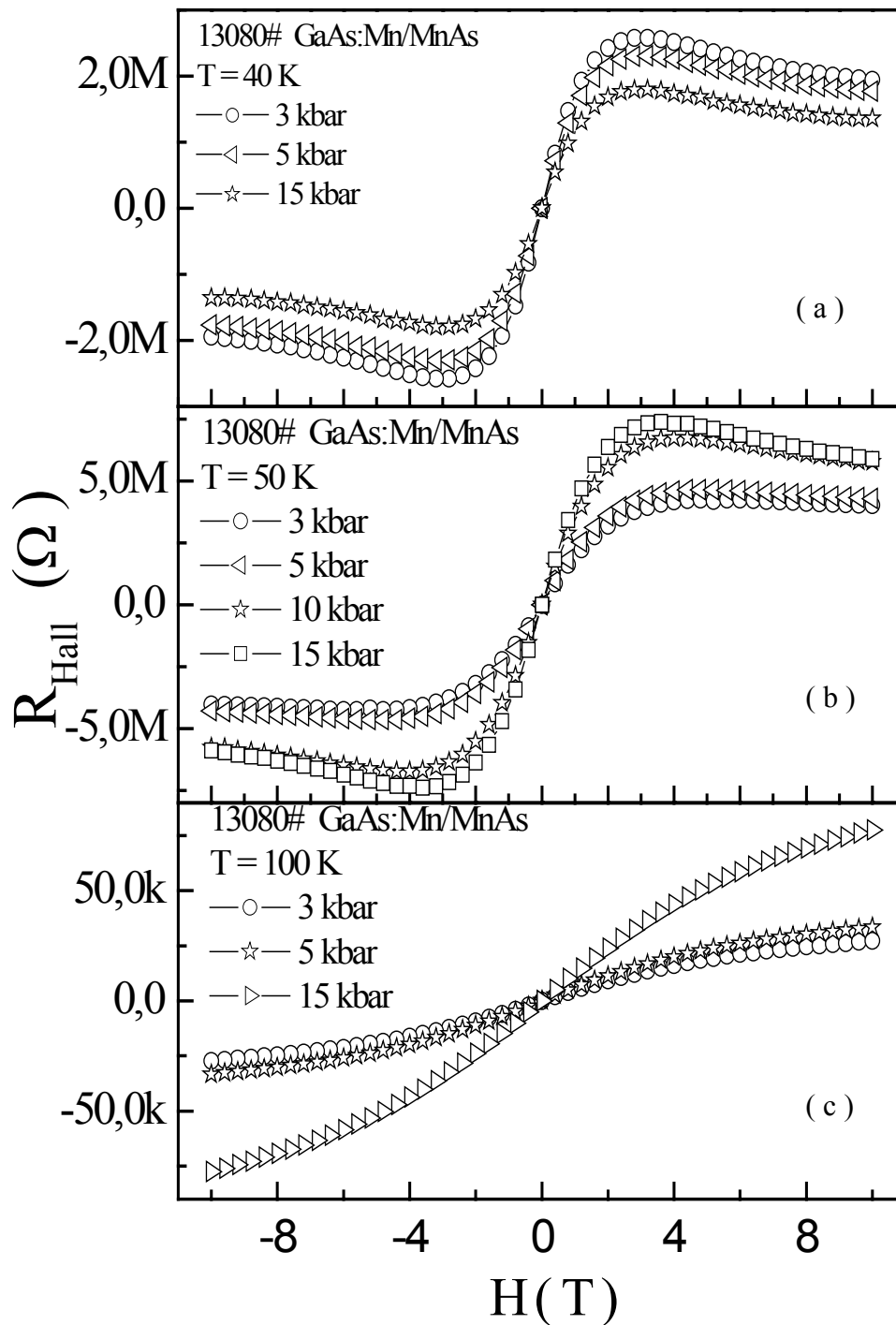


Fig. 5.7. Magnetic field dependence of the Hall resistance of the GaAs: Mn/MnAs hybrid with 150nm thickness for different hydrostatic pressures. (a) $T=40$ K (b) $T=50$ K (c) $T=60$ K.

- 3) The transition temperature from negative to positive MR shifts slightly to higher temperature;
- 4) The magnitude of the observed large positive MR at intermediate temperatures is also almost independent of the external pressure. However, the temperature, where the maximum positive MR occurs, shifts to higher temperatures;
- 5) At $T = 100$ K, the positive MR is enhanced by about 20% due to the increased pressure. This enhancement decreases with increasing temperature, and the MR is nearly the same for all pressures at room temperature.

Fig. 5.6 depicts the temperature dependence of the resistivity of GaAs:Mn/MnAs hybrid with 150 nm thickness at $H = 0$ T for different hydrostatic pressures. It is found that the resistivity increases with increasing applied hydrostatic pressure, and the carrier concentration at room temperature decreases with increasing hydrostatic pressures as shown in the inset of Fig. 5.6. Moreover, the Hall effect at different pressures was also investigated as shown in the Fig. 5.7. The unusual spin-dependent Hall effects discussed in chapter 4 display a similar behaviour at different applied pressures:

- 1) At $T = 40$ K, the Hall resistance saturates at about $H = 2$ T at $P = 3$ kbar, and then decreases slowly to a constant value as shown in the Fig. 5.7(a). The corresponding saturation value shifts to low magnetic field with increasing applied external hydrostatic pressure.
- 2) At $T = 50$ K, the Hall resistance saturates and keeps at a constant value at about $H = 4$ T at $P = 3$ kbar. Again, the corresponding saturation value shifts to low magnetic field with increasing applied external hydrostatic pressure as shown in the Fig. 5.7(b). Moreover, the effect of increasing applied pressure is equal to the effect of the decreasing temperature, i.e., the Hall resistance at $P = 15$ kbar saturates at an intermediate magnetic field about $H = 3$ T and then decreases slowly to a constant value similar to the behavior at $T = 40$ K.
- 3) At $T = 100$ K, the Hall resistance only shows a ‘S’-shape behavior without saturation as shown in Fig. 5.7(c). It increases with increasing applied hydrostatic pressure. At room temperature, the Hall resistance shows a linear behavior again for all pressures, but the Hall resistance increases with increasing pressure. The increasing Hall resistance is mainly attributed to decreasing carrier concentration due to a pressure-induced change of the acceptor depth.

It can be concluded that

- 1) The spin-dependent Hall effect is enhanced by the increasing pressure.
- 2) The maximum of the positive MR and the transition temperature from negative to positive MR shift to higher temperatures.

- 3) Enhanced MR effects indicate that the interaction between the MnAs and paramagnetic matrix is enhanced at $T=100\text{ K}$.

Therefore, these results are consistent with what happens in II-VI DMS and InMnAs, i.e., an enhanced p-d exchange interaction by increasing applied hydrostatic pressure. Unfortunately, these effects are partly compensated by the variation of the carrier density. As for the paramagnetic GaAs:Mn alloys, more investigations especially low-temperature photoluminescence measurements under hydrostatic pressure are needed.

5.3. Transport AFM measurements of GaAs:Mn/MnAs hybrids

In order to obtain more information about how carrier transport between the ferromagnetic MnAs clusters and paramagnetic GaAs:Mn matrix takes place, atomic force microscope (AFM) experiments in the conducting mode have been performed, where an individual MnAs cluster can be controlled by the conducting AFM and the local conductivity via the cluster can be measured by applying an electrical voltage over the tip-sample contact. As we know, the van der Pauw method yields a macroscopic measurement of the average electrical behaviour of the whole sample. Therefore, it is impossible to determine the local conductivity by such a measurement. In contrast in an AFM measurement, in which nano-scale resolution can be achieved, it is in principle possible to study local differences in conductivity between regions with and without MnAs clusters, and even the transport behaviour between a single cluster and the matrix.

The tapping mode is adopted for the all topography measurements, and the contact mode is used for transport AFM experiments, in which the current is applied between tip and sample. In the transport AFM measurements, a metallized AFM tip with Pt-coating serves as the scanning electrical nanoprobe. In order to locally probe the electrical transport properties, the GaMnAs:MnAs sample was placed in an AFM system operating in air at room temperature. The tip is positioned above the sample at a specific location and then lowered until it makes physical and electrical contact with the sample surface. When the bias voltage is applied between the bottom of the sample and the tip, the voltage gradient is perpendicular to the sample surface. The local current at the specific location is measured by a current amplifier in the circuit. Due to the nano-scale resolution of the tip, one can detect how the current transport varies when either cluster or matrix is contacted.

When a small positive bias voltage was applied, there was no current measurable. However, with increasing the bias voltage to a higher value, a small current is observed in the region with MnAs clusters and no current can be found in the region of the GaAs:Mn matrix. With

the applied bias voltage increasing further to the highest value $V=11$ V, it was found that the contrast between the regions with and without MnAs clusters becomes more significant, i.e, there is an obvious current in the region with MnAs clusters and only small current observed in the region without MnAs clusters as shown in the Fig. 5.8(b).

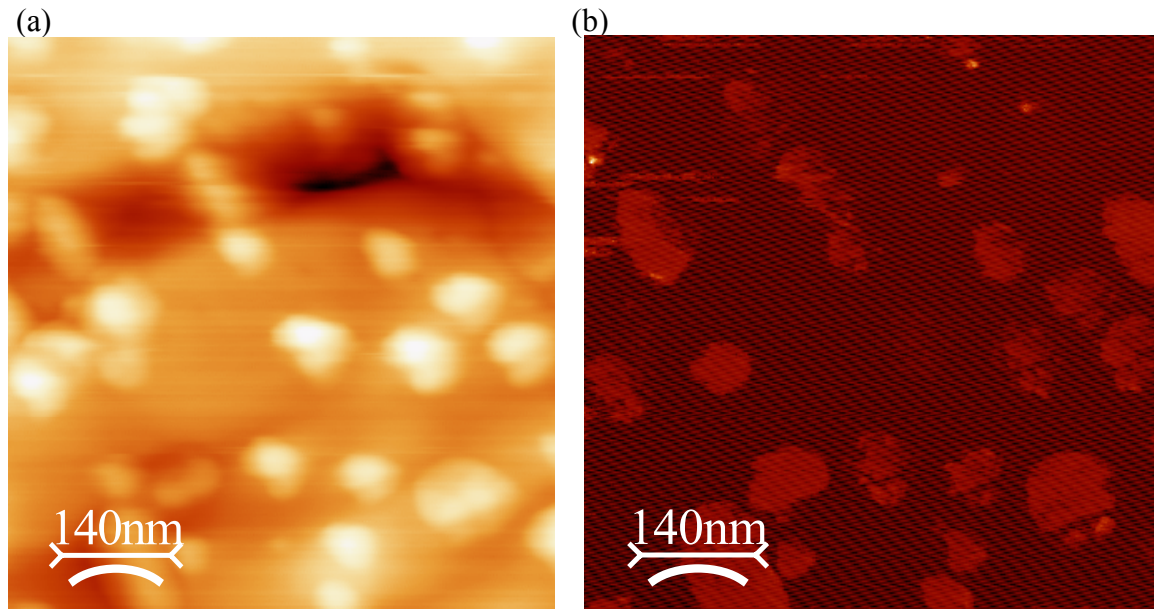


Fig. 5.8. (a) Topography scan of the GaMnAs: MnAs hybrid; (b) The corresponding conductivity scan with positive bias voltage. The darker patches correspond to lower current.

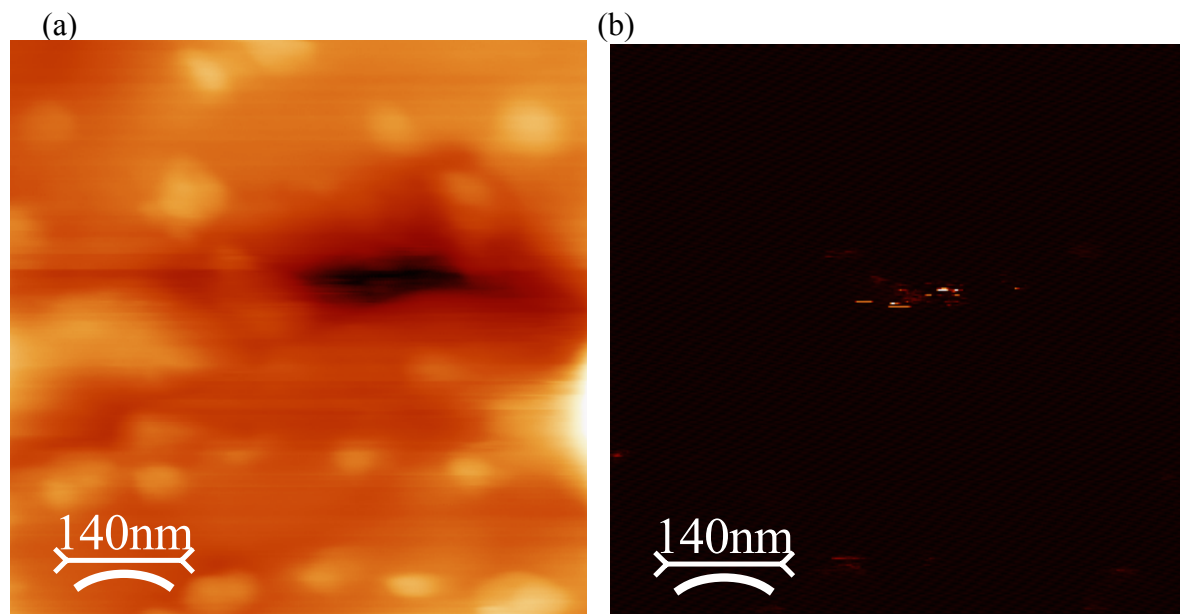


Fig. 5.9. (a) Topography scan of the GaAs:Mn/MnAs hybrid; (b) The corresponding conductivity scan with negative bias voltage. The darker patches correspond to lower current.

Moreover, on reversing the applied voltage, the current is cut off and no current can be observed even with the highest voltage as shown in the Fig. 5.9(b). Fig. 5.8(a) and Fig. 5.9(a) are the corresponding topography scans of same regions, which allows one to identify the clusters positions. It can be easily seen that the current is much higher in the regions with MnAs clusters.

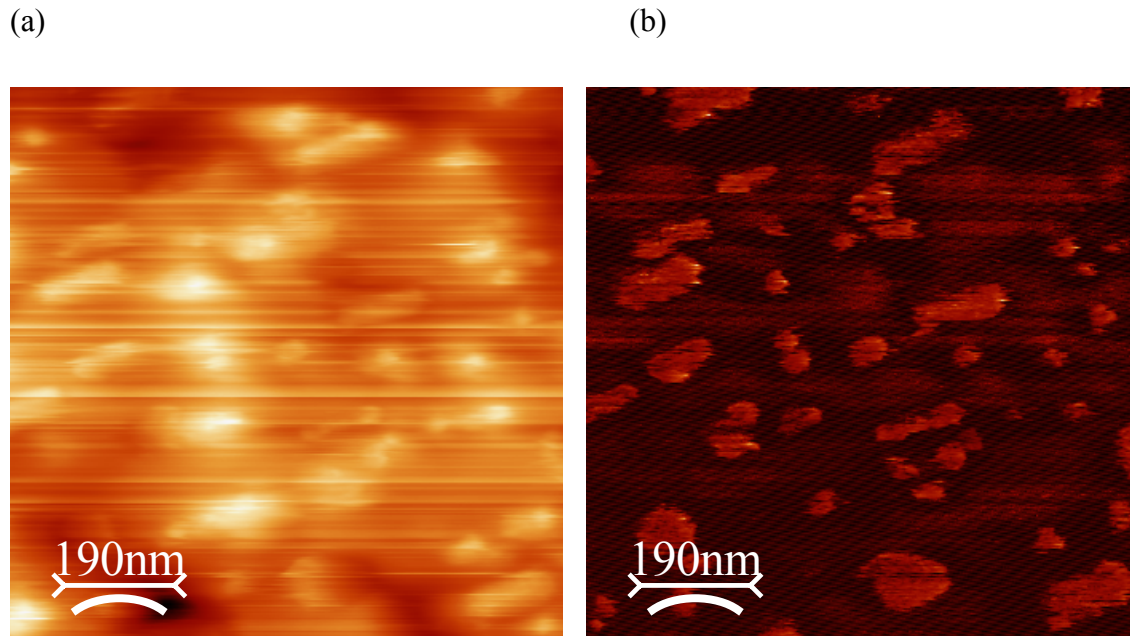


Fig. 5.10. (a) Topography of the modified surface and (b) The corresponding conductivity scan with positive bias voltage.

Another interesting phenomenon is that the observed current is enhanced after several circle scans or etching, which indicates that probably an oxide layer on the surface is removed mechanically (tip) or chemically (etching) as shown in Fig. 5.10. This means that at a particular position the oxide layer can be removed by the tip. However it is found that it starts growing again after some time (the current decreases again). Due to the presence of this oxide layer, the situation becomes extremely complicated. However, according to the experimental results, it is suggested that the imbalance in conductivity for the two applied voltages directions may be induced by the existence of a Schottky barrier at the interface between the MnAs cluster and the matrix. When the positive voltage is applied, the height of the Schottky barrier decreases which leads to the current passing easily through regions with MnAs clusters. In contrast, the height of the barriers seems to increase under a negative bias voltage, leading to the vanishing of the current. More detailed experiments are needed in the future to obtain a more conclusive picture.

In summary, first AFM measurements on the GaAs:Mn/MnAs hybrids have been performed. It is comparatively easy to select individual clusters with the AFM tip. It is also found that it

is feasible to measure the local conductivity of a cluster in the hybrids using a conducting tip in contact mode. Compared with the small currents observed in the GaAs:Mn matrix region, a significantly higher current is measured in the region with MnAs clusters when a positive bias voltage is applied. This current vanishes on reversing the applied voltage. The results hint at the existence of a Schottky barrier between the MnAs clusters and the matrix. However, due to the formation of an oxide layer, one has to apply very high voltages to observe a current, which leads to an insufficient amount of data to confirm whether the I-V curve really exhibits a Schottky barrier behaviour. Therefore, the remaining work is to remove the oxide layer without destroying the sample in the future.

References:

- [1] J. Blinowski and P. Kacman, *Phys. Rev. B.* **67**, 121204 (2003).
- [2] K. W. Edmonds, P. Boguslawski, K. Y. Wang, R. P. Campion, S. N. Novikov, N. R. S. Farley, B. L. Gallagher, C. T. Foxon, M. Sawicki, T. Dietl, M. B. Nardelli, and J. Bernholc, *Phys. Rev. Lett.* **92**, 037201 (2004).
- [3] Y. Matsuda and N. Kuroda, *Phys. Rev. B.* **53**, 4471 (1996).
- [4] R. Meyer, M. Dahl, G. Schaack, A. Waag, and R. Boehler, *Solid State Com.* **96**, 271 (1995).
- [5] F. Hamdani, A. R. Goni, K. Syassen, and R. Triboulet, *Phys. stat. sol.(b)* **223**, 171 (2001).

6. Summary and Outlook

The work described in this thesis has to be seen in the context of developing semiconductor technology towards controlling the spin character of carriers in semiconductors. In this spintronic field, one of the present aims is to achieve a controllable ferromagnetic semiconductor at room temperature. One way is to enhance the Curie temperature in the MBE-grown II(Mn)-VI and III(Mn)-V DMS alloys which exhibit an RKKY-like ferromagnetism, by doping to control effective carrier concentration or by annealing to get the optimum effective Mn concentration, and by band structure engineering. Another alternative are hybrid structures including a ferromagnetic component with Curie temperature above room temperature. Therefore, the spin-related transport properties were investigated in GaMnAs-based alloys and hybrids grown by MOVPE and MBE in this thesis. The obtained important results are as follows:

For GaMnAs-based alloys:

- 1) Unusual positive and negative MR, which are very sensitive to the Mn concentration, were observed at low temperatures in paramagnetic GaAs:Mn alloys grown by MOVPE. This phenomenon is very similar to that observed in the II(Mn)-VI DMS. A comprehensive qualitative description of the MR in the II(Mn)-VI and III(Mn)-V DMS with low Mn concentration is obtained. It is suggested that the interplay of two effects plays an important role. One is the magnetic field-dependent spin splitting of the valence band caused by the *sp-d* exchange between the Mn A^0 (d^5+h) centers and the band states, which shifts the position of the Fermi-level. The other is the disorder effect induced by Mn incorporation. The competition of these two effects is responsible for the unusual positive and negative MR effects. It is found by MCD that the FM coupling with a positive $N_0\beta$ in this paramagnetic GaAs:Mn grown by MOVPE is attributed to the Mn acting as effective A^0 (d^5+h) centers. In the ferromagnetic GaMnAs alloys by MBE growth, large negative MR is observed at low temperature. However, the Curie temperature is far below the estimated value due to the inactive interstitial Mn ions. Thus, the nature of the Mn ions in GaMnAs alloys depends strongly on the growth procedures, which leads to various kinds of intrinsic and extrinsic effects.
- 2) A theoretical calculation by a network and a mobility model based on a phenomenological description was successfully used to explain the experimental MR results in the II(Mn)-VI and III(Mn)-V DMS with low Mn concentration. By adjusting

the weighting of the effects of occupation of the four spin-subbands and of disorder, the negative and positive MR behavior is obtained in these two models. The theoretical results are in good agreement with the experimental results.

- 3) By Te doping into paramagnetic GaAs:Mn with small Mn concentration, a control of the carrier concentration by Te incorporation is almost independent of the Mn concentration. The Hall measurements reveal the presence of both two types of free carriers, electron and holes, and it is possible to change the majority carrier type from p to n type with Te co-doping. Te co-doping causes a transition from VB transport to CB transport. In the case of conduction band transport, the s - d exchange interaction induced conduction band splitting and its contributions to the MR is of minor importance, confirming that the $|N_0\beta| \gg |N_0\alpha|$ in (Ga,Mn)As. Consequently, the contribution of the exchange interaction to the MR effect weakens and finally disappear with increasing Te concentration. The MCD measurements reveal that due to Te co-doping the valence band filled with electrons consequently leads to Mn acting as A^- centers and an AFM type coupling between VB states and the Mn spins. This result confirms that the sign and magnitude of exchange integral $N_0\beta$ indicating FM or AFM coupling between spins of the VB carriers and the Mn ions can be tuned by the local electronic structure of the Mn ion.

Therefore, the properties of GaMnAs-based alloys show that GaMnAs can be more easily doped with Mn impurities acting as electrically active, in contrast to a large quantity of transition metals incorporated into II-VI materials only acting as local spins.

For GaAs:Mn/MnAs-based hybrids:

- 4) The series GaAs:Mn/MnAs and GaInAs:Mn/MnAs paramagnetic-ferromagnetic hybrids prepared either by MOVPE directly or by post-growth annealing of $\text{Ga}_{1-x}\text{Mn}_x\text{As}$ alloys grown by low-temperature MBE are studied based on the understanding of GaAs:Mn alloys. Large unusual MR effects are found in the hybrids including MnAs clusters with NiAs structure grown by MOVPE, e.g. a -30% negative MR at low temperature and change to 160% positive MR with increasing temperature at $H=10$ T. The ferromagnetic MnAs cluster leads to a local localization process of the carriers around the clusters and act as a spin-filter, which is suggested to be responsible for the observed unusual coexistence of the large negative and positive MR effects. By varying the growth parameters, it is confirmed that the magnitude of

the spin-filter effect can be tuned by the size and shape as well as by the density of the clusters. The MR and Hall effect investigated in these hybrids confirm that the interplay of the paramagnetic matrix and of the MnAs clusters dominates the spin-dependent transport behaviour. Both, the properties of the matrix and of the MnAs clusters strongly depend on the preparation procedure. As these properties also determine the spin-dependent transport behaviour, it is very sensitive to the preparation procedure.

- 5) The FMR measurements indicate that two type of MnAs clusters form in the post-growth annealing of $\text{Ga}_{1-x}\text{Mn}_x\text{As}$ alloys grown by low-temperature MBE. One of them is confirmed as the same as the one observed in the hybrids grown by MOVPE with NiAs-structure (type I). The other one (type II) is of much lower Curie temperature and different structure. With increasing annealing temperature, the content of type I clusters increases whereas the content of type II clusters decreases. More detailed information is needed about two types of MnAs clusters to find out how these two different MnAs clusters affect the spin-dependent transport in such paramagnetic-ferromagnetic hybrids.
- 6) The geometry dependence of the MR and Hall effect of the GaAs:Mn/MnAs hybrid reveals that the degree of microscopic interaction between the free carriers in the paramagnetic semiconductor host and the ferromagnetic MnAs clusters also strongly depends on the transport geometry and the resulting current path through the sample. The hydrostatic pressure dependence of the MR and the Hall effect are consistent with what happens in II-VI DMS and InMnAs, i.e., an enhanced p-d exchange interaction by increasing applied hydrostatic pressure. However, these effects are partly compensated by the pressure-induced variation of the carrier density.

Therefore, the properties of GaAs:Mn/MnAs-based hybrids indicate that the paramagnetic-ferromagnetic structures exhibit large spin-dependent transport effects. These effects can be tuned by the growth conditions, by the growth procedure, and by external physical parameters. The way to modify the effective carrier concentration in the matrix of the hybrid with 150 nm thickness is very useful to find the optimum property of the matrix for the spin-dependent transport. On the other hand, to investigate the properties of thicknesses less than 150 nm is also necessary for the optimum function of the MnAs clusters. Combining the individual properties of the paramagnetic matrix and MnAs clusters and their interactions can lead to a control of the giant Zeeman splitting in the matrix, the local inhomogeneous inner

magnetic field due to the MnAs clusters, and the interface between the matrix and clusters. These effects can be designed individually or together to optimize spin-transport in the hybrid.

For further investigations of these interesting paramagnetic-ferromagnetic hybrids, some experiments are suggested in the following.

- 1) One is to continue the investigation of the local spin-dependent transport in the ferromagnetic-paramagnetic hybrids by transport AFM. In the case of GaAs:Mn/MnAs hybrid, due to the possible half-metallic character of the ferromagnetic MnAs clusters, it is possible to use one spin orientation channel in the MnAs clusters as a spin filter. A tip with a ferromagnetic coating should be prepared to interact with the spins within the ferromagnetic MnAs clusters. It is possible to prepare a sample holder where a DC magnetic field can be applied. The external small magnetic fields applied in plane of the sample surface should be sufficient for switching the magnetization direction of the MnAs clusters while leaving the magnetization state of the ferromagnetic coating of the tip unaffected. With the changing of the magnetization direction of the ferromagnetic coating of the metallic tip with respect to that of the ferromagnetic MnAs clusters, a large TMR effect should be achieved due to the changing of the tunnel resistance at the bias voltages corresponding to the energetic positions of the two spin components of the exchange-split surface state.
- 2) The temperature and magnetic field dependence of current-voltage characteristics of the hybrid samples grown by MOVPE are useful to investigate the property of the barrier at the interface of the matrix and clusters.
- 3) Injected polarized light is supposed to increase the effective spin carrier concentration in the matrix. Therefore, the spin-dependent transport measurements with illumination by the polarized light are worth looking at.
- 4) Measurements of the temperature dependence of thermal conductivity are useful to investigate whether there is a phase transition at the transition temperature from negative to positive MR.
- 5) Measurements of the temperature dependence of the Thermopower maybe be very useful to understand the special behaviours of carriers and the temperature dependence of the Fermi-level in these GaMnAs-based alloys and hybrids.

Acknowledgements

I would like to express my sincere gratitude to **Prof. Dr. Wolfram Heimbrod**t and **Dr. Peter Klar** made the possibility for my Ph. D studies in Germany, to **European Graduate College (EGC)** has financially supported me during the past three years. It has been really a wonderful and fruitful experience to be part of the meeting of east and west cultures. This experience taught me a great deal about scientific knowledge and the colourful aspects of life. There is no way I can show my thanks directly, but I hope, all of you can feel and understand my sincere thanks.

I would like to gratefully acknowledge **Prof. Dr. Wolfram Heimbrod**t. With his creative supervision and constant encouragement, the dilute magnetic semiconductor becomes close to me, leading to smooth completion of my Ph. D work. Thanks to his valuable discussion on the complicated experimental results, and his understanding and support for a pleasant, stress-free atmosphere for my study. His kindness and cares for me made him as a special supervisor in my whole study career.

I am especially grateful to **Dr. Peter Klar** for his resourceful guidance and invaluable help and support. He helped me in every detail of the work, from the initial stages of the project design, valuable discussions, to the patient revision of this thesis, letting me get the right way to research work. His lectures on magnetism and semiconductors, which are very valuable for me to make a clear physical picture. Thanks to his many helps when I got into difficulty as a foreign resident. In particularly many thanks to his significant understanding about Chinese culture and typical communications.

I am greatly indebted to **Prof. Dr. Peter Thomas** and **Prof. Dr. Florian Gebhard** for accepting me as a member of the EGC to resulting in a financial support for my Ph. D study. I am glad I belongs to a member of EGC because of the support and encouragement from other members of this organization. Especially gratefully thanks to Prof. Dr. Peter Thomas for his theoretical insights for our work and the introduction of the Hungarian culture for my stay in Budapest.

In particular, I would like to acknowledge

Prof. Dr. Sergei Baranovski and *Christoph Michel*, *Dr. Vedran Rajevac* for their wonderful theoretical cooperation;

The group of *Prof. Dr. Mihaly György* at Budapest University of Technology and Economics, for their kind cares when I studied in their group as a exchange student;

The group of *Prof. Dr. Wolfgang Stolz* for their closely cooperation with us and kindly supplied the contacting set-up. Especially, thanks to *Dr. Michel Lampalzer* offering the series samples, *Dr Kerstin Volz* on the STM measurement, and *Stefan Oberhoff* on the AFM measurement;

The group of *Prof. Dr. Alois Loidl* for their experimental cooperation. Especially thanks to *Dr. Hans-Albrecht Krug von Nidda* and *Thomas Kurz* for the SQID and FMR measurements;

Dr. Heinz Sturm for his measurement on the transport-AFM;

Mr. *Sven Kroker* for his annealing procedures on the MBE-GaMnAs samples.

Dr. Torsten Henning and *Jörg Teubert* for the programme;
The workshop group of *Dr. Matthias Born* for their very helpful electric technique;

The workshop group of *Hermann Günther* and *Rüdiger Rink* for their perfect mechanical work;

and thanks to *Ms. Anne Ehlers* and *Ms. Marina Koch* for their kind helps especially in dealing with all kinds of complicated documents.

I am grateful to *Dr. Limei Klar* for her warm helps always to me.

I deeply thank my best friend *Dr. Huijuan Zhou, Ling. Fu* and to more good friends than possibly be named here who accompanied with me during this period abroad.

Sincere thanks must go to all the members of our group: *Dr. Heiko Grüning, Dr. Thorsten Hartmann, Dr. Horst Falk, Martin Güngerich, Jörg Teubert, Jens Kampmann, Christian Karcher, Björn Metzger*, for their kind helps and the pleasant atmosphere, and especially for the ‘Friday wine-drinking’. Thanks to their kind helps and understanding for any troubles and difficulties in my studies and daily life. I am very happy and enjoy the nice time with them.

Forever, grateful thanks to my dear family: my parents, my grandparents, my sister and brother, for their everlasting love.

Curriculum Vitae

Shuangli Ye, born on 10/10/1975 in Xiantao, Hubei Province, People's Republic of China

Bachelor of Science *September 1993 – July 1997*

Hubei University, Wuhan, Hubei, People's Republic of China

Master of Science *September 1997 – July 2001:*

Institute of Solid State Physics, Chinese Academy of Science,

Hefei, People's Republic of China

Advisor: **Prof. Yuping Sun**

Dissertation: *The effect of monovalent-metal substitution on structural and CMR properties of LaMnO_3 Manganates*

PH.D *01.11.2001 –present*

Department of Physics and Material Sciences Center, Philipps-University, Marburg, Germany

Advisor: **Prof. Wolfram Heimbrod**

Dissertation: *Magneto-transport in (Ga,Mn)As-based alloys and hybrids*

Publications:

Spin-dependent localization effects in GaAs:Mn/MnAs granular paramagnetic-ferromagnetic hybrids at low temperatures

C. Michel, C.H. Thien, **S. Ye**, P.J. Klar, W. Heimbrod, S.D. Baranovskii, P. Thomas, M. Lampalzer, K. Volz, W. Stolz, B. Goldlücke
Superlattices and Microstructures. **37**, 321 (2005).

Tuning of average p-d exchange in (Ga,Mn)As by modification of the Mn electronic structure

Th. Hartmann, **S. Ye**, P.J. Klar, W. Heimbrod, M. Lampalzer, W. Stolz, T. Kurz, A. Loidl, H.-A. Krug von Nidda, D. Wolverson, J.J. Davies, and H. Overhof ;
Phy. Rev. B. **70**, 233201, (2004).

Anisotropy of the magneto transport in (Ga,Mn)As/MnAs paramagnetic-ferromagnetic hybrid

S. Ye, P.J. Klar, T. Hartmann, W. Heimbrod, M. Lampalzer, S. Nau, T. Torunski, and W. Stolz, T. Kurz, H.-A. Krug von Nidda and A. Loidl ,
Appl. Phys. Lett. **83**, 3927 (2003).

Influence of co-doping on the magnetoresistance of paramagnetic (Ga,Mn)As

S. Ye, P.J. Klar, T. Henning, M. Lampalzer, W. Stolz and W. Heimbrod,
J. Superconductivity: Incorporating Novel Magnetism **16**, 159 (2003).

Magneto-optical spectroscopy on (Ga,Mn)As based layers - correlation between the p-d exchange integral and doping

T. Hartmann, **S. Ye**, T. Henning, P.J. Klar, M. Lampalzer, W. Stolz and W. Heimbrod,
J. Superconductivity: Incorporating Novel Magnetism **16**, 423 (2003).

conference Presentations:

International workshop spintronics: Spin Injection, transport, and Manipulation

Ruhr-Universität Bochum, Germany, October 11-12, 2004

Poster: Magnetotransport in GaMnAs/MnAs and GaInMnAs/MnAs paramagnetic-ferromagnetic hybrids

S. Ye, P.J. Klar, T. Hartmann,, M. Lampalzer, W. Stolz and W. Heimbrod,

The 20th General Conference of the Condensed Matter Division of the European Physical Society

Prague, July 19-23, 2004

Poster: magnetoresistance and Hall effect investigation in GaMnAs/MnAs paramagnetic-ferromagnetic hybrids

Shuangli Ye, Peter J. Klar, Michael Lampalzer, Wolfgang Stolz and Wolfram Heimbrod

Wandlitz Days on Magnetism workshop: Local Moment Ferromagnets: Unique Properties for Modern Application

Berlin, Germany, March 15-18, 2004

Poster: Experimental and theoretical investigations of the magnetotransport in (GaMn)As/MnAs and (GaInMn)As/MnAs paramagnetic-ferromagnetic hybrids

Shuangli. Y

'11th International Conference on Modulated Semiconductor structures(MSS11)'

Nara, Japan, July 14-18, 2003

Poster: **Correlation of magnetism and magneto-transport in GaAs:Mn/MnAs paramagnetic-ferromagnetic hybrid structures**

S. Ye, P.J. Klar, T. Hartmann, W. Heimbrodtt, M. Lampalzer, W. Stolz, Th. Kurz, H.-A. Krug von Nidda, A. Loidl

2nd International Conference on Physics and Application of Spin Related Phenomena in Semiconductors

Würzburg, Germany, July 23 - 26, 2002

Poster: **Influence of co-doping on the magnetoresistance of paramagnetic (Ga,Mn)As**

S. Ye, P.J. Klar, T. Henning, M. Lampalzer, W. Stolz and W. Heimbrodtt,